

Quantifying the Impact of Tolerance Evolution on Bacterial Populations under Time Inhomogeneous Antibiotic Stress.

Jonas Günzl





Faculty of Mathematics and Natural Sciences

Department of Physics, Institute for Biological Physics

# Quantifying the Impact of Tolerance Evolution on Populations under Time Inhomogeneous Antibiotic Stress

Jonas Günzl (Student ID: 7406746)

Born on 3rd May 1999 in Rostock

## Master Thesis

to achieve the academic degree

Master of Science (M.Sc.)

## Supervisor:

1st: Prof. Dr. Joachim Krug

2nd: Prof. Dr. Berenike Maier

Submitted on: August 19, 2025

## Abstract

In the vast field of microbiology and antimicrobial research the rather general term fitness is often condensed into growth rate at some specific antibiotic concentration. In a constant environment, this measure allows to construct meaningful fitness landscapes for distinguishable genotypes and predicts the evolution of resistance. Such studies usually disregard the clinically relevant regime of microbial death and the typically time dependent antibiotic concentration.

In this work, we present a model for the evolution of antibiotic tolerance, defined as the ability of bacteria to reduce their death rate under high antibiotic concentrations without developing resistance. Under the assumption of periodic antibiotic treatment, we introduce two novel performance measures for tolerant mutants and demonstrate how tolerance can become established within a wild type bacterial population. We introduce the concept of effective fitness, quantifying bacterial net growth over a full cycle of periodic antibiotic exposure. This metric reveals that tolerant mutants can establish in the population despite lacking a direct growth advantage. By deriving a closed-form expression for effective fitness, we identify key parameters of antibiotic tolerance and apply trade-off-based fitness landscape theory to predict tolerance evolution.

Furthermore, we propose survival probability as an alternative metric of reproductive success. Using analytical and numerical analyses based on a simple homogeneous birth-death model, we show that tolerant mutants have an increased chance of surviving antibiotic treatment.

Ultimately, these results imply that tolerant mutants can rescue populations from extinction.

# Contents

1	Inti	roduction	1
<b>2</b>	Cha	aracterizing the Bacterial Response to Antibiotic Treatment	4
	2.1	Resistance and Tolerance - How to Distinguish Different Behaviors?	4
	2.2	Dose-Response Curves	5
	2.3	Quantifying the Treatment Efficacy - Effective Fitness	8
	2.4	A First Interpretation of the Effective Fitness	10
		2.4.1 The Pharmacokinetic Parameter $\alpha \tau$	11
		2.4.2 The Hill Parameter $\nu$ - a Short Intermezzo on the Step DRC	12
		2.4.3 The Resistance Parameter $C$	13
		2.4.4 On the Ratio of $\lambda_{\min}$ and $\lambda_{\max}$	14
	2.5	Biological Context of the $\lambda_{\min}$ - $\lambda_{\max}$ Relation	19
3	Tole	erance Evolution in Trade-Off Induced Fitness Landscape	21
	3.1	Mapping Genotypes to Fitness	21
	3.2	Fitness Graphs and Fitness Landscapes	22
	3.3	The Topography of Trade-Off Induced Landscapes	24
		3.3.1 Gain Intuition on a Toy Model	24
		3.3.2 Ruggedness and Accessibility for Stochastic Landscapes	27
		3.3.3 On the Number of Loci	34
	3.4	Tolerance Evolution in Effective Fitness Landscapes	38
4	Sto	chastic Birth and Death Processes	43
	4.1	The General Birth and Death Process	44
	4.2	The Simple and Homogeneous Birth and Death Process	46
5	$\operatorname{Th}\epsilon$	e Stochastic Model of Periodic Treatment	49
	5.1	Biostatic and Biocidal Interpretation of $\eta$	49
	5.2	Pharmacokinetics and Pharmacodynamics in the Stochastic Model	50
	5.3	The Interpretation of Tolerance in the Stochastic Model	52
	5.4	The Survival Probability Within a Single Treatment Period	52
	5.5	The Survival Probability of Tolerant Mutants	56
6	Nu	merical Simulation of Periodic Treatment	<b>59</b>
	6.1	Remarks on Competition	59
	6.2	The Gillespie Algorithm	60
	6.3	Comparison of Simulations and the Survival Probability	61
	6.4	Comparison of Simulations and the Effective Fitness	61

7	Pop	ulation Rescue Through Antibiotic Tolerance	64
	7.1	Standing Genetic Variation	64
	7.2	De Novo Mutation	66
8	Disc	cussion	69
	8.1	Conclusion	69
	8.2	Outlook	71
		8.2.1 Modified Gillespie Algorithm	71
		8.2.2 Biphasic Evolution in the Stochastic Model	71
		8.2.3 Analytic Results on the Rescue Probability	72
		8.2.4 First Passage Times	73
A	Ren	narks on the Dose-Response Curve and the Effective Fitness	75
	A.1	Reformulation of the Dose-Response Curve	75
	A.2	Analytic Solution of the DRC Integral	76
	A.3	Limits of the Effective Fitness	77
		A.3.1 On the Pharmacokinetic Parameter $\tilde{\alpha}$	77
		A.3.2 On the Hill Exponent $\nu$	77
	A.4	Derivation of Effective Fitness for the Step DRC	79
	A.5	Analysis on the Normalized Effective Fitness as a Function of $\kappa$	80
		A.5.1 The Limit of Large Death Rates $(\kappa \to \infty)$	80
		A.5.2 What Happens for Finite $\kappa$	80
	A.6	The Effective Fitness Under Changes of the MIC	81
В	Ren	narks on the TIL Model	83
	B.1	Proof of the Ordering-Accessibility Equivalence	83
	B.2	Results for Trade-Off Landscapes with 4 Loci and Constant Variance	84
	В.3	Normalization of the Fitness Peak Count	84
	B.4	Evolution Algorithm	85
$\mathbf{C}$	Rob	oustness of the Deterministic Tolerance Evolution Model	87
	C.1	Robustness of the Effective Fitness	87
	C.2	Robustness of the TIL-Model Analysis	91
D	Size	Distributions in the Simple Birth–Death Process	95
$\mathbf{E}$	Sur	vival Probability for Biostatic and Biocidal Treatment	97
	E.1	Proof that $P_{\text{surv}}^{\text{cidal}} < P_{\text{surv}}^{\text{static}}$	97
	E.2	Proof that $P_{\text{surv}}^{\text{cidal}} > P_{\text{surv}}^{\text{static}}$ for $\eta_{\text{max}} < 0$	98

# List of Figures

1	Resistance and Tolerance	5
2	Hill Type Dose-Response Curves	7
3	Analytic Solution of the Hill Model	10
4	Analytic Solution of the Hill and Step Model	13
5	2D Fitness Landscape	14
6	2D Fitness Landscape with $\kappa \& c$	15
7	Family of Dose-Response Curves	16
8	Effective Fitness as Function of $\kappa$	18
9	Family of Dose-Response Curves with $c \neq 0$	19
10	Exemplary Fitness Graphs	23
11	Fitness Graph and Fitness Landscape	23
12	Visualization of the Accessibility Property	25
13	Toy Model Fitness Landscapes	28
14	Toy-Model Behavior of the Effective Fitness	29
15	Landscape with Random Death Rate	30
16	Landscapes for Various TIL Models	31
17	Trade-off Results for Constant Variance $x = 0.3$	32
18	Layer of Peak Genotypes $x = 0.3$	33
19	Trade-off Results for Constant Variance $x = 0.7$	34
20	Layer of Peak Genotypes $x = 0.7$	34
21	Binomial Layer Distribution	35
22	Topography for Variable System Size	36
23	Normalized Number of Fitness Peaks	37
24	Average Path Length in the Toy Model	38
25	Average Length of Evolutionary Paths	39
26	Evolutionary Path in Trade-Off Landscapes	41
27	Evolutionary Path in a Large Trade-Off Landscapes	42
28	Deterministic Cell Count over Time - Motivation for a Stochastic	
	Model	44
29	Extinction Probability in the Simple Birth-Death Process	48
30	DRC of the Stochastic Model	51
31	Survival Probability in a Constant Environment	55
32	Survival Probability in a Step Function Concentration Profile	57
33	2D Topography of the Survival Probability	57
34	2D Topography of the Survival Probability for Prolonged Treatment.	58
35	Survival Probability in a Step Like Concentration Profile for the	
	Wild Type and Tolerant Mutant	58

36	Survival Probability for Wild Type and Tolerant Mutant from Nu-	
	merical Gillespie Simulations.	61
37	Single Gillespie Simulations of a $N_0 = 100$ and $N_0 = 10000$ Wild	
	Type Population	62
38	Average of 500 Gillespie Simulations of a $N_0 = 100$ and $N_0 = 10000$	
	Wild Type Population	63
39	Gillespie Simulations of a Two Phenotype Population with Stand-	
	ing Genetic Variation.	65
40	Rescue and Survival Probability	66
41	Gillespie Simulations of a Two Phenotype Population with De Novo	
	Mutations	67
42	Rescue Probability for Different Mutation Probabilities	67
A.1	The Effective Fitness as a Function of the Resistance Parameter $C$ .	81
B.1	Trade-Off Results for Constant Variance $\lambda_{\text{max}} \in [0.7, 1.0)$	84
B.2	Layer of Peak Genotypes $\lambda_{\text{max}} \in [0.7, 1.0)$	84
В.3	Trade-off Results for Constant Variance $\lambda_{\text{max}} \in [0.3, 0.6)$	85
B.4	Layer of Peak Genotypes $\lambda_{\text{max}} \in [0.3, 0.6)$	85
C.1	2D Fitness Landscape Double Exponential	88
C.2	Construction Scheme for Alternative DRC's	89
C.3	Fitness Topographies for Different Dose-Response Curves	90
C.4	Effective Fitness Over $\phi$ for Constructed DRC	91
C.5	Number of Peaks and Accessibility Property for the Constructed	
	DRC as a Function of $\bar{\phi}$ .	92
C.6	Number of Peaks and Accessibility Property for the Constructed	
	DRC as a Function of the Number of Loci	92
C.7	TIL-Model Path Lengths as a Function of the Fraction $\overline{\phi}$	93
C.8	Exemplary Path in the Topography of the Constructed DRC	93
D.1	Time Evolution of the Wild Type Population Size Distribution	96
D.2	Time Evolution of the Tolerant Mutant Population Size Distribution.	96

## 1 Introduction

With the discovery of the first antibiotics by Fleming [1], a new era of pharmacologic treatment began to arise. Rampant infectious diseases such as tuberculosis, typhus, syphilis, etc. rapidly became less lethal [2] and the average life expectancy significantly increased [3] as those antibiotics became readily available after World War II [2], [4]. Ever since, the world wide consumption has been increasing [5]. However, already as early as 1940, observations indicated that bacteria are able to inactivate the antibiotic [6] and withstand high doses of the drug. This phenomenon is commonly known as antibiotic resistance [7].

The degree of resistance depends on the expression of certain genes, controlling fundamental cell mechanisms, such as matrix influx and efflux or the synthesis of antimicrobial agents. Such mechanisms can be up or dow regulated through mutations, ultimately enhancing the cell's ability to withstand high antibiotic concentrations [8, 9].

It has been shown that the development of antibiotic-resistant bacteria strongly correlates with the rate of antibiotic consumption in a society [10]. Unsurprisingly, drug-resistant infections have become a serious health concern [4, 5, 10, 11] and recent studies estimate, that globally there could be about 10 million deaths associated to antimicrobial resistance in 2050 [12].

Moreover, also a second kind of antimicrobial adaptation has already been discovered in 1944 [13]. It was observed, that a transient exposure to antibiotics did not kill bacteria even at very high dosage. Such a response, whether inherited or not, has been termed as 'tolerance' [14, [15], [7]].

The clinical implications of tolerance evolution on treatment efficacy are often overlooked [16], even though it increases the mortality rate [17] as well as the probability of developing resistant mutations [16]. Furthermore, meaningful fitness measures of tolerant strains remain widely undefined and our understanding of tolerance evolution is far less advanced than that of resistance [18].

In this thesis, we will therefor focus exclusively on the effect of antibiotic tolerance and neglect all other forms of adaptation, such as resistance, resilience or persistence [7, 19].

We examine the advantage of evolving antibiotic tolerance within a clinically relevant pharmacokinetic-pharmacodynamic (PKPD) framework, in which antibiotic concentrations alternate periodically between growth and killing regimes. Building on the well-established theory of Hill-shaped dose-response curves [20, 21, 22, 23, 24], we introduce two fundamentally different performance measures to compare the success of tolerant mutants to the wild type.

These quantities are capable to predict how the empirically observed trade-off be-

tween enhanced survival at high concentration and decreased growth rate in the absence of antibiotic [25, 26, 27, 28] is beneficial and we show that such tolerant mutants can establish in a bacterial population.

In the first part, we present a fully deterministic framework, to describe the population size as a function of time. Using a simple, exponentially decreasing concentration profile, we derive the time integral of the dose response curve over one drug cycle in section 2.3. The exponential of this integral describes the effective change in the amount of viable cells after one treatment period. Under the assumption, that non of the PKPD functions change during the treatment, the solution of the integral is a constant for all subsequent periods and we readily find a solution for the cell count after arbitrarily many drug applications.

For the purpose of this work, we propose to normalize the integral by the time period and interpret the result as an effective growth or death rate, which we call the effective fitness. This quantity has units of a replication rate and yields an approximate solution for the cell count at any real time t > 0 and defines a meaningful fitness measure for any phenotype with a Hill-shaped dose-response curve.

In the following (section 2.4), we demonstrate how tuning two key dose-response curve parameters captures the previously described tolerance trade-off. For any phenotype that is tolerant compared to the wild type in this sense, we compute the effective fitness and obtain a two dimensional topography. This structure illustrates, which tolerance mutations increase the effective fitness and highlights how bacteria may escape extinction through adaptive tolerance evolution.

A more detailed analysis of the emerging fitness landscape and the accumulation of beneficial mutations is conducted within a genotypic model of trade-off induced fitness landscapes. Similar models were previously introduced in the context on antibiotic resistance evolution [29].

Developing intuition on a toy model, we discuss the key properties, the ruggedness and accessibility property, of tolerance trade-off landscapes in section 3.3. Finally, we simulate evolution as random adaptive walks on the fitness landscape (section 3.4) and uncover a biphasic pattern of tolerance evolution, characterized by initial cost acquisition followed by compensatory adaptation.

Concluding on the first part of this thesis, we show that a simple measure on the average replication rate predicts that tolerant mutants can have a selective advantage over the wild type. For large populations, that are far from extinction over multiple periods, this is a meaningful result. However, because effective fitness is defined as the period-averaged replication rate, it fails to capture short-term dynamics occurring within a single or few periods. Moreover, the deterministic

description becomes inaccurate when population sizes are small and extinction risk becomes significant, which is of particular clinical importance.

Accordingly, the second part of this study presents a refined, stochastic description of the periodic treatment, explicitly modeling growth and death as distinct processes and capturing extinction events that are not described by the deterministic approach. Furthermore we distinguish the analysis of biocidal and biostatic antibiotics.

Based on previous results on the fundamental birth and death process [30] [31], we derive an analytically exact result on the probability that any phenotype survives a single dose of the respective antibiotic (section [5.4]). Additionally to the deterministic effective fitness, the survival probability introduces a second, stochastic measure of success.

We demonstrate for both modes of action, that tolerance evolution can increase the survival probability relative to the wild type and potentially threatens the efficacy of clinical treatment.

In section 6 we introduce a numerical Gillespie algorithm 32 of periodic treatment, modeling the stochastic process in computer simulations. This algorithm is exact and tracks the cell number of any phenotype in the population as a function of time 32, 33.

We compare these simulations to the analytic predictions of the survival probability (section 6.3) and the effective fitness (section 6.4) on the respective timescale, highlighting the relevance of both quantities.

Finally, we discuss two scenarios of evolutionary rescue, which is a key concern in the field of evolutionary biology [34, 35]. We show in section [7], that the presence of a small tolerant subpopulation or also de novo evolution of antibiotic tolerance result in characteristic U-shaped rescue curves [35]. The rescue probability is further quantified in Gillespie simulations of the two distinct scenarios (section [7.1] and [7.2]).

Importantly, the rescue probability is a long-term probabilistic measure defined in the limit of many successive drug applications. It is high when the initially small tolerant subpopulation has a high chance of survival and rapidly grows to a supercritical size. Accordingly, the rescue probability correlates with both analytical metrics and ultimately quantifies the chance that prolonged periodic treatment fails due to the presence or evolution of antibiotic tolerance.

In section 8, we summarize the results on periodic antibiotic treatment and explore potential extensions of our study.

# 2 Characterizing the Bacterial Response to Antibiotic Treatment

# 2.1 Resistance and Tolerance - How to Distinguish Different Behaviors?

The failure of antibiotic treatment has long been associated to resistance mutations [16]. Such a mutation is characterized by an increase of the minimum inhibitory concentration (MIC), allowing for growth at high concentrations of the antibiotic [7]. Quantifying the MIC experimentally is relatively easy, since it is only necessary to test for "growth" or "no growth" in different environments [36].

Despite being so convenient in terms of selecting for resistance, the MIC is not capable to distinguish tolerant bacterial strains. By definition, tolerance is the ability to survive a transient exposure to high concentrations of an antibiotic without changing the MIC [7, 14]. It becomes therefore necessary to introduce a second parameter. Brauner et al. proposed the mean duration of killing (MDK), in combination with the MIC for a standardized characterization of the antibiotic sensitivity [7]. The MDK is defined as the typical duration to kill a certain amount of the bacterial population [37].

Unlike the MIC, determining the MDK can be experimentally costly [38], 39, as it requires measuring cell death instead of growth.

Growth rate assays are commonly performed by optical density (OD) measurements [7, 40, 39], where an increase of absorption is related to a positive change in biomass. However, such measurements cannot reliably detect cell death [39]. A common method to capture cell death is to inoculate bacteria in the antibiotics for a desired time and spread a dilution on agar plates. Counting the fraction of regrowing sub-colonies, so called colony forming units (CFU), then yields the fraction of survivors [38], [7]. This has to be repeated for different times and antibiotic concentrations to obtain full time-kill assay.

Figure 1 summarizes the discussed parameters of a bacterial response to antibiotic treatment.

Recently, novel approaches to avoid the time consuming plating and colony counting have been tested. Bren et al. proposed a regrowth approach, which relates the time to reach a certain OD threshold to the fraction of survivors [39]. Another method was used by King et al., who examined a fluorescence based time-kill essay [41]. Both approaches seem to reproduce results from the cell counting approach to a large extent, but problems such as varying lag-times and antibiotic overtake (regrowth) or experimental bias and fitness interference of the flu-

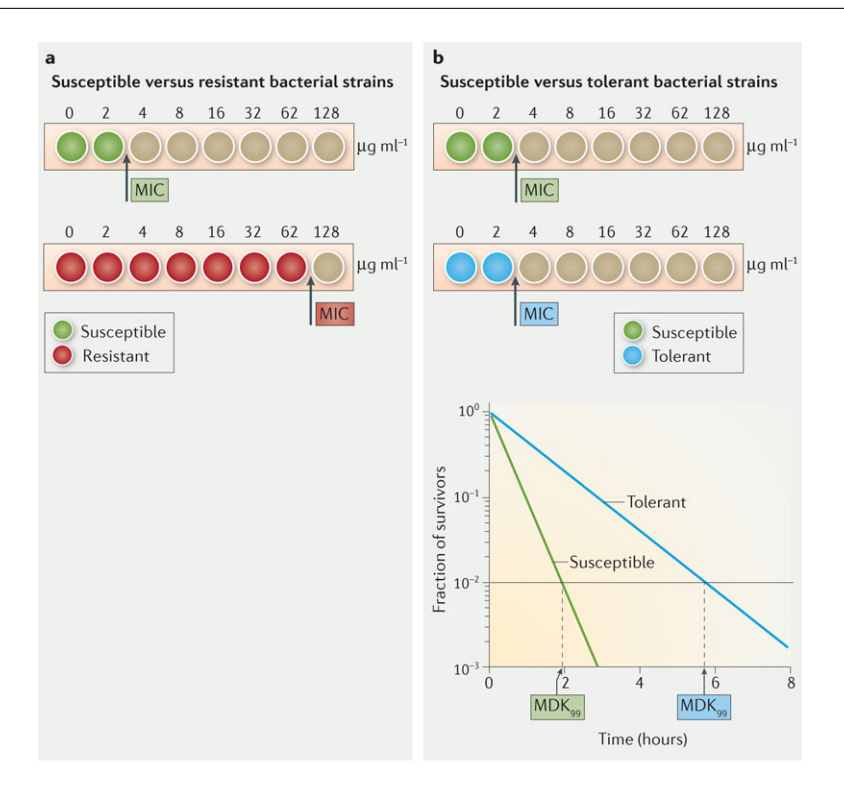


**Figure 1:** a: Wild type (green) and resistant strain (red) in similar antibiotic environments. The resistant strain also grows at high concentrations of the antibiotic because of an increased MIC.

b: Wild type (green) and tolerant strain (blue) in similar antibiotic environments. Similar to the wild type, the tolerant strain does not grow at high antibiotic concentrations (equal MIC). The MDK<sub>99</sub> from time-kill experiments can distinguish the bacterial strains. The figure was published in [7].

orophore have to be tested.

# 2.2 Dose-Response Curves

Distinguishing between tolerance and resistance can be crucial for clinical applications. Wrong treatment might be ineffective or even harmful for the antibiotic efficacy [14, 16].

Still, measurement of bacterial killing at "high"- or "well above MIC" concentrations [7], [14] remains vague to some extent. Moreover, maintaining constant antibiotic concentrations over extended periods can be challenging due to pharmacokinetic factors like drug absorption, distribution and metabolism [42], [43], [44], [23], [21], [45]. It is therefore practical, to define a concentration dependent rate, that describes the effective change of the population size.

Assuming exponential growth and death, such a rate can be extracted from log-linear fits to the discussed time-kill curves [39], [20].

In 1971 Jusko proposed a first mathematical model to describe the fraction of viable cells over time  $\boxed{46}$ . The model describes the amount of viable cells (N)

as a function of the natural growth/death (g/d) rate of the bacteria, an effective concentration (c) in the body compartment of the bacterial infection and a reaction rate (k) of the antibiotic with bacteria. Assuming, that all target cells are similarly susceptible, one finds a simple expression for the rate of change in cell count:

$$\frac{dN}{dt} = (g - d) N - k c N \tag{1}$$

The pharmacodynamic model defined in (1) was revisited and modified by Zhi et al. [47], [48] and became prominent as [20], [49], [45].

First, the Zhi model defines the apparent growth rate at zero concentration:

$$\lambda_{\text{max}} = g - d.$$

The model of Jusko further simplifies as one considers that bacteria are directly affected by the concentration in the central compartment, i.e. there are no transport losses of the antibiotic concentration. Hence, the effective concentration (c) is a readily tunable (in general time-dependent) concentration (c(t)). Moreover the model assumes that no resistance occurs, or, if it does, it can be described by an additional growth rate constant [47].

For such a model, two cases can be distinguished [47, 48, 45]. (1) A linear non-saturable model describing a concentration independent reaction rate of the antibiotic (as in [1]). And (2) a non-linear saturable model, where the reaction rate  $\lambda$  is multiplied with a Michaelis-Menten type factor  $(K_m + c)^{-1}$  [48], which yields

$$\frac{dN}{dt} = \lambda_{max} N - k \frac{c(t)}{K_m + c(t)} N \tag{2}$$

$$= \lambda(c(t)) N. \tag{3}$$

In this context,  $\lambda$  denotes the effective replication rate of bacteria under treatment and the function  $\lambda(c)$  is known as the dose-response curve (DRC) for this model. The DRC essentially depends on three parameters, which are unique to each pair of drug and bacterial strain.  $\lambda_{\text{max}}$  and k were already introduced above and  $K_m$  is a Michaelis-Menten type saturation constant [48]. For the given model  $K_m$  represents the concentration, where the effective reaction rate reached half of its maximum.

In vitro studies were able to show, that such a saturable model appears to be appropriate to predict the fraction of CFU after treatment [48, 45].

An additional generalization of this model incorporates a Hill coefficient ( $\nu$ ) as a fourth parameter [21, 22, 20, 23, 24], which adjusts the steepness of the dose-

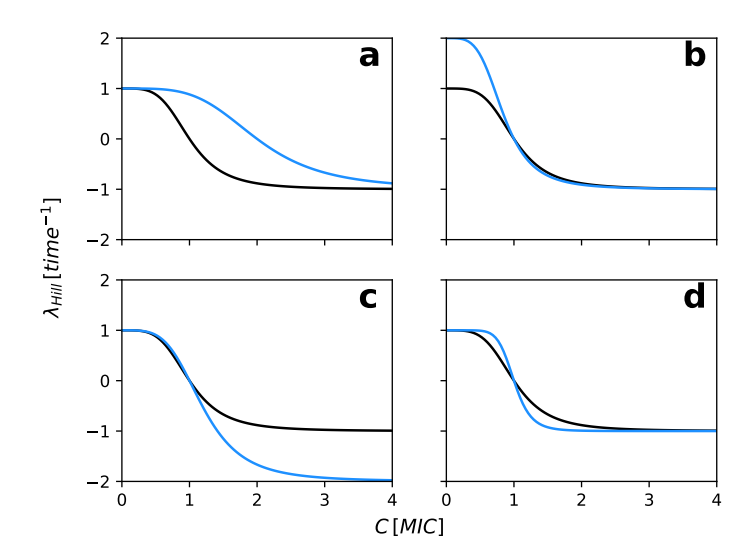


Figure 2: Visualization of the dose-response curve 5 and the influence of the four parameters. The black graph represents a reference strain with  $\lambda_{min} = \lambda_{max} = 1 \text{ time}^{-1}$ , MIC = 1 a.u. and  $\nu = 4$ .

Relative to the reference, the blue graph represents a different strain with doubled: (a) MIC,  $(b)\lambda_{max}$ , (c)  $\lambda_{min}$  and (d)  $\nu$ .

response curve:

$$\lambda(c(t)) = \lambda_{max} - k \frac{c(t)^{\nu}}{K_m^{\nu} + c(t)^{\nu}}.$$
(4)

However, for meaningful comparison with experiments and accurate modeling, it is preferable to define the dose-response curve using the previously established MIC and the maximum rate of cell death under treatment ( $\lambda_{\min}$ ) [20], [50] (see Appendix [A.1] for derivation):

$$\lambda_{\text{Hill}}(c(t)) = \lambda_{max} - (\lambda_{max} + \lambda_{min}) \frac{\left(\frac{c(t)}{MIC}\right)^{\nu}}{\left(\frac{c(t)}{MIC}\right)^{\nu} + \frac{\lambda_{\min}}{\lambda_{\max}}}.$$
 (5)

This 'Hill-Type' dose-response curve and the effect of the four parameters is further explored in figure 2.

Equation (5) provides a convenient parametrization of the DRC, allowing for independent adjustment of the null fitness, i.e. the growth rate in the absence of antibiotic stress, and maximum death rate ( $\lambda_{\text{max}}$ ,  $\lambda_{\text{min}}$ ) and the MIC appearing as a variable in the equation.

Furthermore, the DRC converges to the apparent null fitness  $\lambda_{\text{max}}$  of the bacteria for  $c \to 0$  and the maximum killing rate  $-\lambda_{\text{min}}$  for  $c \to \infty$ .

It is important to note, that  $\lambda_{\min}$  in equation (5) is positive by convention. This makes  $\lambda_{\max}$  and  $\lambda_{\min}$  both positive rates and negative signs are model intrinsic.

### 2.3 Quantifying the Treatment Efficacy - Effective Fitness

The dose-response curve (5) quantifies the concentration dependent reaction of a bacterial genotype to a particular antibiotic (pharmacodynamics). With this, we can now solve the differential equation (3) and discuss how the amount of viable cells changes over time. The general solution is given by

$$N(t) = N_0 \exp\left(\int_{t_0}^t \lambda(c(t'))dt'\right) \tag{6}$$

with  $\lambda(c)$  defined in (5).

Typically, clinical drug administration is considered to be periodic in time [44] [45], 21] and the effective change of the population size after one dosing period should be determined. It is therefore meaningful, to introduce the 'effective fitness'

$$\Lambda(\tau) = \frac{1}{\tau} \int_{t_0}^{t_0 + \tau} \lambda(c(t')) dt'$$
 (7)

as a functional of the dose-response curve and the concentration profile, as well as the period length  $\tau$ .

Using this definition, the effective change in viable cells after one drug dosing is given by:

$$N(\tau) = N_0 \exp(\Lambda \tau)$$
.

In this sense,  $\Lambda(\tau)$  describes an effective growth/death rate of the bacterial population after one drug cycle.

This reveals a first theoretical insight on the problem: The treatment efficacy of a certain drug on a given bacterial strain can be quantified by the effective fitness (7) which generally depends on the time between two drug administrations  $\tau$ , the concentration profile c(t) and the shape of the DRC.

Essentially, the bacterial population grows, if  $\Lambda(\tau) > 0$  and it dies, if  $\Lambda(\tau) < 0$ . Otherwise, the size of the population remains constant over time.

In this sense, the effective fitness provides a good measure of the treatment efficacy. Nevertheless, it can be important to compute the time resolved population size, as N(t) is generally non monotonic (see Figure 3) and the population might be extinct before the end of the treatment period. However, this is a stochastic effect, and for now, we will focus on finding a deterministic measure of the cell count after one period.

In the following analysis it is therefore considered, that  $0 < t \le \tau$ . Using the definition of the effective fitness (7), the general solution (6) can be expressed as

$$N(t) = N_0 \exp\left(\Lambda(t) \ t\right). \tag{8}$$

Thus, the main goal remains to solve the integral of the dose-response curve for a given time profile of the antibiotic concentration.

A whole field of research in clinical pharmacology is dedicated to the analysis of meaningful PKPD functions and dosing optimization [51], [52], which is not explored in detail here. For the purpose of this discussion, it is sufficient to note, that multiple studies [44], [45], [21] propose a double exponential function with a decay rate  $\alpha$  and take up rate  $\beta$  of the form

$$c(t) = c_{\text{max}} \left( e^{-\alpha (t - t_0)} - e^{-\beta (t - t_0)} \right). \tag{9}$$

Unfortunately, the integral in (8) can not be solved analytically for the DRC (5), given the general concentration profile (9). We present some numerical results for such general profiles in Appendix (7.1) but let us examine a simpler profile here. We consider very large  $\beta$  now, which corresponds to an immediate availability of the drug at the infection site. For such a scenario, the pharmacokinetic function for one dose of the drug reduces to

$$c(t) = c_{\text{max}} e^{-\alpha (t - t_0)} \tag{10}$$

and the time integral of (5) can be solved analytically. Such a profile is commonly assumed in models of time dependent treatment [53], 54

For  $\alpha, \nu \neq 0$  and  $0 < t \leq \tau$  one obtains:

$$\tilde{\Lambda}_{\text{Hill}}(t) = \int_{t_0}^{t_0+t} \lambda_{\text{Hill}}(c(t'))dt'$$
(11)

$$\tilde{\Lambda}_{\text{Hill}}(t) = \lambda_{\text{max}} t + \frac{\lambda_{\text{max}} (1 + \phi)}{\alpha \nu} \ln \left( \frac{C^{\nu} e^{-\alpha \nu t} + \phi}{C^{\nu} + \phi} \right)$$
(12)

where  $C = \frac{c_{\text{max}}}{MIC}$  and  $\phi = \frac{\lambda_{\text{min}}}{\lambda_{\text{max}}}$  (detailed derivation in the Appendix A.2). Finally, the exponential of (12) represents the relative change in viable cells over one period of drug dosing:

$$\frac{N(t)}{N_0} = e^{\tilde{\Lambda}_{\text{Hill}}(t)}.$$
(13)

The setup is visualized in figure 3 where the antibiotic concentration and the relative change of viable cells of two bacterial strains are shown for 3 drug administrations.

The two bacterial strains analyzed can be viewed as a susceptible wild type and a tolerant strain, as the MIC remains the same, but the mutant exhibits better survival under transient drug exposure.

It is important to note, that unlike the previously defined effective fitness  $\Lambda$ ,  $\tilde{\Lambda}$  is not an effective growth or death rate. It is just the solution of the integral.

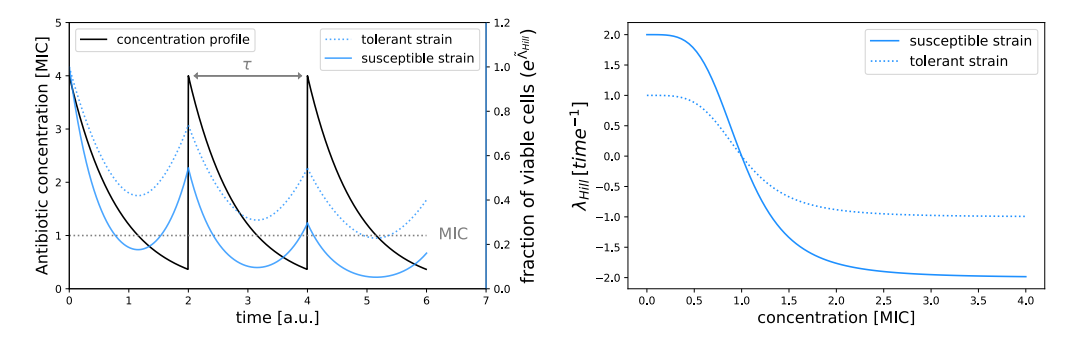


Figure 3: Solution of equation (13) for three periodic drug administrations with period length  $\tau=2$  t.u.. For a simple exponential concentration profile  $(c_{\text{max}}=4, \alpha=1.2\,\text{time}^{-1})$ , the relative change of viable cells of two bacterial strains is visualized over time (left). Both strains share the same MIC=1 a.u.,  $\nu=4$  and  $\phi=1$ , but the tolerant mutant (dashed lines) has only half the growth rate of the susceptible strain (solid lines):  $\lambda_{\text{max}}^{(\text{sus})}=2\,\lambda_{\text{max}}^{(\text{tol})}$ . The respective dose-response curves of both bacterial strains are shown on the right.

However, both quantities are related:

$$\Lambda(t) = \frac{1}{t}\tilde{\Lambda}(t)$$

which yields the same expression as (7), if  $t = \tau$ .

Given the result in (12), the effective fitness of this setup is given by

$$\Lambda_{\text{Hill}}(\tau) = \lambda_{\text{max}} + \frac{1}{\tau} \frac{\lambda_{\text{max}} (1 + \phi)}{\alpha \nu} \ln \left( \frac{C^{\nu} e^{-\alpha \nu \tau} + \phi}{C^{\nu} + \phi} \right)$$
(14)

and has the dimension  $\left[\frac{1}{\text{time}}\right]$ , as desired.

This quantity is further explored in the following section.

# 2.4 A First Interpretation of the Effective Fitness

The effective fitness in (14) represents a key result of the analysis for the presented scenario. Nevertheless, some crucial questions are yet undiscussed. How is a resistance or tolerance mutation represented in this formula? How can a population switch from negative to positive  $\Lambda$ ? How does the pharmacokinetic function influence the result?

It is therefore desirable, to develop some understanding and intuition for this quantity and gain some insight on the effective fitness.

We start by recalling the previous result in a slightly different form:

$$\Lambda_{\text{Hill}}(\tau) = \lambda_{\text{max}} \left[ 1 + \frac{(1+\phi)}{\nu \alpha \tau} \ln \left( \frac{C^{\nu} e^{-\nu \alpha \tau} + \phi}{C^{\nu} + \phi} \right) \right]. \tag{15}$$

<sup>&</sup>lt;sup>1</sup>At the time of completing this work, I became aware that Helen Alexander had independently derived a similar result in Chapter 3 of her PhD thesis [54]. This work is yet unpublished and I arrived at this result prior to knowledge of her contribution.

Provided that the ration of  $\lambda_{\min}$  and  $\lambda_{\max}$  ( $\phi$ ) remains constant, the 'null fitness' ( $\lambda_{\max}$ ) does not shape the qualitative behavior of the effective fitness. It rather determines the scale of the response, i.e. for large/small  $\lambda_{\max}$ , the population grows (and dies) more rapidly/slowly. But importantly, the sign of the effective fitness does not change, since  $\lambda_{\max} > 0$  by definition.

The sign of  $\Lambda_{\text{Hill}}$  is essentially determined by the second term in (15), that depends on the dimensionless quantities:  $\alpha \tau$ ,  $\nu$ ,  $\phi = \frac{\lambda_{\min}}{\lambda_{\max}}$  and  $C = \frac{c_{\max}}{MIC}$ .

#### 2.4.1 The Pharmacokinetic Parameter $\alpha \tau$

We will begin by focusing on the pharmacokinetic parameter  $\tilde{\alpha} = \alpha \tau$ , as the model's response is very illustrative in this case. Every other parameter is treated as a finite constant for now.

In the picture of a periodic antibiotic treatment the parameter  $\tilde{\alpha}$  relates the rate of drug degradation to the timescale of the treatment period. More explicitly, if  $\tilde{\alpha} \gg 1$  then the decay rate  $\alpha$  is large compared to the time between two drug administrations. Hence, the drug concentration reaches sub MIC conditions well before the next dosing and it is expected, that the effective fitness converges to the null fitness for  $\tilde{\alpha} \to \infty$ .

We can readily prove the expected result analytically:

$$\lim_{\tilde{\alpha} \to \infty} \left( \overline{15} \right) = \lambda_{\max} \left[ 1 + \underbrace{\lim_{\tilde{\alpha} \to \infty} \frac{(1+\phi)}{\nu \, \tilde{\alpha}} \, \ln\left(\frac{C^{\nu} e^{-\nu \, \tilde{\alpha}} + \phi}{C^{\nu} + \phi}\right)}_{=0} \right]$$
(16)

Vice versa, the limit of  $\tilde{\alpha} \to 0$  models the case of very slow drug degradation. The pharmacokinetic function is almost all the time close or equal to the maximum concentration  $c_{\text{max}}$ .

If this concentration is significantly higher than the MIC, it is expected, that the effective fitness is close to the maximum death rate  $(-\lambda_{\min})$ . Otherwise, if the drug concentration is initially already below the MIC, the effective fitness should be positive and converge to  $\lambda_{\max}$  in the limit of  $c_{\max} \ll MIC$ .

We can also check our expectations here and compute:

$$\lim_{\tilde{\alpha} \to 0} \left( \boxed{15} \right) = \lambda_{\max} \left[ 1 + \lim_{\tilde{\alpha} \to 0} \frac{(1+\phi)}{\nu \, \tilde{\alpha}} \, \ln \left( \frac{C^{\nu} e^{-\nu \, \tilde{\alpha}} + \phi}{C^{\nu} + \phi} \right) \right] \tag{17}$$

$$= -\lambda_{\min} \frac{C^{\nu} - 1}{C^{\nu} + \phi} \tag{18}$$

$$= \lambda_{\text{Hill}}(c_{\text{max}}). \tag{19}$$

The computation of (18) is not trivial and a detailed derivation can be found in the appendix A.3.1.

Recalling, that  $C = \frac{c_{\text{max}}}{MIC}$  and  $\phi = \frac{\lambda_{\text{min}}}{\lambda_{\text{max}}}$ , three interesting cases can be found:

$$\lim_{\tilde{\alpha} \to 0} \Lambda_{\text{Hill}} \begin{cases} \to \lambda_{\text{max}} & \text{if } c_{\text{max}} \ll MIC \\ = 0 & \text{if } c_{\text{max}} = MIC \\ \to -\lambda_{\text{min}} & \text{if } c_{\text{max}} \gg MIC \end{cases}$$
 (20)

which reflects our expected results.

Clinically, the case of high initial concentrations is particularly interesting, since the bacteria are not killed otherwise.

In this scenario, the effective fitness is negative for some small  $\tilde{\alpha}$  and positive, i.e. equal to  $\lambda_{\max}$ , for  $\tilde{\alpha} \to \infty$ . Since the effective fitness is continuous for  $\tilde{\alpha} \in (0, \infty)$ , there is a point where the effective fitness as a function of the pharmacokinetic parameter  $\tilde{\alpha}$  switches its sign.

It is hard to analytically prove the uniqueness and the exact point of such a transition, but it is enough to notice the existence here.

From a pharmacological perspective it is desirable to further analyze the influence of the pharmacokinetic function and to optimize clinical dosing for effective treatment. However, the focus of this study is the bacterial response, particularly antibiotic tolerance, to a specific dosing protocol. Therefore, the following sections examine the survival strategies of a homogeneous population, i.e. how the shape of the dose-response curve influences the effective fitness.

#### 2.4.2 The Hill Parameter $\nu$ - a Short Intermezzo on the Step DRC

For the analysis of very large Hill exponents it is illustrative, to examine the influence of  $\nu$  on the dose-response curve (5) first. It is readily observed, that

$$\lim_{\nu \to \infty} (5) = \lambda_{\text{step}} = \begin{cases} \lambda_{\text{max}} & \text{for } c(t) < MIC \\ -\lambda_{\text{min}} & \text{for } c(t) > MIC \end{cases}$$
 (21)

which is a step function (see figure 4).

Given this step profile, an effective fitness can be computed in full analogy to the discussion above, which is shown in the Appendix A.4. The result is a function of the three untouched parameters:

$$\Lambda_{\text{step}} = \begin{cases}
\lambda_{\text{max}} \left( 1 - \frac{1+\phi}{\tilde{\alpha}} \ln \left( C \right) \right) & \text{for } \tilde{\alpha} \ge \ln(C) \\
-\lambda_{\text{min}} & \text{for } \tilde{\alpha} < \ln(C)
\end{cases}$$
(22)

where the condition " $\tilde{\alpha} \geq \ln(C)$ " indicates that the initial antibiotic concentration falls to the MIC level within the timescale of a single period. Note, that C > 1 is always assumed here, since trivial results are obtained in the opposite case. For consistency, one can prove (see appendix A.3.2) that

$$\lim_{\nu \to \infty} \langle \overline{15} \rangle = \Lambda_{\text{step}}. \tag{23}$$

The discussed dose-response curve (21) has already been used for community studies [55], [56] and can be highly useful to test results of the Hill model.

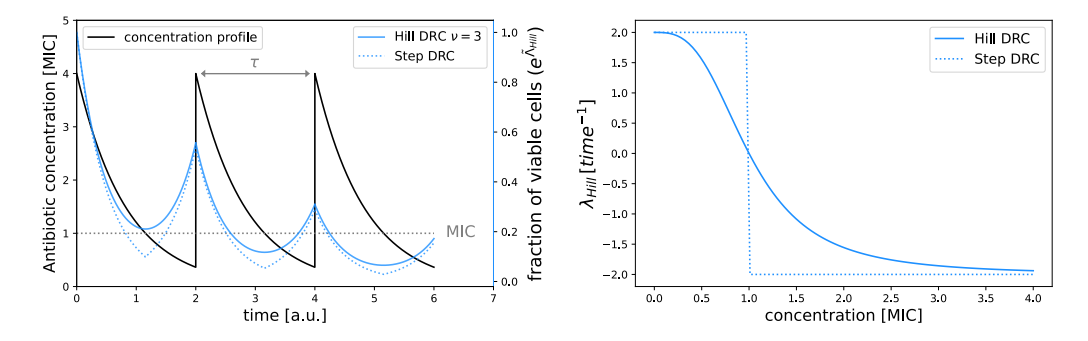


**Figure 4:** Analytic solution of the Hill-Type dose-response curve (solid blue) together with the Step Function (dashed blue) for a given concentration profile (black) around the MIC (grey). The Hill type DRC resembles the susceptible strain from figure 3 and the step function is the respective limit for  $\nu \to \infty$ .

#### 2.4.3 The Resistance Parameter C

The Resistance parameter was introduced as a dimensionless quantity  $C = \frac{c_{\text{max}}}{MIC}$  that relates the maximum antibiotic dosage to the MIC of the microbe. It is expected, that the effective fitness of a highly susceptible phenotype, i.e.  $MIC \ll c_{\text{max}}$  or  $C \gg 1$ , is lower than a resistant species with  $C \to 1$ . This can be seen if we recall our fitness function (15) and compute the respective limit:

$$\lim_{C \to \infty} \left( \overline{15} \right) = \lambda_{\max} \left[ 1 + \lim_{C \to \infty} \frac{(1+\phi)}{\nu \,\tilde{\alpha}} \, \ln \left( \frac{C^{\nu} e^{-\nu \,\tilde{\alpha}} + \phi}{C^{\nu} + \phi} \right) \right] \tag{24}$$

$$= -\lambda_{\min}. \tag{25}$$

Appendix A.1 visualizes the convergent behavior for different choices of parameters and verifies our analytic computation. Furthermore, we note, that the effective fitness is monotonically decreasing in the resistance parameter, as expected. For the case where  $C \to 1$ , it is enough to note that the dose-response curve will only be integrated over its positive (growth) region. Therefore, the effective

fitness can be nothing but positive. Because (15) is a continuous function of C, the intermediate value theorem implies that there must exist a point  $C_{\text{crit}}$  where the effective fitness becomes zero.

#### 2.4.4 On the Ratio of $\lambda_{\min}$ and $\lambda_{\max}$

In the derivation of (15) the ratio  $\phi = \frac{\lambda_{\min}}{\lambda_{\max}}$  was introduced as a dimensionless parameter. This expression is analytically correct and provides a useful parametrization of the effective fitness from a theoretical point of view. However, it suggests that the maximum death rate  $\lambda_{\min}$  is not an independent parameter and cannot be changed without changing the null fitness  $\lambda_{\max}$ . This is not generally true and it is important to keep the parametrization with both rates  $\lambda_{\min}$  and  $\lambda_{\max}$  in mind.

Therefore, we start by computing the effective fitness (15) for various tuples  $(\lambda_{\min}, \lambda_{\max})$ . The result is a two dimensional fitness landscape presented in figure

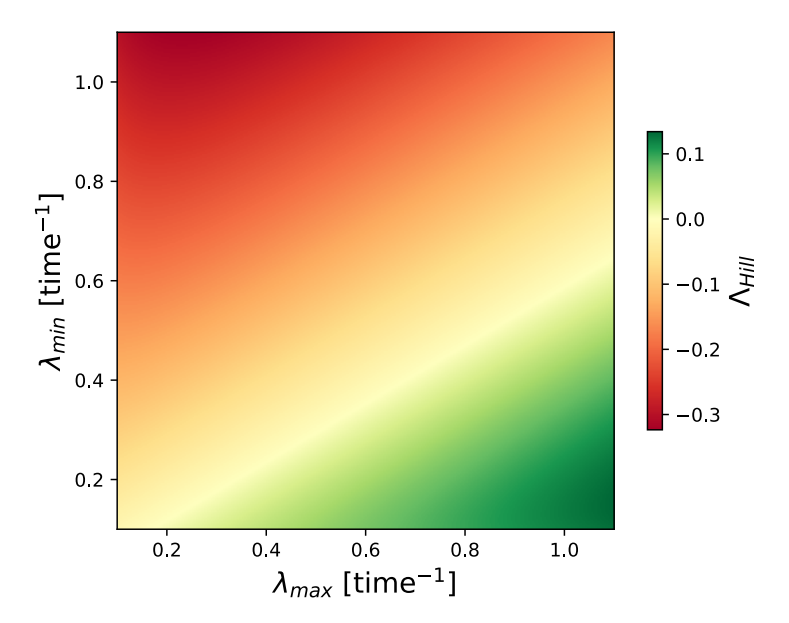


Figure 5: The Effective Fitness in a two dimensional landscape of null fitness ( $\lambda_{\rm max}$ ) and maximum death rate ( $\lambda_{\rm min}$ ).  $\Lambda_{\rm Hill}$  is computed for an exponential concentration protocol with  $\tilde{\alpha}=2.4$  and  $c_{\rm max}=4\,MIC$  and with a Hill parameter  $\nu=4$ .

As expected, the effective fitness decreases for increasing  $\lambda_{\min}$  or decreasing  $\lambda_{\max}$  and increases in the opposite case. The transition from negative (red area) to positive (green area) fitness is visualized in light yellow.

The topography of this landscape is characterized by the choice of the previously discussed parameters  $(C, \tilde{\alpha} \text{ and } \nu)$  and a general  $\lambda_{\min}$ - $\lambda_{\max}$  phenotype can

be anywhere in this landscape.

However, Tuomanen et al. [57] observed a strict proportional relationship between growth and death rates in *Escherichia coli* under  $\beta$ -lactam treatment. This relationship was also reported by Lee et al. [40] and is repeatedly assumed in studies on bacterial death [58, 56, 39, 59]. It is therefore meaningful to consider  $\lambda_{\min}$  to be an affine function of  $\lambda_{\max}$ :

$$\lambda_{\min} = \kappa \lambda_{\max} + a. \tag{26}$$

Note, that

$$\phi = \frac{\lambda_{\min}}{\lambda_{\max}} = \kappa + \frac{a}{\lambda_{\max}}$$

and therefore  $\phi \neq \kappa$  in general.

The functional dependency can be visualized in the previously introduced landscape (see Figure 6) and we can study the effective fitness as a function of  $\kappa$  and a now. Note that  $\kappa$  and a are restricted to a regime, where  $\frac{\lambda_{\min}}{\lambda_{\max}}$  is positive. For simplicity, we first consider the a special case where, a = 0.

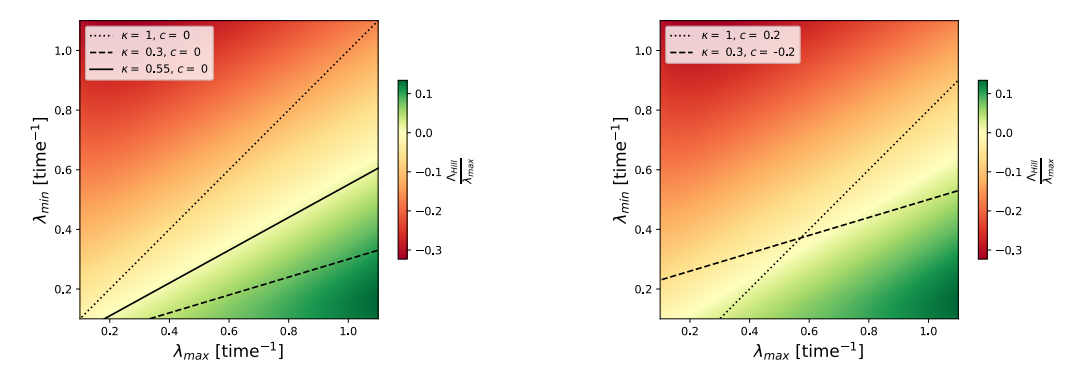


Figure 6: Visualization of some exemplary affine functions  $\lambda_{\min}(\lambda_{\max})$  in the Fitness Landscape from figure 5.

The left plot visualizes a setup where a=0, corresponding to a linear dependency. Essentially, the barrier of  $\Lambda=0$  is not crossed by any line of constant  $\phi$ . Thus, phenotypes that do not change the relation of  $\lambda_{\min}$  and  $\lambda_{\max}$  cannot switch from negative to positive fitness in this case.

The right plot visualizes a scenario, where  $a \neq 0$  and thus the fraction  $\phi$  is not a constant anymore. In such a scenario, a phenotype with constant  $\kappa$  and c can switch from positive to negative fitness by tuning its maximum death rate  $\lambda_{\min}$ .

If a = 0,  $\lambda_{\min}(\lambda_{\max})$  is a linear function and thus  $\phi = \kappa$ . In this case, the effective fitness (15) can be written in the form

$$\frac{\Lambda_{\text{Hill}}}{\lambda_{\text{max}}}(\kappa) = 1 + \frac{(1+\kappa)}{\nu \,\tilde{\alpha}} \, \ln\left(\frac{C^{\nu} e^{-\nu \,\tilde{\alpha}} + \kappa}{C^{\nu} + \kappa}\right) \tag{27}$$

where everything else than  $\kappa$  is kept constant. Accordingly,  $\frac{\Lambda_{\text{Hill}}}{\lambda_{\text{max}}}$  - which is termed as normalized effective fitness in the following - is invariant along the lines of constant  $\kappa$ .

Moreover, if a point where  $\Lambda_{\text{Hill}} = 0$  exists for a certain choice of  $C, \nu, \lambda_{\min}, \lambda_{\max}$  and  $\tilde{\alpha} = \alpha \tau$ , then there also exist infinitely many other points. Such a line is associated to a family of dose-response curves, which essentially yield the same normalized effective fitness  $\frac{\Lambda_{\text{Hill}}}{\lambda_{\max}}$  (see figure 7).

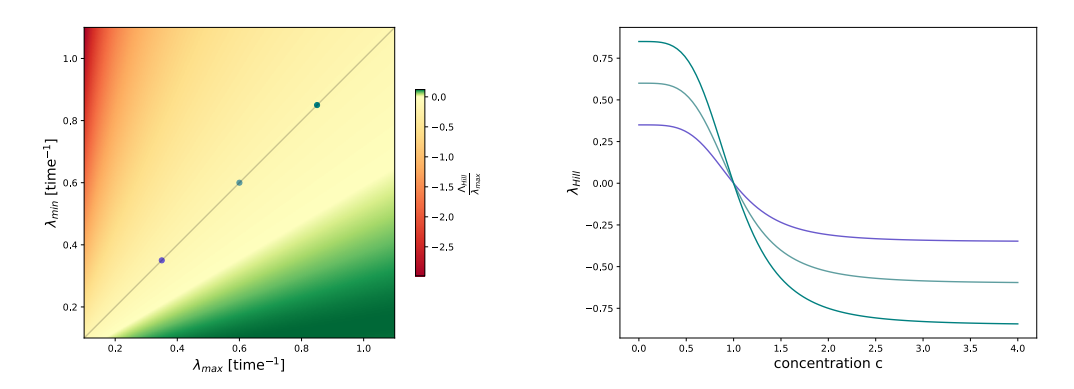


Figure 7: Left: Two dimensional  $(\lambda_{\max}, \lambda_{\min})$ -Landscape of the normalized effective fitness. The other parameters are taken from figure [5] ( $c_{\max} = 4 \,\mathrm{MIC}, \,\tilde{\alpha} = 2.4, \,\nu = 4$ ). Linear functions  $\lambda_{\min}(\lambda_{\max}) = \kappa \,\lambda_{\max}$  are surfaces of constant normalized fitness and are associated to a family of Dose-Response curves (right plot). The grey line exemplarily shows this for  $\kappa = 1$ , where three dots represent three different dose-response curves.

*Right:* The three exemplary dose-response curves for the " $\kappa = 1$  - family". All dose-response curves have the same normalized effective fitness  $\frac{\Lambda_{\rm Hill}}{\lambda_{\rm max}}$ .

This motivates to visualize (27) as a function of  $\kappa$  (see figure 8) and to find the root of this function (if it exists).

First, recall that  $\lambda_{\max}$  and  $\lambda_{\min}$  are positive and therefore  $\kappa \geq 0$ . For such  $\kappa$  and  $\tilde{\alpha}, \nu, C \neq 0$  the normalized effective fitness is everywhere continuous and differentiable.

Starting the analysis for small  $\kappa$ , i.e.  $\lambda_{\text{max}} \gg \lambda_{\text{min}}$ , one readily notes that  $\kappa = 0$  is a trivial solution for (27) = 0. One concludes, that if the first derivative of the normalized fitness at  $\kappa = 0$  satisfies

$$\left. \frac{\partial}{\partial \kappa} \frac{\Lambda_{\text{Hill}}}{\lambda_{\text{max}}} \left( \kappa \right) \right|_{\kappa = 0} = \frac{e^{\tilde{\alpha} \nu} - 1}{\tilde{\alpha} \nu C^{\nu}} - 1 > 0 \tag{28}$$

it follows, that

$$\frac{\Lambda_{\text{Hill}}}{\lambda_{\text{max}}}(\kappa) > 0 \quad \text{for some } \kappa > 0.$$
(29)

If this does not hold for a certain set of parameters, then the effective fitness would be negative everywhere (irrespective of  $\kappa$ ) and the antibiotic would kill the bacteria in any scenario. It is therefore reasonable to assume (28) for the purpose

of this work.

Now, if  $\kappa$  is large, i.e.  $\lambda_{\text{max}} \ll \lambda_{\text{min}}$ , the normalized effective fitness becomes

$$\lim_{\kappa \to \infty} (27) = 1 + \frac{C^{\nu}}{\tilde{\alpha} \nu} \left( e^{-\tilde{\alpha} \nu} - 1 \right)$$

(see Appendix A.5.1 for derivation).

Notably, if this limit is larger than zero, then the effective fitness is everywhere positive and there is no scenario, where the antibiotic kills the bacteria.

It is therefore reasonable, to assume

$$\lim_{\kappa \to \infty} \left( 27 \right) = 1 + \frac{C^{\nu}}{\tilde{\alpha} \nu} \left( e^{-\tilde{\alpha} \nu} - 1 \right) < 0 \tag{30}$$

here.

Equations (29) and (30), together with the Intermediate Value Theorem imply, that if condition (28) holds, then there exists a second point at which  $\frac{\Lambda_{\text{Hill}}}{\lambda_{\text{max}}}(\kappa) = 0$ . Rolle's theorem also implies the existence of a maximum point, where  $\frac{\partial}{\partial \kappa} \frac{\Lambda_{\text{Hill}}}{\lambda_{\text{max}}}(\kappa) = 0$ .

The appendix A.5.2 provides more profound calculations and it is argued, that the maximum is unique.

We can furthermore find, that for the discussed parameter range, defined by (82) and (28), we find the maximum point  $\phi_{\text{max}}$  in the interval (0, 1]. However, computing the exact point  $\phi_{\text{max}}$  where the effective fitness becomes maximal remains a task for numerical calculations.

At this point it is important to emphasize, that the appearance of the unique maximum is exclusive to the Hill shaped dose-response curves. Our parametrization [5] implies, that  $\lim_{\lambda_{\min}\to 0} \lambda(c) = 0$  for all concentrations if the other parameters ore finite. Thus, we find that

$$\lim_{\phi \to 0} \Lambda_{Hill} = 0.$$

However, this does not hold for other dose-response curves, especially not for the step function (see appendix C.1 for details).

This rather technical analysis of the fitness landscape is treated in figure 8. For three different choices of the system parameters  $C, \tilde{\alpha}, \nu$  the normalized effective fitness is visualized as a function of  $\kappa$ . One can see, that the fitness function is only positive, if (28) is fulfilled. And if it is positive, there exists a unique maximum and a second zero point.

In summary we have now shown, that the normalized effective fitness only

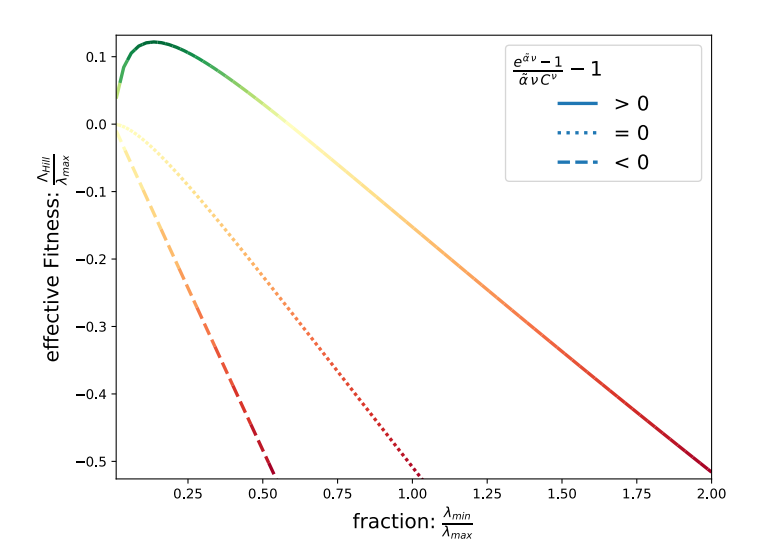


**Figure 8:** Effective fitness  $\Lambda_{\text{Hill}}$  divided by the null fitness  $\lambda_{\text{max}}$  as a function of  $\kappa$  in the color code of figure [7].

The solid line represents the scenario from above  $(c_{\text{max}} = 4 \,\text{MIC}, \, \tilde{\alpha} = 2.4, \, \nu = 4)$  which essentially fulfills (28). Both of the other scenarios do not satisfy (28) and therefore  $\forall \kappa : \frac{\Lambda_{\text{Hill}}}{\lambda_{\text{max}}}(\kappa) < 0$ .

depends on the ratio of null fitness and max. death rate. Furthermore for a given set of parameters  $(\tilde{\alpha}, \nu, C)$ , a unique maximum at some  $\kappa_{\text{max}}$  was found to exist under certain constraints. However, all the analysis only holds for the normalized effective fitness, while the quantity of interest remains the effective fitness.

It is therefore important to also consider the  $\lambda_{\max}$  factor for physical interpretations. It is readily observed that the extra factor will only affect the magnitude of the fitness function and introduces a linear gradient to the contours of constant  $\kappa$ . Accordingly, if  $\Lambda_{\text{Hill}}(\kappa)$  is negative for some (unchanged)  $\kappa$ , it will be beneficial to minimize  $\lambda_{\max}$  (dormant bacteria). Otherwise, phenotypes with positive effective fitness tend to maximize their  $\lambda_{\max}$ .

Most importantly we note, that mutations which do not alter the ratio  $\frac{\lambda_{\min}}{\lambda_{\max}}$  cannot change the sign of the effective fitness. This observation does not hold, if the constraint a=0 is relaxed.

If  $a \neq 0$ , the analysis from above has to be revisited. The most striking difference was already mentioned in figure  $\boxed{6}$ , where it was noted that the effective fitness can switch its sign also for constant  $\kappa$  and c.

One notes that an offset  $a \neq 0$  influences the maximum death rate independent of the null fitness. Accordingly the shape of the dose-response curve changes to some extent and the normalized effective fitness becomes:

$$\frac{\Lambda_{\text{Hill}}}{\lambda_{\text{max}}}(\kappa) = 1 + \frac{\left(1 + \kappa + \frac{a}{\lambda_{\text{max}}}\right)}{\nu \,\tilde{\alpha}} \, \ln\left(\frac{C^{\nu} e^{-\nu \,\tilde{\alpha}} + \kappa + \frac{a}{\lambda_{\text{max}}}}{C^{\nu} + \kappa + \frac{a}{\lambda_{\text{max}}}}\right). \tag{31}$$

Repeating the analysis for families of dose-response curves (see figure 7 for a = 0), one finds that the normalized effective fitness is not a constant for a given  $\kappa$ -a-family. Figure 9 visualizes this for three exemplary DRC's.

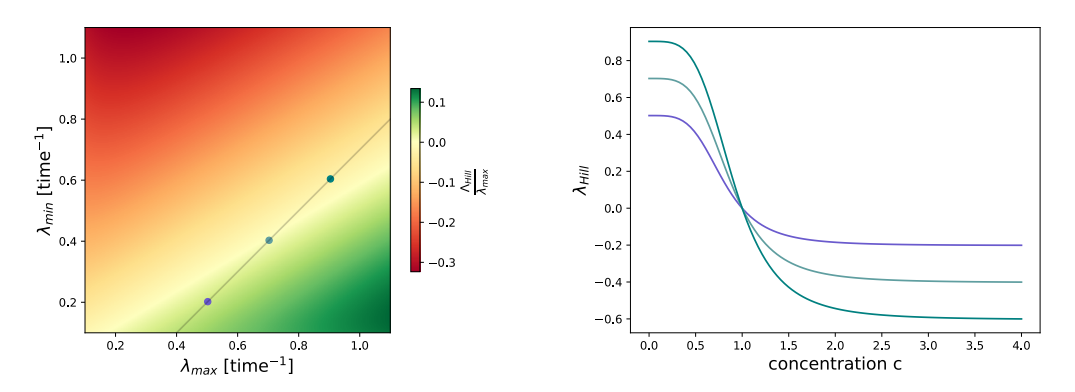


Figure 9: Left: Two dimensional ( $\lambda_{\max}$ ,  $\lambda_{\min}$ )-Landscape of the normalized effective fitness. The other parameters are taken from figure  $5 (c_{\max} = 4 \,\mathrm{MIC})$ ,  $\tilde{\alpha} = 2.4$ ,  $\nu = 4$ ). Linear functions  $\lambda_{\min}(\lambda_{\max}) = \kappa \lambda_{\max} + a$  are surfaces of constant normalized fitness and are associated to a family of Dose-Response curves (right plot). The grey line exemplarily shows this for  $\kappa = 1$  and c = -0.3, where three dots represent three different dose-response curves. Right: Three exemplary dose-response curves for the " $\kappa = 1$ ,  $\kappa = -0.3$  - family". All Dose

*Right:* Three exemplary dose-response curves for the " $\kappa = 1$ , a = -0.3 - family". All Dose response curves have now a different normalized effective fitness.

The biological context of a  $\lambda_{\min}$ - $\lambda_{\max}$  relation has been reviewed in previous studies [39, 56, 57] and we will address this in the next section. These studies suggest that  $\lambda_{\min}$  and  $\lambda_{\max}$  are correlated ( $\kappa > 0$ ) also for  $a \neq 0$  [39, 56], which implies a trade-off behavior, i.e. decreasing the growth rate also decreases the death rate. Typically such a trade-off is associated with antibiotic tolerance [39, 60, 61, 62], which was found to emerge under periodic antibiotic stress [63, 37]. With the effective fitness  $\Lambda_{\text{Hill}}$  we have now introduced a framework to understand, how such a trade-off can be beneficial and that there exists an optimal ratio  $\frac{\lambda_{\min}}{\lambda_{\max}}$  for a given set of parameters.

In the following, we stick to the finding that a reduction in the death rate comes with a cost in the null fitness, but return to the effective fitness as a function of a two dimensional phenotype ( $\lambda_{\min}$  and  $\lambda_{\max}$ ). Hence, we consider mutations which can in principle change both  $\lambda_{\min}$  and  $\lambda_{\max}$  independently under the constraint of a trade-off.

This will be further reviewed in a genotypic model (section 3), which has been used for similar applications before 29.

# 2.5 Biological Context of the $\lambda_{\min}$ - $\lambda_{\max}$ Relation

The previous section outlined all relevant parameters of the effective fitness, highlighting that any measure of antibiotic tolerance is crucially determined by the relation of  $\lambda_{\min}$  and  $\lambda_{\max}$  [39, [60, [61], [62]]. Here, we want to briefly discuss the

# 2 CHARACTERIZING THE BACTERIAL RESPONSE TO ANTIBIOTIC TREATMENT

biological context of  $\lambda_{\min}$  and  $\lambda_{\max}$  and why it is meaningful to consider a relation between both parameters.

In accordance with the definition of Brauner et al. [7], antibiotic tolerance is

the ability [...] of microorganisms to survive transient exposure to high concentrations of an antibiotic without a change in the MIC.

This is a rather general definition and can be caused by several mechanisms such as cell aggregation [64, 65], increased lag time [7] or slow growth [7, 56]. However, since our model assumes that the population is always in an exponential phase (growth or death), we do not account for any lag effects. Furthermore, we do not resolve any spatial effects and we will therefore stick to 'tolerance by slow growth' [7] here.

In the example of  $\beta$ -lactam treatment, targeting the process of bacterial cell wall synthesis during cell division [66], the treatment efficacy crucially depends on the growth rate. Hence, the rate of killing is proportional to the rate of cell division [57]. Hence, growth inhibiting conditions are known to increase tolerance to antibiotics [57], [25].

In general, such growth inhibition can be an inherited genotypic change, reducing the natural growth rate, or a phenotypic response to some environmental changes. Bren et al. [39] explained a phenotypic response with a resource allocation model, in which the growth rate  $\lambda_{\text{max}}$  can be manipulated by varying the amount of supplied nutrients. For different growth media, they where able to show that the death rate  $\lambda_{\text{min}}$  can be described as a linear function of the growth rate (as in [26]), where the parameters  $\kappa$  and a depend on the choice of carbon source.

In this sense, the decrease in death rate, and thus the adaptation to antibiotic stress, can be fully understood as a rapidly (depending on the lag time) changing phenotypic response.

In another study Mizrahi et al. [56] evolved a susceptible isolate and observed antibiotic tolerance in the evolved strains. Sequencing the whole genome of these strains revealed, that many of them accumulated similar mutations. These mutation where found to (1) be linked to  $\beta$ -lactam resistance and (2) impact cell growth [56]. Many of the observed mutations had simultaneous decreases in death and growth rates [56] and it is therefore biologically meaningful to consider a genotypic trade-off model. We refer to the trade-off in  $\lambda_{\min}$  and  $\lambda_{\max}$  as tolerance trade-off.

# 3 Tolerance Evolution in Trade-Off Induced Fitness Landscape

In the previous section the effective fitness  $\Lambda_{\text{Hill}}$  (14) was introduced as a fitness measure for bacterial populations under periodic antibiotic stress. We have seen that this is a function of some environmental parameters, essentially the maximum drug concentration and the period length, and the phenotype, which is the MIC,  $\lambda_{\min}$ ,  $\lambda_{\max}$  and  $\nu$ .

For the purpose of this analysis, we will focus on antibiotic tolerance, which is related to an enhanced survival at high antibiotic concentrations and a fitness cost at low concentrations [39, 60, 61, 62]. Whether inherited or not, such a trade-off adaptation is commonly observed in tolerant isolates (see section [2.5]). Hence, the two phenotypes  $\lambda_{\min}$  and  $\lambda_{\max}$  will be of particular interest and we will build upon the results of section [2.4.4].

The growth-death trade-off introduces an additional constraint on the optimization of  $\lambda_{\min}$  and  $\lambda_{\max}$ . Hence, the two phenotypes cannot be optimized independently and we will see that high fitness phenotypes usually have an optimal ratio  $\phi$ .

The phenomenon of trade-offs is certainly not universal to any drug response, but it has been observed in previous studies. Lazar et al. [38] noted that some strains are highly susceptible to single drugs but less if drugs are combined. Stiffler et al. [67] reported, that cefotaxime resistance emerged from ampicilin susceptible strains, but not from ampicilin resistant ones. This indicates that in a high ampicilin environment certain mutations are deleterious at low cefotaxime but beneficial at high cefotaxime. And Das et al. [29] observed, that enhanced resistance often reduces the null fitness of a bacterial strain.

For a theoretical description of such trade-offs, a new type of fitness landscapes have been proposed:  $Trade-off\ Induced\ Fitness\ Landscapes\ (TIL)$ . Conceptually, we will use a similar model as in [29] and construct fitness landscapes for  $\lambda_{\min}$ - $\lambda_{\max}$  phenotypes. We show, how biallelic genotypes map to phenotypes and how these relate to the complete two dimensional fitness landscape (figure [5]).

Moreover, we will discuss topological properties of the constructed trade-off landscape and see how such landscapes can model tolerance evolution.

# 3.1 Mapping Genotypes to Fitness

In analogy to previously published models [68], [29], we will use a biallelic genotype  $\sigma$  of length L, i.e. a genotype of L loci. Thus, each site  $\sigma_i$  can be either mutated  $(\sigma_i = 1)$  or unmutated  $(\sigma_i = 0)$ , which yields  $2^L$  possible genotypes. In this

framework, we will refer to the all zeros genotype  $\sigma = 0$  as the wild type and the full mutant as  $\sigma = 1$ .

Here, mutations only affect the null fitness  $\lambda_{\min}$  and the death rate  $\lambda_{\max}$ , while leaving the MIC and also the Hill exponent unchanged. These mutations are assumed to be non epistatic, such that they combine multiplicatively [68]:

$$\lambda_{\min}^{\sigma} = \exp\left[\sum_{i} \sigma_{i} \ln(\lambda_{\min}^{i})\right]$$
 (32)

$$\lambda_{\max}^{\sigma} = \exp\left[\sum_{i} \sigma_{i} \ln(\lambda_{\max}^{i})\right]. \tag{33}$$

Furthermore, each mutation comes with a trade-off, decreasing the death rate at high concentrations while also inhibiting growth at low concentrations, i.e.  $\lambda_{\min}^i < 1$  and  $\lambda_{\max}^i < 1$ . In general, all the  $\lambda_{\min}^i$  and  $\lambda_{\max}^i$  are drawn from a probability distribution, which remains to be specified. This establishes a definite mapping from any genotype to the respective ( $\lambda_{\min}$ - $\lambda_{\max}$ ) phenotype.

The fitness of each phenotype is determined by a second mapping, i.e. a fitness curve, which in general is a function of some environmental parameters and the phenotype-specific parameters. In the context of periodic antibiotic treatment, it is convenient to use the previously established effective fitness, which is a function of C and  $\tilde{\alpha}$  (environmental), as well as the two phenotype specific parameters  $\lambda_{\min}^{\sigma}$  and  $\lambda_{\max}^{\sigma}$ , as a fitness proxy:

$$\Lambda_{\text{Hill}}^{\sigma} = \lambda_{\text{max}}^{\sigma} + \frac{\lambda_{\text{max}}^{\sigma} \left(1 + \frac{\lambda_{\text{max}}^{\sigma}}{\lambda_{\text{min}}^{\sigma}}\right)}{\tilde{\alpha} \nu} \ln \left(\frac{C^{\nu} e^{-\tilde{\alpha} \nu} + \frac{\lambda_{\text{max}}^{\sigma}}{\lambda_{\text{min}}^{\sigma}}}{C^{\nu} + \frac{\lambda_{\text{max}}^{\sigma}}{\lambda_{\text{min}}^{\sigma}}}\right). \tag{34}$$

Eventually, (32) and (33) together with this function make a useful model to describe the growth-death trade-off in a genotypic framework.

# 3.2 Fitness Graphs and Fitness Landscapes

Given the definite mapping from genotype to fitness proxy, fitness graphs are helpful to understand the topology of the resulting landscape. A general fitness graph  $\mathcal{F}$  of a alleles and L loci is a directed Hamming graph  $\mathbb{H}_a^L$ , where neighboring genotypes (nodes) are connected through edges directed towards increasing fitness [69]. For the purpose of this work we chose a biallelic model (a = 2), which has been extensively used in previous studies [70], [71], [68], [29]. Our fitness graph therefore consists of  $N = 2^L$  Nodes and  $E = \frac{L}{2} 2^L$  Edges. Figure 10 displays some exemplary fitness graphs for L = 2 and L = 3.

These visualizations of the fitness function appear to be quite different from the previously discussed landscapes (figure 5), but they are, in fact, closely related.

Given the complete two dimensional fitness map of all possible ( $\lambda_{\min}$ - $\lambda_{\max}$ ) phenotypes, every genotype can be found as one point in this landscape (figure 11). In this sense, the genotype-phenotype map induces a discrete sub-landscape, where only certain phenotypes are realized by the model.

The structure of such a sub-landscape crucially depends on the mapping, i.e. the choice of  $\lambda_{\min}^i$  and  $\lambda_{\max}^i$ , and the number of loci L. The effect of both will be addressed in the next section (figure 3.3). At this stage, it is enough to observe that for a "good" mapping the full landscape represents the  $L \to \infty$  limit of the trade-off-induced sub-landscape.

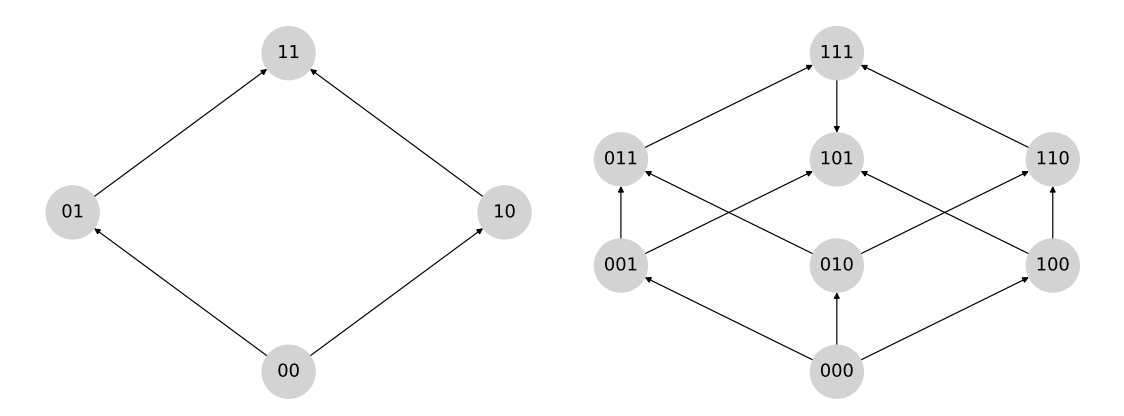


**Figure 10:** Fitness graphs for L=2 (left) and L=3 (right) loci. Each node is connected to its nearest neighbors by an edge that points in the direction of increasing effective fitness. The environmental parameters were chosen in accordance with the previous section:  $c_{\text{max}}=4\,\text{MIC}$ ,  $\tilde{\alpha}=2.4,\ \nu=4$ .

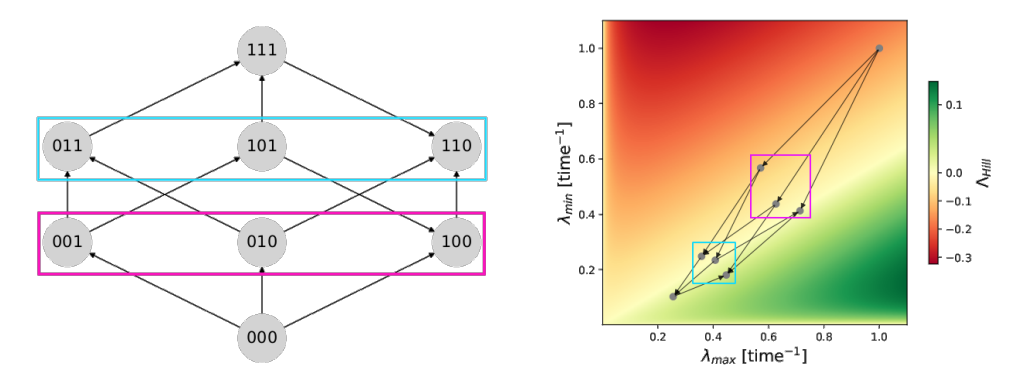


Figure 11: Fitness Graph with L=3 loci (left) and their corresponding location in the complete phenotypic landscape (right). The colored ellipses illustrate where genotypes of intermediate layers in the fitness graph are found in the complete landscape. For this visualization we sampled  $\lambda_{\min}^i$  and  $\lambda_{\max}^i$  from uniform intervals with  $\lambda_{\min}^i \in [0.3, 0.6)$  and  $\lambda_{\max}^i \in [0.5, 0.8)$ .

### 3.3 The Topography of Trade-Off Induced Landscapes

Previous studies on general fitness landscapes identified and discussed topological properties to a large extent [69, [71], [70]. In the context of antimicrobial resistance, this has been done also for trade-off induced landscapes, similar to our model [68, [29]]. Therefore, we will focus on the key features, i.e. ruggedness and peak accessibility, here.

In the following, it will be convenient to use a set notation of the genotypes, which represents each genotype by a set of mutated sites [69]. Thus, any genotype can be found as a subset of the full mutant  $\mathcal{L} = \{1, ..., L\}$ .

Accordingly, the wild type will be the empty set  $(\sigma = \emptyset)$  and  $\sigma = \{1, 3, 7\}$  has mutations on the first, third and seventh position.

Given this notation, it is convenient to define subsets and supersets of a genotype and an accessibility property.

For a general genotype  $\sigma$ , its subsets are elements of the power set  $\mathcal{P}(\sigma)$ , while the superset genotypes are found in  $\{X \cup \sigma | X \in \mathcal{P}(\bar{\sigma})\}$ , where  $\bar{\sigma} = \mathcal{L} \setminus \sigma$  is the complement of  $\sigma$ . Figure 12 visualizes both sets for two exemplary genotypes (nodes in grey circles).

In accordance with Das et al. [29] a fitness landscape has the subset-superset accessibility property, if

any peak genotype is accessible from all its subsets and supersets via all direct paths.

In the framework of *fitness graphs*, a peak genotype, i.e. a local fitness peak of the landscape, is a node with only incoming edges. If a landscape has multiple of such peak genotypes, it is called "rugged".

It has been observed [69] that trade-off induced fitness landscapes can be rugged but still highly accessible. Therefore, we will investigate both properties in the following.

#### 3.3.1 Gain Intuition on a Toy Model

A crucial finding of the analysis in chapter 2.4.4 was, that the normalized effective fitness has a maximum at  $0 < \frac{\lambda_{\min}}{\lambda_{\max}} < 1$  for a certain choice of the parameters. Hence, we can readily argue, that genotypes with  $\phi^{\sigma} = \frac{\lambda_{\min}^{\sigma}}{\lambda_{\max}^{\sigma}} < 1$  will always have higher fitness than the wild type  $(\phi_{\text{wt}} = 1)$  and we expect that peak genotypes will have  $\phi \approx \phi_{\max}$ .

However  $\phi_{\text{max}}$  only maximizes the normalized effective fitness and we will have not yet argued about the true effective fitness. This introduces another constraint on the optimization and global fitness peaks will additionally have relatively high

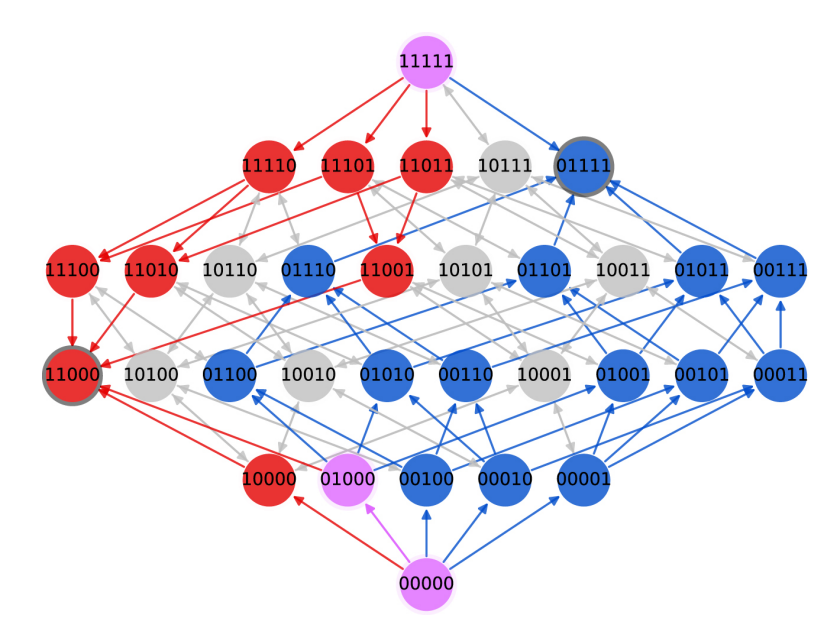


**Figure 12:** Visualization of the subset-superset accessibility property for a landscape of L=5 loci. The landscape has two fitness peaks (grey circles) and their respective complete sub- and superset is highlighted in red/blue. Purple genotypes are in the sub- or superset of both fitness peaks. The figure was published by Krug and Oros 69.

null fitness. Hence, genotypes with  $\phi^{\sigma} \approx \phi_{\text{max}}$  are good candidates to be found as peaks, but do not necessarily have to be peaks.

We can check our expectation in a first toy model, where every mutation contributes equally with  $\lambda_{\min}^i \equiv \beta$  and  $\lambda_{\max}^i \equiv \gamma$ . We will label the fraction of both parameters as  $\frac{\beta}{\gamma} \equiv \phi$ . Thus, the phenotype will just depend on the number of mutations  $n^{\sigma}$  in the respective genotype:

$$n^{\sigma} = \sum_{i} \sigma_{i}.$$

In this toy model, all genotypes with the same  $n^{\sigma}$ , i.e. genotypes in the same layer, will also have the same fitness. Therefore, we will always find a whole layer of peaks and the number of peaks will depend on the number of genotypes in the respective layer [72].

The simplest, non-trivial case is  $\beta \in (0, 1)$  and  $\gamma = 1$ , which is a reduction of death rate without a null fitness cost. With this, we have

$$\phi^{\sigma} = \beta^{n^{\sigma}} \quad \text{and} \quad \lambda_{\text{max}} = 1$$
 (35)

and we can immediately find the peak layer as

$$n_{\text{peak}} = \arg\max_{n^{\sigma}} \left[ \frac{\Lambda_{\text{Hill}}}{\lambda_{\text{max}}} \right]$$
 (36)

that is the number of mutations maximizing the normalized effective fitness. Importantly, we note that the landscape of our toy model can have multiple peaks if  $0 < n_{\text{peak}} < L$ .

Since all genotypes with the same number of mutations have the same  $\phi$  in the toy model, it will be convenient to introduce  $\phi^{(n^{\sigma})}$  here. Thus,  $\phi^{(0)}$  is the fraction for the wild type,  $\phi^{(n_{\text{peak}})}$  the one of the peak layer and  $\phi^{(L)}$  for the full mutant respectively. If we exclude neutral mutations, this quantity is well defined in the toy model, since (35) defines a bijective map between  $\phi^{\sigma}$  and  $n^{\sigma}$ . However, we will also use this quantity in the TIL model later (section 3.3.2), indicating the number of mutations that led to a certain  $\phi$ .

We note, that the construction of our toy model imposes a general order on  $\phi$ . Since  $\beta \in (0, 1)$  and  $\gamma = 1$ , every mutation reduces the fraction of null fitness and maximum death rate and we have

$$\phi^{(L)} < \dots < \phi^{(0)}. \tag{37}$$

Furthermore, we have argued in section 2.4.4 that the effective fitness as a function of  $\phi$  has a unique global maximum. Hence, we can find a certain fitness rank order 70 of the genotypes in the toy model. This property was termed ordering condition in previous studies and is derived in 29. Importantly, if the ordering condition holds for any two-face of the fitness graph, i.e. a subgraph consisting of a reference genotype and two single mutants and a double mutant of that reference strain, the subset-superset accessibility property holds 29. In appendix 8.1 we furthermore show, that the opposite argument, i.e. accessibility implies the ordering condition, also holds and therefore both properties are equivalent. Accordingly, the peak accessibility is guaranteed in the toy model, and we can conclude this for any fitness landscape that has the general ordering 37 in the following.

If we now also let  $\gamma \in (0, 1)$ , one has to distinguish three cases. If we have (1)  $\beta > \gamma$ , the fraction  $\phi$  would increase with every mutation and the effective fitness of any genotype will be smaller than the one of the wild type . Thus, there would not be any beneficial mutations. Therefore, the wild type will always be the unique peak in such a landscape. Otherwise, if (2)  $\gamma = \beta$ , every genotype has  $\phi = 1$ . In this case, it was already observed, that the effective fitness is essentially determined by the sign of the normalized effective fitness and the null fitness. Thus, if the normalized effective fitness is smaller than zero for  $\phi = 1$ , the genotype minimizing the null fitness, i.e. the full mutant, will have maximal fitness. Else, if the effective fitness is positive, the wild type will be the only peak genotype.

In the third case (3), where  $\beta < \gamma$ , each mutation decreases  $\phi$  and therefore we expect a single layer of peak genotypes as before. This layer will be called the peak layer or high fitness layer in the following and can in general have any number of mutations  $n^{\sigma}$ . The fitness of that layer is determined by the choice of  $\beta$  and  $\gamma$  (see figure 13).

Clinically, it is most relevant to consider bacteria that adapt to a certain antibiotic treatment and eventually become tolerant. In terms of fitness landscapes, the initial wild type is not yet adapted to the treatment and has negative effective fitness. But every mutation increases the fitness as the bacteria adapt to the drug, hence  $\beta \leq \gamma$ . Otherwise, non of the mutations would fixate due to selection and there is no evolution from the wild type.

Assuming now that  $\beta \leq \gamma$ , we have

$$\phi^{\sigma} = \left(\frac{\beta}{\gamma}\right)^{n^{\sigma}} < 1$$

for every genotype  $\sigma$ . This preserves the previously discussed order in  $\phi$  (equation (37)) and thus the accessibility property of the normalized effective fitness landscape also holds for  $\gamma \neq 1$ .

Figure 14 also illustrates, that the number of mutations in the peak genotypes crucially depends on the phenotypes, i.e.  $\beta$  and  $\gamma$ . For small  $\phi^{i}$ , every mutation changes the phenotype significantly and the fitness maximum is found within few evolutionary steps. In extreme cases  $(\phi^{i} \to 0)$  the model becomes unreasonable, since the DRC is zero everywhere, if either  $\lambda_{\min} \to 0$  or  $\lambda_{\max} \to \infty$ . This problem is kept in mind also for large  $n^{\sigma}$ , which can be particularly relevant if L becomes large.

Furthermore, it is observed again that  $\gamma$  has a trivial multiplicative effect on the effective fitness, if  $\phi^{i}$  is kept constant and does not change the effective fitness qualitatively (figure 14 right plot).

Summarizing the toy model, we find that such a landscape can have multiple peaks and thus can be rugged. Moreover, also the accessibility property holds, if the parameters are restricted to  $\frac{\beta}{\gamma} < 1$ . In the following we will randomly sample the phenotypes  $\lambda_{\min}$  and  $\lambda_{\max}$  and examine how the result deviates from the toy model.

#### 3.3.2 Ruggedness and Accessibility for Stochastic Landscapes

Building on the deterministic toy model, we now aim to examine the structure of a landscape in which phenotypes are drawn from a probability distribution. For

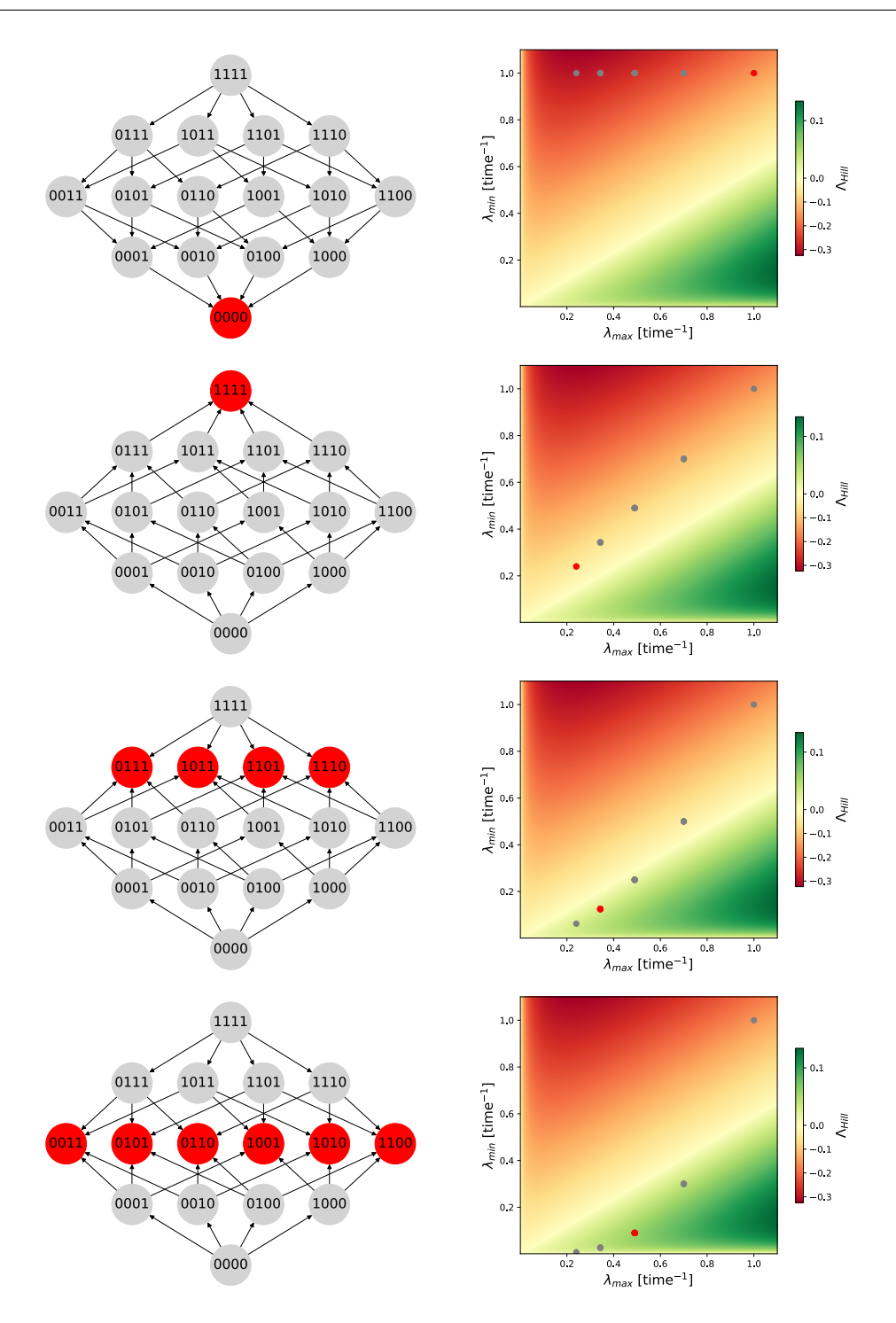


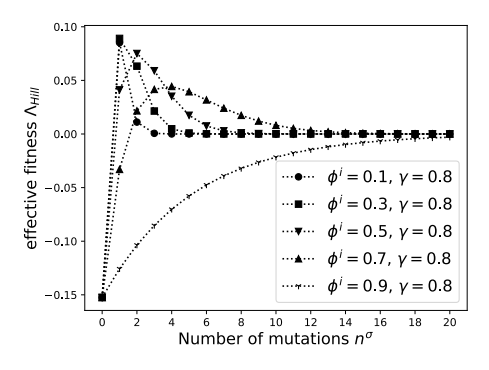
Figure 13: Four different realizations of Toy Model fitness landscapes. The respective fitness graph is shown on the left, while the location in the fitness landscape is shown on the right. (1): We have  $\beta = 1$  and  $\gamma = 0.7$ , hence  $\beta > \gamma$ . Therefore the wild type is the only fitness peak. (2): We have  $\beta = 0.7$  and  $\gamma = 0.7$ , hence  $\beta = \gamma$ . Therefore the full mutant is the only fitness peak

(3/4) We have  $\beta = 0.5/0.3$  and  $\gamma = 0.7$ , hence  $\beta < \gamma$ . We find that this yields intermediate peak layers in the fitness graph.

simplicity, we sample  $\lambda^i_{\min}$  and  $\lambda^i_{\max}$  from uniform intervals

$$\lambda_{\min}^i \in [a, b)$$

$$\lambda_{\max}^i \in [c, d)$$



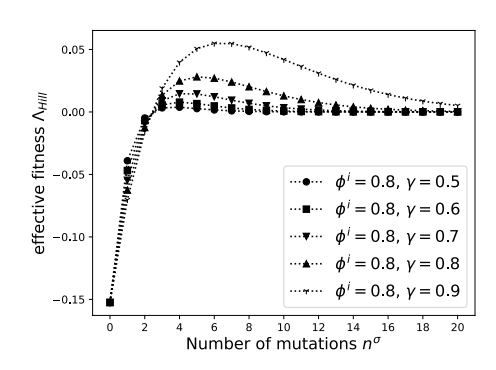


**Figure 14:** Effective fitness  $\Lambda_{\text{Hill}}$  as a function of the number of mutations  $n^{\sigma}$ . It is seen, that the effective fitness has exactly one maximum and therefore the accessibility property holds [69].

 $\overrightarrow{Left}$ : The maximum of the fitness function is found already at few mutations, if  $\phi$  is small and shifts to higher numbers, as  $\phi$  becomes larger.

*Right:* The height of the peak increases with increasing  $\gamma$ .

with  $a < b \le 1$  and  $c < d \le 1$ .

This will map every genotype to a unique phenotype and the fitness is no longer degenerate as in the toy model. Hence, we will find a unique global and, potentially, multiple local fitness peaks. However, they do not necessarily have to occur in the same layer.

In accordance with our previous findings, we first note, that any choice of probability distributions that on average increase  $\phi^{\sigma}$ , i.e. a>c and/or b>d, will have many phenotypes with lower fitness than the wild type. In the context of evolution, this is again not very interesting and will not be considered in the following. Hence, we will stick to either equal or fitness increasing probability distributions, meaning that for every mutation i we have  $\frac{\langle \lambda_{\min}^i \rangle}{\langle \lambda_{\max}^i \rangle} \leq 1$ .

We start with  $\lambda_{\max}^i = 1$  and  $\lambda_{\min}^i \in [a, b)$ , which is a semi random non-trade-off model and makes the phenotypes one dimensional. Thus, the fraction  $\phi^i$  is fully determined by the death rate  $\lambda_{\min}^i$ . Similar to the toy model we expect, that peak phenotypes will have  $\phi^{\sigma} \approx \phi_{\max}$ , but such phenotypes are not necessarily unique anymore. Figure 15 illustrates a four locus case for  $\lambda_{\min} \in [0.3, 0.7)$  where multiple fitness peaks are found in the landscape.

In such a semi-random non trade-off model, the graph topology only depends on the probability distribution of  $\lambda_{\min}$  and we find that  $\forall i, j \in [0, L] : \lambda_{\min}^i \lambda_{\min}^j < \lambda_{\min}^i \Rightarrow \phi^i \phi^j < \phi^i$ . Since this must hold for any two mutations on any background genotype, we conclude directly that the accessibility property must hold for such landscapes (see section 3.3.1).

Unfortunately, the argument is restricted to the semi-random non trade-off model and does not hold once we consider two dimensional phenotypes, i.e. random  $\lambda_{\min}$  and  $\lambda_{\max}$ , again.

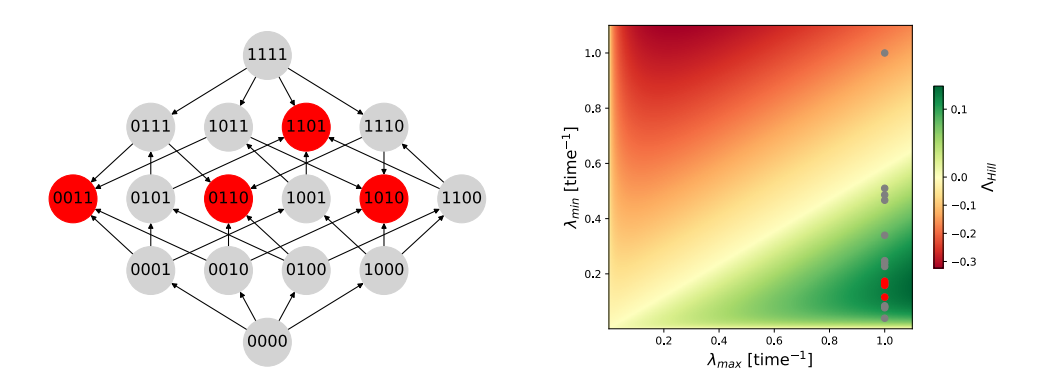


Figure 15: Fitness Graph (left) and full two dimensional Landscape (right) for L=4 with randomly sampled death phenotypes ( $\lambda_{\min}^i \in [0.3, 0.7)$ ) and no trade-off ( $\lambda_{\max}^i = 1$ ). Fitness peaks are colored in red.

For the further characterization of such landscapes, we will numerically analyze multiple setups. A setup always refers to a certain choice of probability distributions, since we keep the general PKPD setting unchanged. We chose L=4 to ensure a decent landscape size with still manageable complexity. For every setup we will identify the number and location of the fitness peaks and check for the subset-superset accessibility property.

Since  $\lambda_{\min}$  and  $\lambda_{\max}$  are drawn from two i.g. different uniform distributions, every setup can be described by four parameters:

$$\langle \lambda_{\min}^i \rangle = \hat{\mu}_{\min} \quad \operatorname{Var}(\lambda_{\min}^i) = \hat{\sigma}_{\min}$$
  
 $\langle \lambda_{\max}^i \rangle = \hat{\mu}_{\max} \quad \operatorname{Var}(\lambda_{\max}^i) = \hat{\sigma}_{\max}$ 

which is the mean and variance of the two probability distributions. For convenience, we will also introduce  $\bar{\phi} = \frac{\langle \lambda_{\min}^i \rangle}{\langle \lambda_{\max}^i \rangle}$ , representing the behavior of an associated toy model with  $\hat{\mu}_{\min} = \beta$  and  $\hat{\mu}_{\max} = \gamma$ . Furthermore, if not stated otherwise, we will set  $\hat{\sigma}_{\min} = \hat{\sigma}_{\max}$  and thus

$$\lambda_{\min}^{i} \in [a, a+x)$$
  
 $\lambda_{\max}^{i} \in [c, c+x)$ .

It is important to note, that x is not an entirely independent parameter, since the boundary condition  $0 < \lambda_{\min/\max} \le 1$  has to be satisfied.

Furthermore, we readily observe, that in the limit of  $x \to 0$  our model will converge to the previously discussed toy model.

Figure 16 is a first illustration of how the parameters shape the fitness landscape. Each plot visualizes the location of all genotypes and the behavior of the

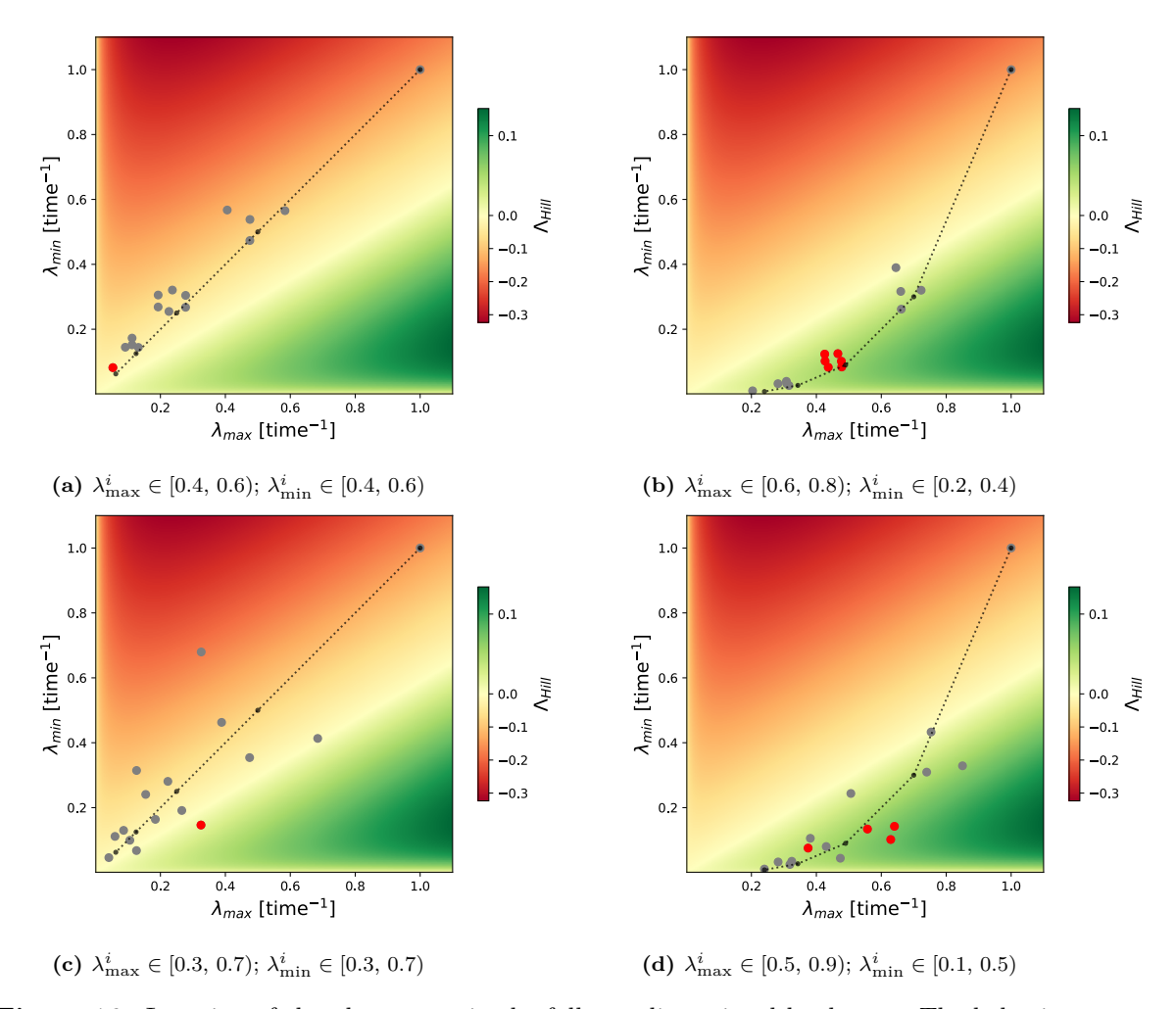


**Figure 16:** Location of the phenotypes in the full two dimensional landscape. The behavior of the distribution mean is shown with black markers (dotted line) and peak genotypes are highlighted in red. Especially (d) illustrates, that high fitness genotypes are good candidates to be fitness peaks, but are not necessarily peaks.

associated toy model in the full two dimensional landscape for different mappings. We find, that all the sampled phenotypes  $\sigma$  can be described as random deviations from the corresponding toy model  $\bar{\phi}^{\sigma} = \bar{\phi}^{n\sigma}$ , where the distribution depends on x.

For small x, phenotypes are found close to the toy model and our previous results are highly useful here (see 16a and 16b). Again, peak genotypes (red markers) are likely to be found in one layer. Otherwise, as x increases, the distribution of phenotypes is rather broad and the toy model results do not readily apply here. However, the topology of trade-off-induced landscapes is found to strongly depend on the choice of uniform intervals. To further investigate this, we perform numerical simulations for various setups. In each simulation, we quantify the number of fitness peaks in the landscape and test their accessibility.

We will start by sampling phenotypes from equal probability distributions

$$\lambda_{\text{max}}^i, \lambda_{\text{max}}^i \in [0.5, 0.8)$$

and successively reduce  $\hat{\mu}_{\min}$  with everything else, especially the interval width x, constant. Each of these scenarios is associated with its respective toy model  $\bar{\phi}$ . Figure 17 illustrates the mean number of peaks and the subset-superset accessibility property as a function of  $\bar{\phi}$ . Both observables are averages over multiple realizations on every setup.

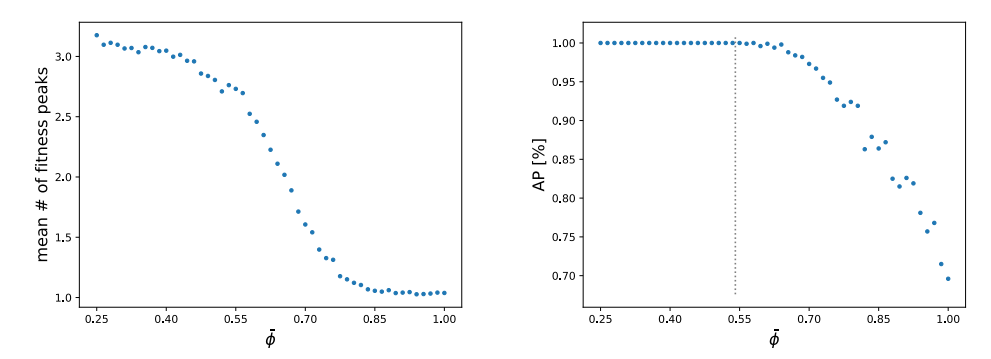


**Figure 17:** Mean number of peaks (left) and percent of AP-fulfilling landscapes (right) as functions of the associated trade-off. The black dotted line indicates the fraction at which both intervals start to overlap and it is observed that this overlap reduces the accessibility of the landscapes.

Every point represents an average over 1000 realizations on every setup. Each setup has  $\lambda_{\max}^i \in [0.5, 0.8)$  and therefore  $\bar{\phi} = \frac{\langle \lambda_{\min}^i \rangle}{0.65}$ .

In analogy to our observations on the toy model, we find that the number of fitness peaks increases as  $\bar{\phi}$  decreases. In this scenario, peaks tend to occur in intermediate layers (see figure 18), rather than in the full mutant. Since intermediate layers contain more genotypes than periphery layers (full mutant and wild type), more genotypes are found as peaks.

Crucially, we note that some setups violate the subset-superset accessibility property. One can show, that the ordering of  $\phi$  (37), which implies the ordering condition on the fitness values [29], is a necessary condition for the AP to hold (see appendix [B.1] for the proof). In the context of the TIL model, (37) can be written as  $\forall i, j \in [0, L] : \phi^i \phi^j < \phi^i$ .

We note, that this property can be violated if

$$\exists j \in [0,\,L]: \phi^j > 1 \quad \Leftrightarrow \quad \exists j \in [0,\,L]: \lambda^j_{\min} > \lambda^j_{\max}.$$

Hence, setups with overlapping probability distributions, i.e. distributions that allow for such mutations, are expected to break the AP.

The right plot in figure 17 proves this observation empirically. It indicates the respective fraction  $\bar{\phi}$ , where both intervals do not overlap anymore and we observe, that non-overlapping setups have the AP, while the accessibility of the landscape reduces with an increasing overlap.

Similar results can be found in the Appendix B.2 for different  $\hat{\mu}_{\text{max}}$ .

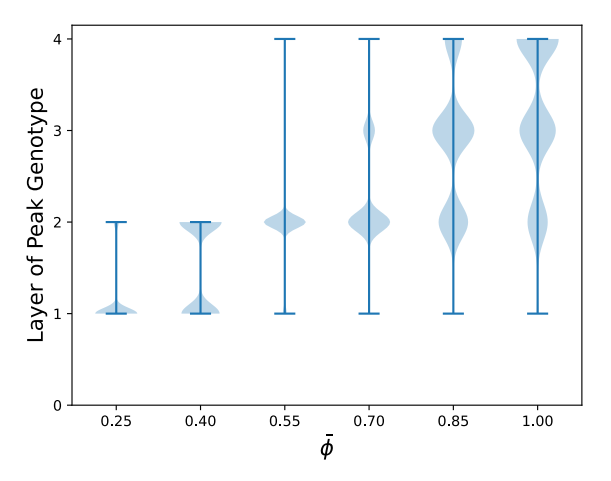
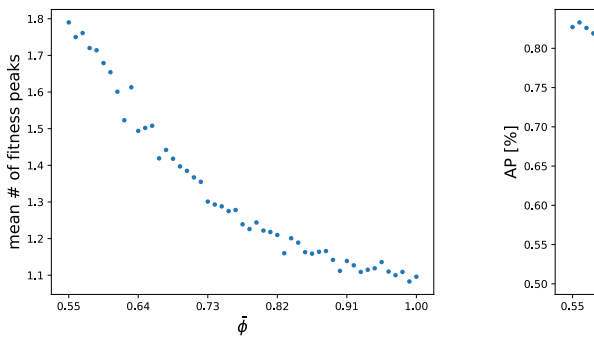


Figure 18: Violin Plot of the peak genotype layer for five exemplary setups with  $\lambda_{\max}^i \in [0.5, 0.8)$  and x = 0.3. For decreasing  $\bar{\phi}$  the peak genotypes tend to occur for fewer mutations ("lower" layers) and cumulated in one layer. Note, that widths of different violins are not normalized to the number of peaks and therefore cannot be compared.

As a final step, we will now increase the width of our probability distributions. According to our previous findings (figure 16) it is expected that high fitness genotypes, especially fitness peaks, now distribute over multiple layers. Hence, the probability of whole peak-layers decreases and we expect less peak genotypes in the landscape (see figure 19 left plot). Furthermore, the violin plot figure 20 supports our assumption and indicates, that fitness peaks are not exclusively found in single layers.

Moreover, increasing the interval width will also increase deviations from the associated toy model  $\bar{\phi}$ . For large enough x, both probability distributions always overlap and therefore the general rank order of the toy model, i.e.  $\forall i, j \in [0, L]$ :  $\phi^i \phi^j < \phi^i$ , is ultimately lost. Thus, edges of the fitness graph are less prone to have a general direction and the accessibility significantly decreases (figure 19 right plot).

In summary, we find that our trade-off landscape does not have universal negative epistasis and does not generally fulfill the subset-superset accessibility property.



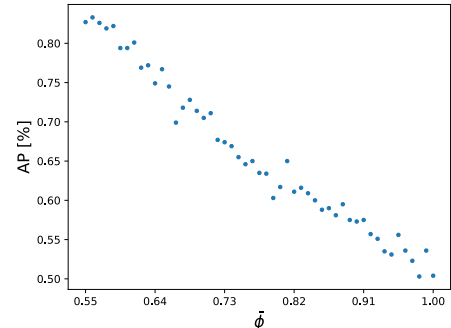


Figure 19: Mean number of peaks (left) and percent of AP-fulfilling landscapes (right) as functions of the associated trade-off. Every point represents an average over 1000 realizations on every setup. Each setup has  $\lambda_{\max} \in [0.3, 1.0)$  and therefore  $\bar{\phi} = \frac{\langle \lambda_{\min}^i \rangle}{0.65}$ .

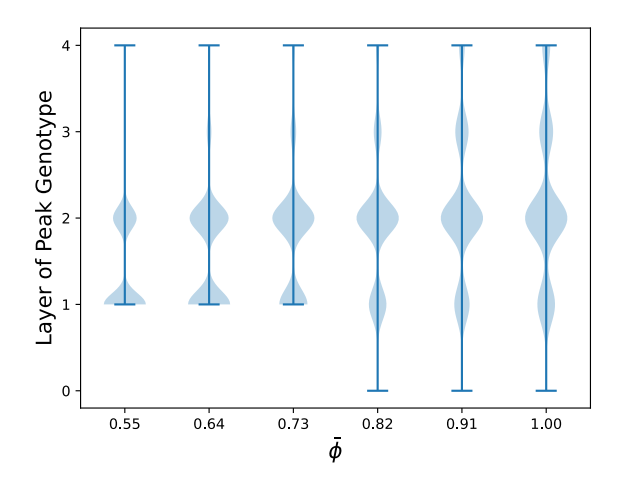


Figure 20: Violin Plot of the peak genotype layer for five exemplary setups with  $\lambda_{\max}^i \in [0.3, 1)$  and x = 0.7. The peak genotypes are not exclusively found in one layer anymore, but tend to distribute in the fitness graph. Note, that widths of different violins are not normalized to the number of peaks and therefore cannot be compared.

#### 3.3.3 On the Number of Loci

For now, we have restricted our analysis to four loci landscapes. This restriction was arbitrary to some extent and chosen such that fitness landscapes maintain manageable complexity. However, previous studies have shown, that the choice of L crucially affects the topology of trade-off induced landscapes, especially the number of fitness peaks [29, 68, 69].

Furthermore, studies on inherited tolerance mechanisms have shown, that several hundreds of genes can be related to single drug tolerance [73] and interestingly, the number of genes associated with increased tolerance is significantly higher than for resistance [7]. We will therefore investigate how the landscape topology changes under increasing system size.

Recalling the definition of a fitness graph from 3.2 one notes, that the number of

nodes (N) and edges (E) directly follow from the number of loci:

$$N = 2^{L}$$
$$E = \frac{L}{2} 2^{L}.$$

Furthermore, we find L+1 layers, where each layer groups  $\binom{L}{n}$  genotypes that have a total of n mutations. This is a binomial distribution and is visualized for L=4 and L=7 in figure [21].

In the previous sections it was discussed to large extent that, at least for the mean field (toy model), there exists an optimal number of mutations  $n_{\rm opt}$ , maximizing the effective fitness. This number is fully determined by the PKPD parameters and the mean of respective probability distributions. Notably, it does not depend on the number of loci in the landscape and can be found as the number of mutations in the peak layer of the associated toy model. We highlight the respective optimum layer in figure 21

Since the optimum number of mutations does not depend on the number of

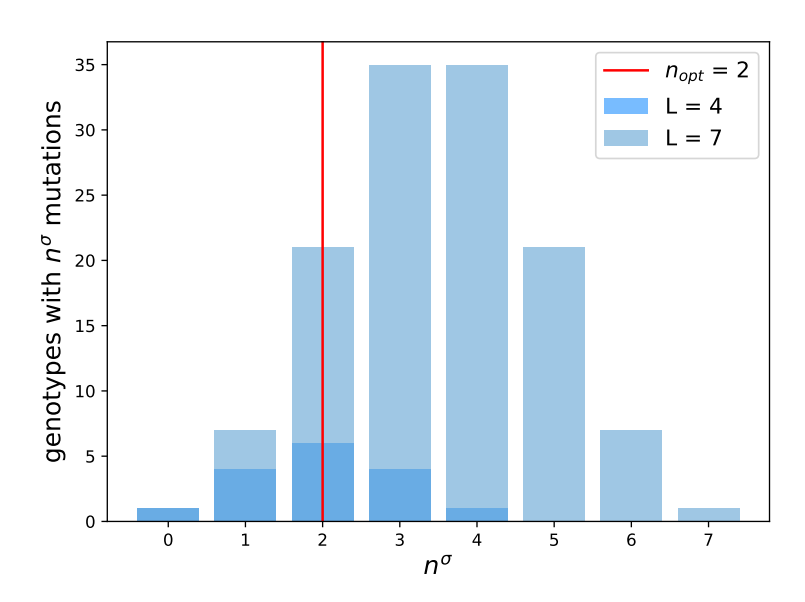


Figure 21: Binomial distribution of the number of genotypes per layer of the fitness graph for L=4 and L=7. The red line indicates the optimal number of mutations for an exemplary setup with  $n_{\text{opt}}=2$ .

One can see that many additional genotypes in the L=7 landscape appear far away from the optimum layer and are thus very unlikely to become fitness peaks. However, also the number of genotypes in the high fitness region around the optimum increases and thus we also expect the number of peaks to increase. However, this increase is not proportional to the amount of additional peaks.

loci, may of the additional genotypes appear in a region far away from the fitness optimum and are thus unlikely to become peaks (see figure 21). Accordingly, such genotypes will not contribute to the observed number of peaks  $n_{\text{peaks}}$  in the landscape.

Nevertheless, also the number of nodes in the optimum layer increases, such that more genotypes are mapped to high fitness phenotypes. The left plot in figure 22 indicates that this will also increase the absolute number of peaks found for large systems. This increase is however not proportional to the number of additional genotypes.

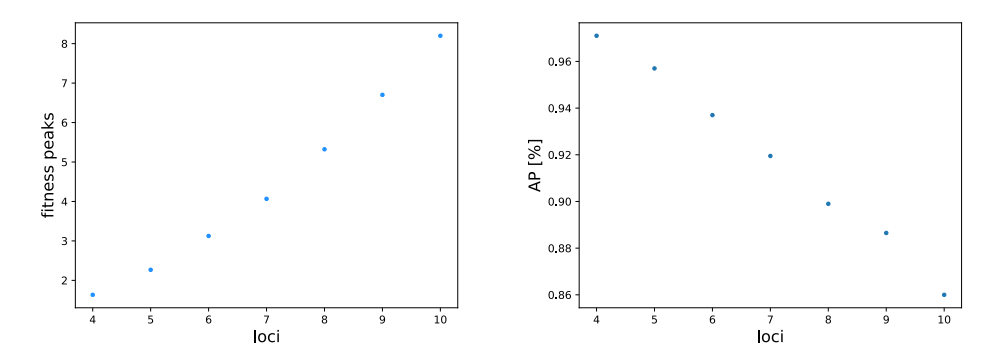


Figure 22: Left: Total number of fitness peaks as a function of L. Right: Percent of AP-fulfilling landscapes as functions of the number of loci L. In both plots every data point represents an average over 2000 realizations on the respective number of loci with  $\lambda_{\text{max}} \in [0.5, 0.8)$  and  $\lambda_{\text{min}} \in [0.3, 0.6)$ .

In order to compare the ruggedness of landscapes with different L, we propose to normalize the number of fitness peaks by the amount of relevant genotypes  $n_{\rm rel}(L)$ . In the context of the ruggedness analysis, we consider those genotypes that have a non negligible probability to become a fitness peak (see B.3 for details).

For every empirically observed number of fitness peaks (left plot of figure 22), we compute the fraction

$$\frac{n_{\rm peaks}}{n_{\rm rel}(L)}$$

and visualize the result in figure 23. Interestingly, this fraction is not a constant for different L and we observe, that the relative number of peaks decreases for larger landscapes. Accordingly, these landscapes are less rugged.

Similar to a decrease in the relative number of fitness peaks, we observe that the accessibility decreases for larger systems.

One can show analytically, that the probability of a direct accessible path between two general genotypes decreases with increasing topological distance if the fitness graph is fully isotropic and the edges do not have a general direction [69].

For a binary, fully random and entropy maximizing Hamming Graph the average distance between two random genotypes is given by:

$$\langle D \rangle = \frac{L}{2}.$$

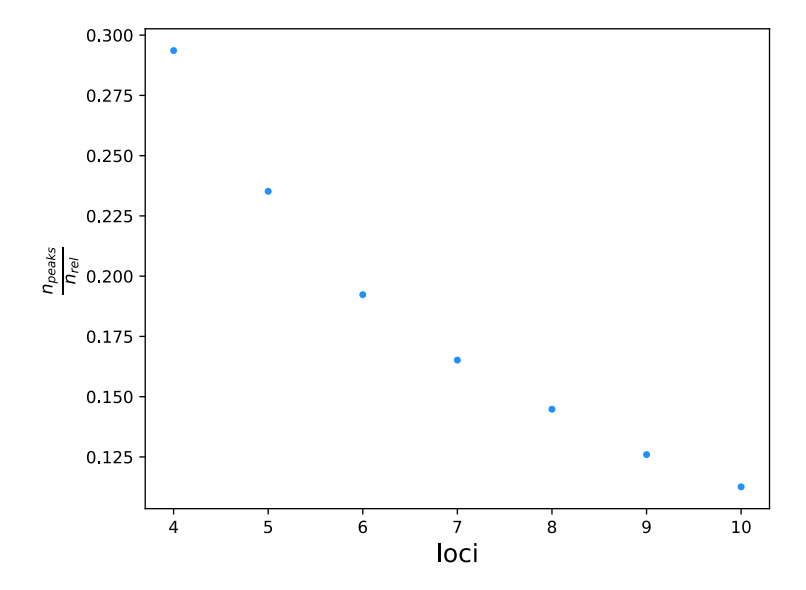


Figure 23: Visualization of the relative count of fitness peaks for landscapes of different L. We observe the percentage of relevant genotypes that are peaks decreases for landscapes with a higher number of loci. Thus, even though the absolute number of peaks increases, the large landscapes are relatively less rugged.

Hence, the accessibility from all sub-/superset genotypes becomes less likely for large L.

This does not hold for the toy model, where edges have a general direction with probability p=1 and the distance between  $\sigma'$  and  $\sigma''$  is thus given by  $D=|n_{\sigma'}-n_{\sigma''}|$ .

Here, growth-death trade-off induced fitness graphs are deviations from the toy model ground state and the direction of any graph edges follows a Bernoulli distribution with  $p \neq 0.5$  in general. Hence, the average distance  $\langle D \rangle$  is expected somewhere between the two extreme cases and we expect that the accessibility of large systems decreases. This is observed in simulations and indicated in the right plot of figure [22].

Summarizing on the structure of large fitness landscape, we have found, that for an increased number of loci, most additional genotypes are negligible for the analysis of the number of peaks. We have found furthermore, that the relative number of peaks decreases and that also less realizations of the larger systems empirically have the accessibility property.

Ultimately, we can now use our knowledge about the landscape topology to understand how bacterial populations evolve under antibiotic stress and how tolerance emerges in clonal populations.

### 3.4 Tolerance Evolution in Effective Fitness Landscapes

We discussed some basic properties of the constructed trade-off induced fitness landscapes in the previous sections. However, the analysis was rather technical and we also want to address the biological picture to some extent here.

Fitness graphs are highly useful to understand evolutionary dynamics of bacteria [69] since graph edges indicate which mutation will be beneficial and eventually fixates. Thus, they reflect that selection would always drive a species towards increasing fitness until a peak genotype is reached.

We model evolutionary paths with a random adaptive walk [74], selecting a random mutation of the active genotype, which is accepted if it is beneficial and rejected otherwise (see [B.4] for the detailed algorithm).

From graph theoretical perspective, evolution from wild type  $(\sigma^0)$  to fitness peak  $(\sigma')$  is a non-cyclic, direct or indirect path on the fitness graph (Hamming graph). The average length  $\langle l \rangle$  of such a path depends non-trivially on the system size L and the probability distributions.

Analytical computation of such average path lengths is thus highly non trivial for general landscapes, but we can gain some intuition again on the toy model. Here, all evolutionary paths are direct paths of length  $l=n^{\sigma'}$ , which is simply the number of mutations in the peak layer. This increases for  $\beta \approx \gamma$  (or  $\bar{\phi} \to 1$ ) and we find a step like function for the path length (figure 24 left).

Again, we can interpret the random landscape as some deviation from the toy

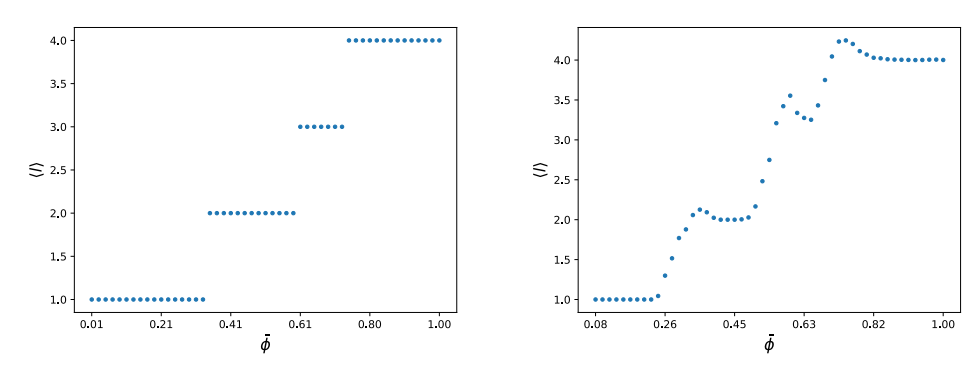


Figure 24: Length of evolutionary paths for the Toy Model (left) and some small perturbation (right) as a function of  $\bar{\phi}$  for L=4. In the toy model all paths from wild type to peak genotype are direct paths and have length  $n^{\sigma'}$ , i.e. the number of mutations in the peak layer. Hence, the average path length is a step function. For this visualization we chose  $\lambda_{\text{max}} = 0.7$  or  $\lambda_{\text{max}} \in [0.7, 0.8)$  respectively.

model and increasing the interval width x will be some perturbation on the step like function of the average path length. In figure  $\boxed{24}$  (right) that variance is small and the step like behavior is well preserved. However, we find that the function overshoots the toy model result at transition regions. Since peak genotypes of the random model can generally occur in different layers, we do not necessarily have a

whole layer of peaks as in the toy model. Hence, the probability of indirect paths contributing to the average increases, which becomes particularly relevant at the transition points. This result compares to the findings in [72], where evolution to a fitness peak is generally indirect in a semi random and fully random TIL model.

As x increases, the peak region expands to multiple layers (see figure 20), and the contribution of indirect paths gradually becomes the dominant factor in the average path length (see figure 25).

Interestingly, the average path length has a maximum for  $\bar{\phi} < 1$  and decreases again as  $\bar{\phi} \to 1$ . In the first place, this seems rather counter intuitive, since we expect to find fitness peaks to be the full mutant or at least some highly mutated genotype. However, the probability of sampling non favorable mutations, i.e. mutations with  $\phi^i > 1$ , increases as  $\bar{\phi} \to 1$ . For the extreme case  $(\bar{\phi} = 1)$  half of the possible mutations have a lower fitness than the wild type and are therefore never realized in the evolution. Hence, the fitness graph reduces to a sub graph, where only few indirect paths contribute to the average path length.

Furthermore, the violin plots in section 3.3.2 suggest that even as  $\bar{\phi}$  approaches 1, peaks do not necessarily appear in higher layers with increasing interval width x. Therefore, the average path length becomes considerably shorter than the expectation predicted by our toy model.

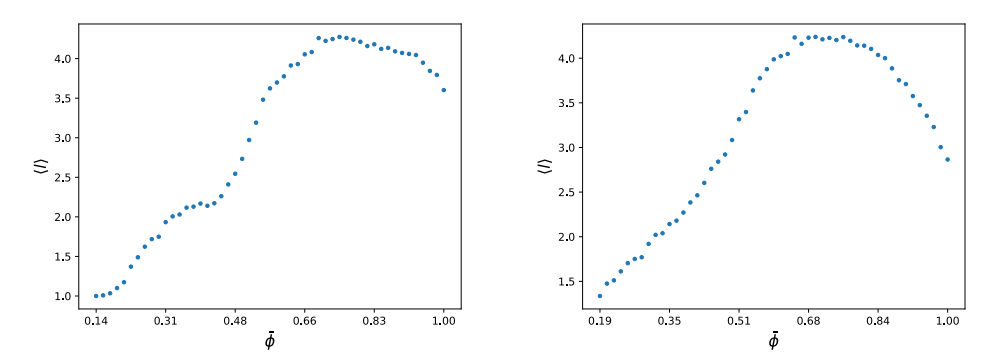


Figure 25: Length of evolutionary paths for  $\lambda_{\max} \in [0.7, 0.9)$  (left) and  $\lambda_{\max} \in [0.7, 1.0)$  (right) as a function of  $\bar{\phi}$  for L=4. The average path length decreases with decreasing  $\bar{\phi}$ , which simply follows the decreasing distance between wild type and fitness peak. Due to the contribution of indirect paths to the average, the average path length is non monotonic and the maximum of  $\langle l \rangle$  occurs for  $\bar{\phi} < 1$ .

In the following, we choose  $\bar{\phi} \approx 0.7$ , generating well accessible landscapes (figure 17 right) and relatively long paths, which eventually reveals some insightful dynamics. Figure 26 visualizes an exemplary path (purple) from wild type to peak genotype in the fitness graph (left) as well as in the full two dimensional landscape (right).

## 3 TOLERANCE EVOLUTION IN TRADE-OFF INDUCED FITNESS LANDSCAPE

Interestingly such paths exhibit a reproducible biphasic behavior, which has been observed on trade-off induced fitness landscapes before [72]. At first, simply accumulating mutations and approaching the high fitness layer drives the evolution. Whereas in a second phase, the evolution approaches a highly rugged region in the fitness topography. Here, reversing and adding mutations can be similarly beneficial and thus certain non-optimal mutations revert while more beneficial ones are added. This does not significantly change the average number of mutations and we observe this as a fluctuation in the "band of maxima" [72]. This proceeds until, eventually, a fitness peak is found.

The length of the second phase correlates with the number of realizable indirect paths, which becomes large if many mutations are beneficial (small  $\bar{\phi}$ ), peak genotypes occur in different layers (large x) and also the system size becomes large. All these findings are combined in a last simulation (figure 27).

In order to avoid a large number of topological negligible peaks, we chose  $\lambda_{\min} \in [0.5, 0.7)$  and  $\lambda_{\max} \in [0.8, 1.0)$ . Thus, single mutations do not significantly change the phenotype and we have a large region that can be realized in the evolution.

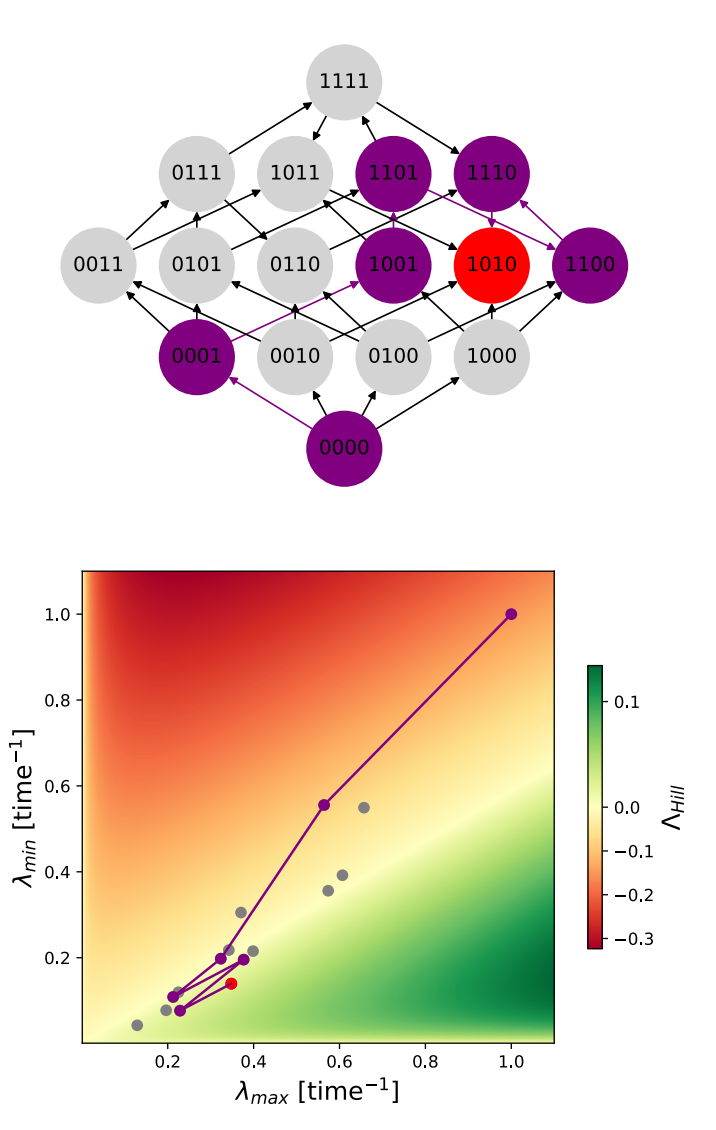


Figure 26: Exemplary evolution from the wild type to a fitness peak (red). The genetic path (purple) is shown on the fitness graph (left), as well as in the full two dimensional landscape (right). The trade-off landscape was constructed with  $\lambda_{\text{max}} \in [0.5, 0.8)$  and  $\lambda_{\text{min}} \in [0.3, 0.6)$ .

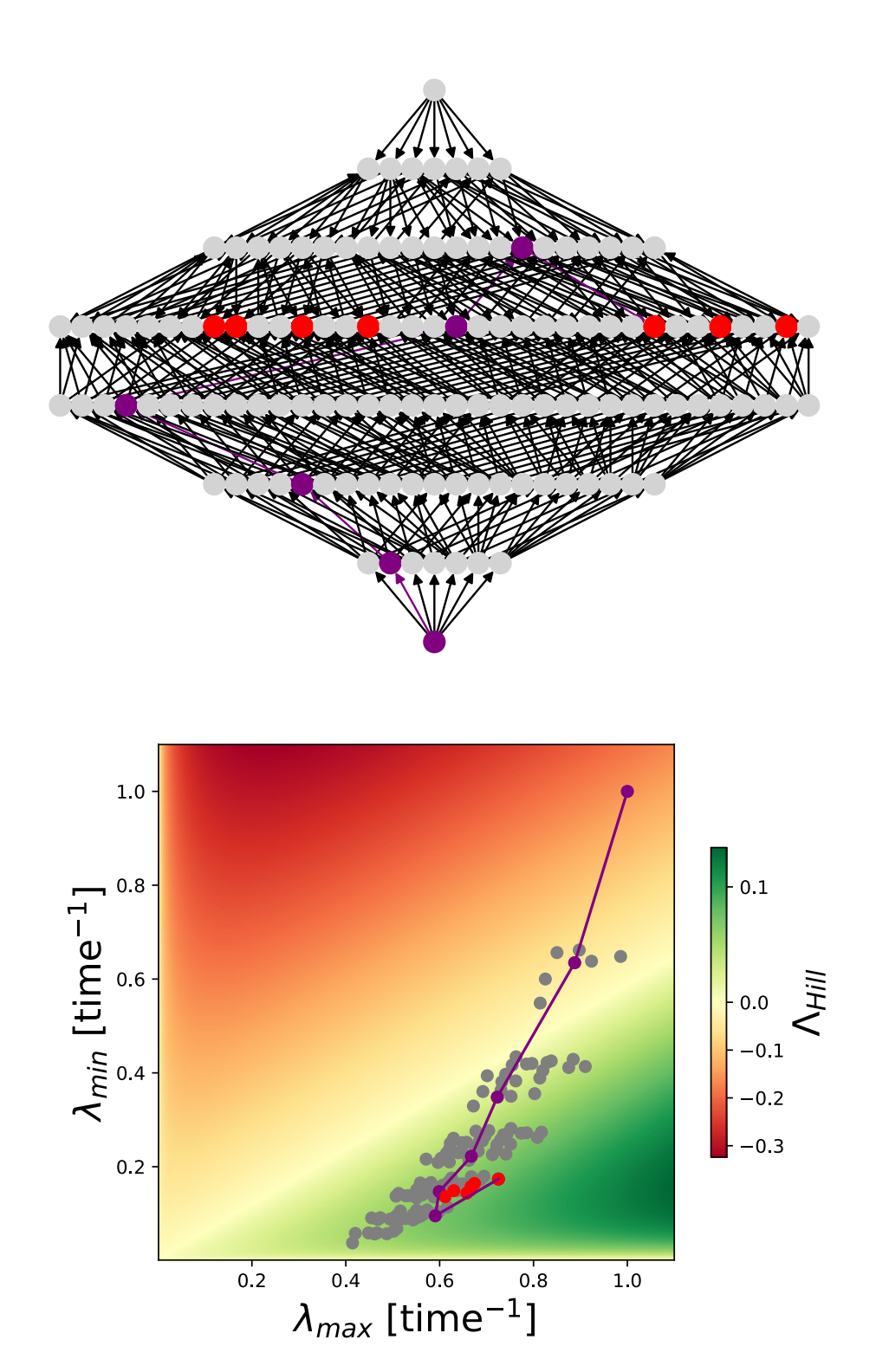


Figure 27: Evolution from the wild type to a fitness peak (red) in a landscape that favors long paths. The genetic path (purple) is shown on the fitness graph (left), as well as in the full two dimensional landscape (right). The trade-off landscape with L=7 loci was constructed with  $\lambda_{\min} \in [0.5, 0.7)$  and  $\lambda_{\max} \in [0.8, 1.0)$ .

### 4 Stochastic Birth and Death Processes

With the first part of this work we have now introduced a fitness measure, comparing the performance of different phenotypes under periodic antibiotic stress. In the context of such dosing protocols, featuring a death and some regrowth regime, we were able to show that certain tolerance mechanisms are beneficial. Using Regoes idea of Hill Type dose-response curves (5) together with an exponential dosing profile, we derived a fitness function of a time inhomogeneous treatment, that remains reasonably well interpretable.

However, it is important to emphasize that the effective fitness is a deterministic mean field description of the time dependent population size N(t) after one period. It is therefore expected to be an exact measure in the limit of large populations, but it is not capable to capture the dynamics within a treatment period (see figure 28), any random deviations from the mean and, most importantly, extinction events.

Our effective fitness framework stands in contrast to the intrinsic stochasticity of biological mechanisms, particularly those related to growth and death. We are therefore interested in finding a more realistic description of the population size under periodic treatment, which accounts for growth and death as two separated stochastic processes.

Building up on Kendall's birth and death model  $\boxed{30}$ , we motivate the description of the stochastic replication process in terms of the time evolution of the probability mass function  $P_n(t)$ . Assuming, that the populations have the Markov property, we show that this is given by the master equation and furthermore motivate a convenient description of the appearing transition rates.

Within this stochastic framework we compute the time dependent survival probability for one period of antibiotic treatment and compare analytic predictions to numerical Gillespie simulations.

We demonstrate that the stochastic model converges to the previously discussed mean-field description, i.e. the effective fitness, in the limit of large populations. In contrast, extinction events in small populations are not captured by the deterministic model (figure [28]). As a result, the survival probability becomes a distinct feature of the stochastic framework, providing a second, complementary measure of success under antibiotic treatment.

In the context of clinical treatment, eradication of pathogenic bacteria remains the ultimate goal. Using our stochastic model, we ultimately investigate whether a tolerant mutant can rescue a whole population from extinction and potentially threaten the treatment success.

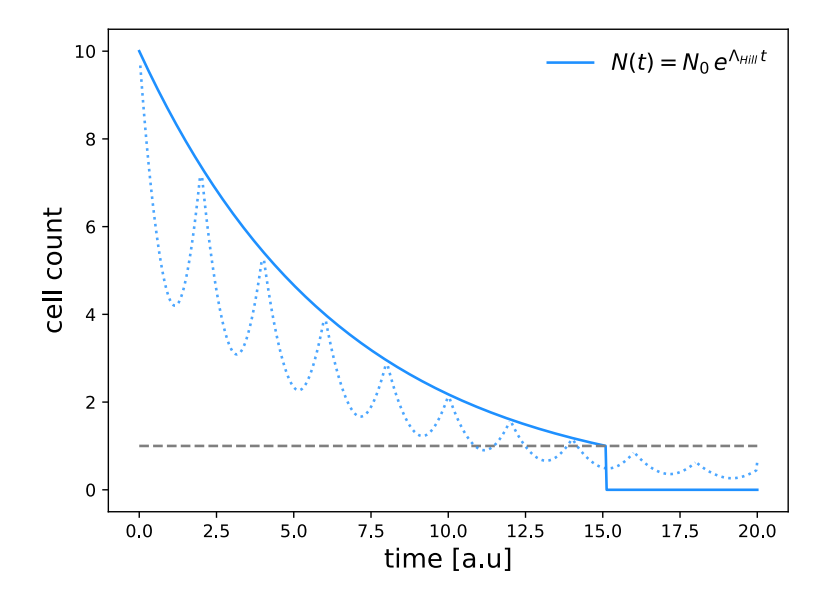


**Figure 28:** The effective fitness captures change of the population size after one period of antibiotic treatment. The death and regrowth character (dotted line), emerging from a time dependent dosing protocol, is not captured by solution that is predicted from the effective fitness (solid line).

Furthermore, the deterministic model describes the population size as a continuous variable, where N=0 (extinction) is never reached. In principle, we can demand that a population is extinct, whenever N<1, which, however, seems suboptimal since regrowth from extinction cannot be excluded (see period 6 & 7 of the dotted line).

Furthermore, stochastic deviations from the mean can significantly influence the time of extinction, which makes a stochastic description inevitable.

#### 4.1 The General Birth and Death Process

In his pioneer work on a stochastic description of population growth, Kendall [30] introduced a formulation for the general birth and death process. Given a value-discrete time dependent random variable  $n_t$ , which we interpret as population size, the birth and death process allows for three possible transitions within a time increment dt:

Birth:  $n_{t+dt} = n_t + 1$ 

Death:  $n_{t+dt} = n_t - 1$ 

None:  $n_{t+dt} = n_t$ 

Together with the respective transition probabilities:

$$p_{\text{Birth}} = g(t) n_t dt + \mathcal{O}(dt)$$

$$p_{\text{Death}} = d(t) n_t dt + \mathcal{O}(dt)$$

$$p_{\text{None}} = 1 - (g(t) + d(t)) n_t dt + \mathcal{O}(dt)$$

this defines the general stochastic birth and death process [30], [31]. We interpret q and d as growth and death rates respectively.

This is a Markov process and we can write the Master equation for the probability distribution [30]:

$$\frac{dP_n}{dt} = g(n-1)P_{n-1} + d(n+1)P_{n+1} - (g+d)nP_n.$$
 (38)

The random variable  $n_t$  is non-negative and the state  $n_t = 0$  is an absorbing state of the system. Accordingly, the equation above describes the system for  $n_t \ge 1$  and we have

$$\frac{dP_0}{dt} = dP_1 \tag{39}$$

as a second equation for the time evolution of the absorbing state.

For the general birth and death process, both rates g and d can generally be any function of time and environment, where typical environmental factors are the presence of antibiotics or other individuals in a population. Species interactions are found to have a significant impact on the competition [75, 76, 77] [78] and it is typically assumed that either the birth- or death rate are functions of the population size (birth- or death competition) [33].

The phenomenon of stress due to competition in a living population appears naturally and can be found in all kinds of interacting communities [76]. However, in the context of bacteria, we can also apply additional external stress with the supply of antibiotics at a certain concentration. Again we can distinguish two modes of action: biostatic- and biocidal treatment. A biostatic drugs is a growth inhibiting antimicrobial, reducing the birth rate g, whereas biocidal drugs increase the death rate d [33].

In this work, we aim to analyze the stochastic birth and death process of bacteria that are exposed to a time dependent periodic antibiotic stress. In combination with the general size and time dependency of the g and d, solving (38) and (39) is a hard problem.

A general solution was presented by Kendall [30] and is known as:

$$P_0(t) = \xi_t \tag{40}$$

$$P_n(t) = \{1 - P_0(t)\} (1 - \epsilon_t) \epsilon_t^{n-1} \text{ for } n \ge 1$$
 (41)

where

$$\xi_t = 1 - \frac{e^{-\rho}}{W(t)} \tag{42}$$

$$\epsilon_t = 1 - \frac{1}{W(t)} \tag{43}$$

with

$$\rho(t) = \int_0^t \{d(t') - g(t')\} dt' \tag{44}$$

$$W = e^{-\rho} \left\{ 1 + \int_0^t e^{\rho(\tau)} d(\tau) \, d\tau \right\}. \tag{45}$$

The latter becomes intractable for an exponential concentration profile together with hill shaped replication rates.

# 4.2 The Simple and Homogeneous Birth and Death Process

The underlying complexity of the general birth–death process arises from the rates g and d, which are, in general, functions of time and the environment. However, this complexity can be significantly reduced if we treat both rates as constant and homogeneous in the population. This is known as the simple birth and death process 30.

In this specific case, an exact solution of the master equation is known. Here, we will only sketch the derivation, but more detailed explanations, also on other birth-death processes, can be found in Chapter 8 of Baileys book [31].

Using the probability generating function

$$G(z,t) = \sum_{n=0}^{\infty} P_n(t)z^n$$

we can write the master equation (38) and (39) as a partial differential equation of  $\mathcal{G}$ :

$$\frac{\partial \mathcal{G}}{\partial t} = \left[ g z (z - 1) + d (z - 1) \right] \frac{\partial \mathcal{G}}{\partial z}.$$
 (46)

We can solve this equation by the method of characteristics and obtain

$$\mathcal{G}(z,t) = \left(\frac{df(z,t) - 1}{gf(z,t) - 1}\right)^{n_0} \tag{47}$$

where  $n_0$  is the population size at time t = 0 and

$$f(z,t) = \frac{(z-1)e^{(g-d)t}}{gz-d}.$$

Ultimately, we obtain the desired probability distribution  $P_n(t)$  from the series expansion of (47) in powers of z [31]:

$$P_n(t) = \sum_{j=0}^{\min(n_0,n)} \binom{n_0}{j} \binom{n_0+n-j-1}{n_0-1} \sigma(t)^{n_0-j} \rho(t)^{n-j} (1-\sigma(t)-\rho(t))^j$$
(48)

$$P_0(t) = \sigma^{n_0} \tag{49}$$

with the two functions

$$\sigma(t) = \frac{d\left(e^{(g-d)t} - 1\right)}{g e^{(g-d)t} - d}$$
(50)

$$\rho(t) = \frac{g\left(e^{(g-d)t} - 1\right)}{g\,e^{(g-d)t} - d}.\tag{51}$$

Notably, we obtained a manageable expression for the extinction probability  $P_0(t)$ , which we proceed to discuss briefly.

One can readily verify that  $\sigma(t) < 1$  for all t, g, d > 0, implying that the extinction probability decays exponentially with the initial population size  $n_0$ . This result is consistent with expectations for a simple homogeneous birth–death process, where interactions between individuals are absent. In such a scenario, the whole population can be described as  $n_0$  independent and identical birth–death processes, which makes the individual extinction events multiplicative.

Furthermore, we observe that the extinction probability converges for long times [31], as

$$\lim_{t \to \infty} \sigma(t) = \begin{cases} 1 & \text{for } g \le d \\ \frac{d}{g} & \text{for } g > d \end{cases}$$
 (52)

Figure 29 illustrates how the extinction probability varies with time and the initial population size. This result will be further reviewed in numerical simulations later (see section 6). Additionally, the time evolution of the full probability distribution is briefly discussed in the Appendix D.

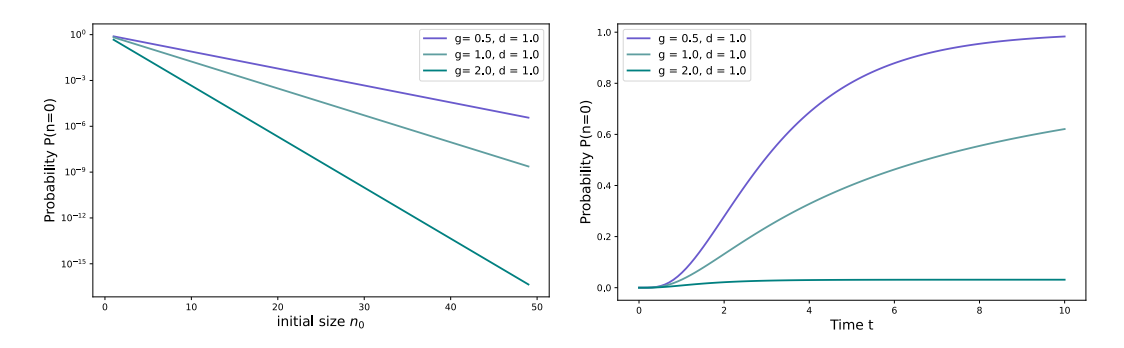


Figure 29: Visualization of the extinction probability for three fundamental scenarios. Left: Extinction probability as a function of initial population size at t = 2. One observes that the extinction probability decreases exponentially in  $n_0$ , where the slope corresponds to the logarithm of  $\sigma$ .

Right: Extinction probability as a function of time for  $n_0 = 5$ . In both cases where  $g \le d$ , the system ultimately converges to P(n = 0) = 1, indicating certain extinction. In contrast, when g > d, the extinction probability remains small but, notably, greater than zero.

At this stage, it is important to emphasize once again that the results presented in this section are valid only under the assumption of constant birth and death rates. Consequently, additional work is required to adapt these results to our case, where the rates g and d vary over time due to the periodic antibiotic concentration profile.

### 5 The Stochastic Model of Periodic Treatment

We start our stochastic analysis, rewriting the very first equation (1) of this work:

$$\frac{dN}{dt} = (g - d) N - \eta(c) N. \tag{53}$$

Here, we describe the effect of the antibiotic with the function  $\eta(c)$ , which corresponds to the previously defined dose–response curve [33], [79]. In contrast to the previous approach, growth, death and antibiotic effect are now treated as three distinct parameters, rather than considering only the net replication rate.

However, except for the summation over the distinct rates, the model described by (53) is equivalent to Regoes differential equation (3). The new parameter  $\eta$  is closely related to Regoes dose-response curve  $\lambda(c)$  (shift by a constant g-d) and now contains all the concentration dependence of the model. Note that  $\eta$  also has units of time<sup>-1</sup> and can be interpreted as a third, additive stochastic rate additionally to g and d.

### 5.1 Biostatic and Biocidal Interpretation of $\eta$

We consider here, that the antibiotic effect is additive (as in [33]), but multiplicative effects are also considered in other studies [79]. From the equation (53) we note, that the effect of the antibiotic can be interpreted as either growth inhibiting:

$$g \to g - \eta$$

$$d \to d \tag{54}$$

or death promoting:

$$g \to g$$

$$d \to d + \eta. \tag{55}$$

In the deterministic description of population size, both modes of action are equivalent, as only the sum of all rates determines the overall replication rate. Thus, the effective fitness is universal to biostatic and biocidal drugs.

In contrast, the stochastic model explicitly distinguishes between growth and death processes. This distinction changes the dynamics within one period of treatment and thus also the chance of surviving one dose of the respective drug action. We will further explore this in section 5.4 and 6.

Experimentally, the difference between the two modes of action is well motivated by the existence of biostatic (growth inhibiting) drugs like tetracycline or erythromycin, and biocidal (death promoting) drugs like ciprofloxacin or streptomycin [33]. The nowadays most prescribed drugs, the  $\beta$ -lactam antibiotics [80] are associated to the biocidal category [81].

# 5.2 Pharmacokinetics and Pharmacodynamics in the Stochastic Model

We have now motivated, that a stochastic model considers all rates g, d and  $\eta$  instead of just the sum of all rates. Since the natural growth and death rate are assumed to be constant for a given phenotype, the only dose dependence is depicted by the stress response  $\eta(c)$ . In accordance with our previous discussion, this is given by the shifted Hill-Type dose-response curve

$$\eta_{\text{Hill}}(c(t)) = \eta_{\text{max}} \frac{\left(\frac{c(t)}{MIC}\right)^{\nu}}{\left(\frac{c(t)}{MIC}\right)^{\nu} - \frac{\eta_{\text{max}}}{g-d} + 1}.$$
(56)

which is readily obtained from (5), by subtracting  $\lambda_{\text{max}}$ , inverting the sign (because  $\eta$  is a positive rate) and identifying

$$\lambda_{\text{max}} = g - d \tag{57}$$

$$\lambda_{\min} = g - d - \eta_{\max}. \tag{58}$$

In this representation  $\eta_{\text{max}}$  is the effect of the antibiotic at infinite concentration. The value of  $\eta$  has an upper bound for biostatic drugs, since full growth inhibition  $(g - \eta_{\text{max}} = 0)$  is the best possible treatment. We thus have  $0 \le \eta_{\text{max}} \le g$  here, whereas biocidal drugs can in principle have any value  $\eta_{\text{max}} \ge 0$ .

Given the exponentially decaying pharamacokinetics (PK) (10) and the explicit pharmacodynamic (PD) function (56), the equations (44) and (45) are fully determined. Ultimately, this yields the full probability distribution (41), and thereby also the extinction probability  $P_0$  of a general phenotype at time t.

Unfortunately, the resulting integral in (45) is analytically intractable for our PKPD model.

In a related study, Alexander [54] examines the extinction probability of a single individual in the limit of long treatment durations  $(t \to \infty)$  for the same PKPD protocol. However, the resulting expression, which involves hypergeometric functions, does not accurately describe the survival probability for finite, potentially very small  $(t < \tau)$  timescales. Here, we want to focus on finding an expression for

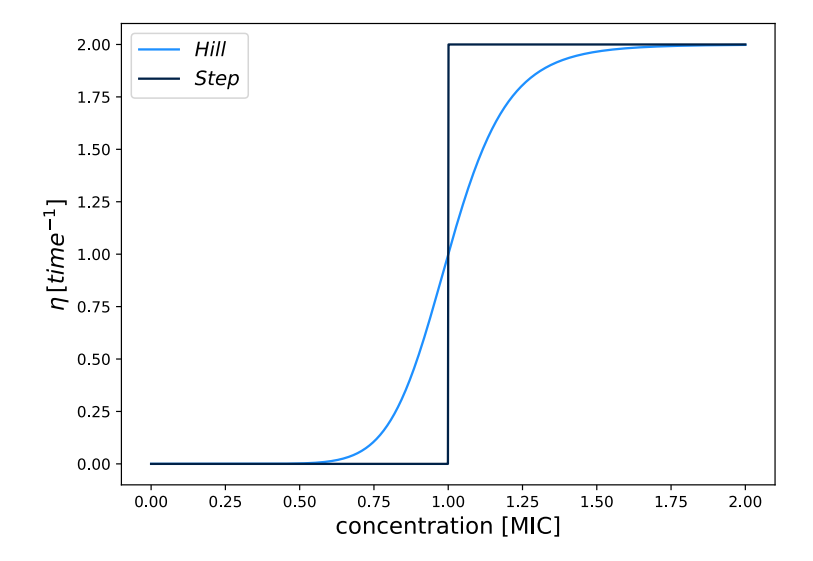


**Figure 30:** The new pharmacodynamic function  $\eta(c)$  in the Hill model (blue) and in the step function limit (black). For the step function, the complex concentration dependency reduces to two regimes, where  $\eta(c)$  is constant.

the probability of extinction or establishment on timescales of one treatment period. The result on the long time establishment is briefly revisited in section 8.2.3.

In order to obtain some analytical insight on the probability distribution  $P_n(t)$ , we will consider the limit of infinitely steep dose-response curves  $(\nu \to \infty)$ . Such an approximation is well motivated by empirical observations on dose-response curves of  $\beta$ -lactam antibiotics [82].

In this limit,  $\eta(c)$  becomes a step function:

$$\eta(c) = \begin{cases}
0 & \text{for } c \le MIC \\
\eta_{\text{max}} & \text{for } c > MIC
\end{cases}$$
(59)

and the previously complex time dependency is now captured in  $\tau$  and  $t_{\text{mic}}$ , i.e. the period length and the time at which the concentration drops to the MIC. Figure 30 illustrates  $\eta(c(t))$  and we will refer to this PKPD model in the following, if not stated otherwise.

Similar to the Hill model equivalence before, the step function  $\eta$  relates to the step function dose-response curve  $\lambda_{\text{step}}$  by a shift of  $-\lambda_{\text{max}}$  and respecting the opposite sign.

The results on  $\lambda_{\text{step}}$  were previously discussed in section 2.4.2 and appendix C.1 and we will compare our stochastic analysis to the deterministic limit later (see 6.4). Therefore, we now aim to derive the probability that a phenotype with a step function  $\eta(c)$  survives one period of biostatic or biocidal antibiotic treat-

ment. Additionally to the effective fitness, this will introduce a second measure to compare the performance of a phenotype exposed to antibiotic stress.

### 5.3 The Interpretation of Tolerance in the Stochastic Model

Similar to the effective fitness, the survival probability provides a single scalar measure that quantifies the performance of a bacterial strain, allowing for direct comparison between phenotypes. For the purpose of this work, we are particularly interested to investigate, how the survival probability of a tolerant mutant compares to the wild type.

Following the definition of  $\boxed{7}$  we interpret Tolerance as a transient reduction in the death rate at high antibiotic concentrations. Furthermore, we discussed in section  $\boxed{2.5}$  that such a tolerance response typically comes with a cost in the null fitness  $\boxed{39}$ ,  $\boxed{56}$ . Previously the tolerance trade-off was modeled as simultaneous, random reduction of  $\lambda_{\min}$  and  $\lambda_{\max}$  in the genotypic TIL-Model. Both of these parameters do not occur in our stochastic formulation. However, we can find a similar interpretation of the trade-off here.

Tolerant strains are, by definition, less susceptible to an antimicrobial agent at high concentration [7]. Since the antibiotic response is essentially reflected by a single scalar parameter within our step function DRC, we can understand tolerance as a reduction of the maximum drug effect  $\eta_{\text{max}}$ .

Furthermore we assume, that the natural death rate d is a constant for all phenotypes and that only the natural growth rate g alternates. Thus, we can model the tolerance trade-off as a simultaneous reduction of the antibiotic susceptibility  $\eta_{\text{max}}$  and the growth rate g, which is empirically meaningful [25, [26], [27], [28].

We will see later, that tolerance increases the survival probability (section 5.5) and, moreover, that a tolerant mutant can rescue a wild type population from extinction (section 7).

Using a survival probability topography, one could in principle repeat a TIL-model analysis for the two phenotypes  $\eta_{\text{max}}$  and g now. However, this would not be very insightful and we want restrict our focus to two phenotypes: the wild type and a tolerant mutant. These two strains are further defined in the following.

### 5.4 The Survival Probability Within a Single Treatment Period

With the simple but justified assumption of a step like antibiotic effect, we have now heavily reduced the time induced complexity of our stochastic model. However, the assumption of population homogeneity in section 4.2 is not yet motivated here.

In fact, if we are only interested in the survival probability and independence of all birth-death processes is guaranteed, we do not have to assume any homogeneity in the population. Considering a population of size n with  $M \leq n$  distinct phenotypes of subpopulation sizes  $n_{\rm m}$  ( $m \in \{1, M\}$ ), the survival probability of the whole population is give as:

$$P_{\text{surv}}(t) = 1 - \prod_{m} P_0(t|n_{\text{M}}).$$
 (60)

Since the simple and homogeneous birth-death process is known from section [6], equation (60) can be readily evaluated. However, it is crucial to justify the fundamental premise of independence, which was also required in the derivation of the results (48) and (49).

Interactions between microbes are frequently observed and exhibit interesting phenomena [64, 75], 83]. Particularly for  $\beta$ -lactam antibiotics, collective dynamics fundamentally influence the antibiotic treatment [84], which cannot be covered in this work. However, any form of interaction depends upon the presence of other individuals to interact with and collective dynamics will be less expressed, if the population density is small.

Mathematically, we already have a fitness measure for the deterministic (large population) limit and furthermore find that that the survival probability increases geometrically in the population size. Clinically interesting phenomena, such as extinction or rescue events, thus emerge for small colonies. We therefore focus on this limit in the following analysis, justifying the assumption of independent stochastic replication of the bacteria.

We have seen that a general solution (60) of the population survival probability readily follows from the results of homogeneous subpopulations. We will therefore focus on the analysis of independent, homogeneous populations of size  $n_0$  with rates g, d and step like  $\eta(c)$ , i.e. we omit the index m.

We have now motivated to apply our known results from the simple birth and death process (equation (48) and (49)), to estimate the survival probability for one period of antibiotic treatment.

The full time dependency of the system is described by the step function  $\eta(c(t))$  (59), which has a single discontinuity at the MIC and is constant otherwise. Hence, the time

$$t_{\text{MIC}} = \frac{\ln\left(C\right)}{\alpha}$$

at which the antibiotic concentration drops to the MIC together with the period length  $\tau$  are the two important timescales of the stochastic model.

First, we consider a scenario where  $\tau \leq t_{\text{MIC}}$ , which is that the concentration never falls below the MIC. This describes a stochastic birth-death process with time independent rates g, d and  $\eta$ . Thus, (48) and (49) are the analytically exact results for the size distribution and the survival probability. Distinguishing the modes of action, we have

$$P_{\text{surv}}^{(>)}(\tau) = 1 - \left[ \frac{d \left( e^{(g-d-\eta_{\text{max}})\tau} - 1 \right)}{(g-\eta_{\text{max}}) e^{(g-d-\eta_{\text{max}})\tau} - d} \right]^{n_0}$$
 (61)

for biostatic treatment and

$$P_{\text{surv}}^{(>)}(\tau) = 1 - \left[ \frac{(d + \eta_{\text{max}}) \left( e^{(g - d - \eta_{\text{max}})\tau} - 1 \right)}{g e^{(g - d - \eta_{\text{max}})\tau} - d - \eta_{\text{max}}} \right]^{n_0}$$
 (62)

in the biocidal case. Here, the (>) superscript indicates that the solution describes "greater than MIC" conditions. Vice versa, (<) superscripts will describe "lower than MIC" concentrations in the following.

One can prove, that for  $\eta > 0$ , the expression (62) is always smaller than (61) (see appendix E.1) which is a first insight on the effect of the mode of action.

In order to illustrate the result, we will now choose some default parameters now, which we refer to as the *reference* or wild type strain in the following. For this strain we choose the natural rates g = 1 and d = 0.3 and the maximum effect of the antibiotic as  $\eta_{\text{max}} = 0.9$ . Furthermore, if not stated otherwise, we will always set our initial population to  $n_0 = 10$ . Figure 31 illustrates this result for both drug modes for the introduced reference strain.

It is already very insightful to note that the treatment efficacy depends on the type of antibiotic, since this was not predicted by the effective fitness. However, we can also find a far more general result. If we consider some agent that has the exact opposite effect of the antibiotic (negative  $\eta$ ) and demand that g > d, we find that

$$P_{\rm surv}^{cidal} > P_{\rm surv}^{static}$$

which is exactly the opposite as before. This relation is proven in appendix E.2. We can thus argue, that for any homogeneous bacterial population, that is described by the simple birth and death process with g > d, a change in the death rate will always have a greater impact than an equivalent change in the growth rate.

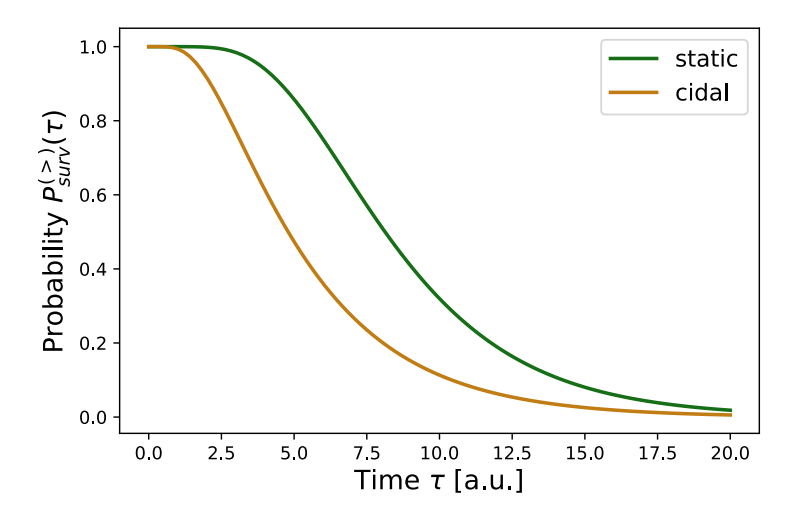


Figure 31: Survival Probability as a function of time for the "greater than MIC" regime, a positive  $\eta$  (antibiotic agent) and  $n_0 = 10$ . It is observed, that  $P_{\text{surv}}^{\text{cidal}} < P_{\text{surv}}^{\text{static}}$  for  $\tau > 0$ , but both curves eventually converge to zero for our reference strain with g = 1, d = 0.3 and  $\eta_{\rm max}=0.9$ . This convergence was already found in the discussion of the simple birth-death process (equation (52)).

This argument already hints at the antibiotic tolerance discussion, which we proceed in section 7.

Considering  $\tau \geq t_{\text{MIC}}$  now, we cannot directly apply the birth death result, since the stochastic rate  $\eta$  changes during the treatment. However, the step function separates the period into two separated regimes where the assumptions of the simple birth-death process hold. Accordingly, the total survival probability has the structure:

$$P_{\text{surv}}(\tau) = 1 - P \text{ [ext. in first phase]} - P \text{ [surv. in first phase]} P \text{ [Ext. in second phase]}$$

where the first phase corresponds to the regime above the MIC, and the second to the regime below it.

Again the first term is obtained directly from the simple birth-death process and we are left with finding an expression for the extinction probability in the second phase.

After time  $t = t_{\text{MIC}}$ , the size distribution  $P_n^{(>)}(t_{\text{MIC}}, n_0)$  is given by (48) and thus the extinction probability in the second phase writes as:

$$P_{\text{ext}}^{(<)}(\tau - t_{\text{MIC}}) = \sum_{n_{\text{MIC}}} P_0^{(<)}(\tau - t_{\text{MIC}}, n_{\text{MIC}}) P_{n_{\text{MIC}}}^{(>)}(t_{\text{MIC}}, n_0)$$
 (63)

$$P_{\text{ext}}^{(<)}(\tau - t_{\text{MIC}}) = \sum_{n_{\text{MIC}}} P_0^{(<)}(\tau - t_{\text{MIC}}, n_{\text{MIC}}) P_{n_{\text{MIC}}}^{(>)}(t_{\text{MIC}}, n_0)$$

$$= \sum_{n_{\text{MIC}}} \left[ \frac{d \left( e^{(g-d)(\tau - t_{\text{MIC}})} - 1 \right)}{g e^{(g-d)(\tau - t_{\text{MIC}})} - d} \right]^{n_{\text{MIC}}} P_n^{(>)}(t_{\text{MIC}}, n_0)$$
(63)

which is the probability that  $n_{\text{MIC}}$  individuals have survived the first phase and go extinct until the end of treatment.

Combining (61)/(62) and (64), we obtain a closed form for the survival probability if  $\tau > t_{\rm MIC}$ :

$$P_{\text{surv}}(\tau) = 1 - P_{\text{ext}}(\tau) \tag{65}$$

$$P_{\text{surv}}(\tau) = 1 - \left[ P_{\text{ext}}^{(>)}(t_{\text{MIC}}) + P_{\text{ext}}^{(<)}(\tau - t_{\text{MIC}}) \right].$$
 (66)

With this, we have found an exact expression for the survival probability as a function of the period length  $\tau$ .

However, the evaluation of (66) requires to determine the full probability distribution at time  $t = t_{\text{MIC}}$ , i.e. infinitely many computations of the sum in (48). Here, we will only consider the first k values of the probability mass function  $P_n(t_{\text{MIC}})$  such that:

$$\sum_{n=1}^{k} P_n(t_{\text{MIC}}) \ge \epsilon$$

where  $\epsilon \leq 1$  is some threshold value. If not stated otherwise, we will set  $\epsilon = 0.95$ . Apart from the repetitive sum evaluation, even the computation of a single value  $P_n(t_{\text{MIC}})$  becomes computationally unfeasible if n or  $n_0$  become large. But since we are interested in small populations, that effectively die when  $t < t_{\text{MIC}}$ , our setup inherently avoids this problem. Hence, evaluating (48) k times is feasible here.

The result for the wild type is shown in figure 32 again for both modes of action. Additionally to the pharmacodynamic parameters  $(g, d, \eta)$ , we have to assume a specific pharmacokinetic profile for this visualization. Here, we chose  $C = \frac{c_{\text{max}}}{MIC} = 15$ ,  $\alpha = 0.7 \, \text{time}^{-1}$  and therefore

$$t_{\rm mic} = \frac{\ln(C)}{\alpha} = 3.87 \,\mathrm{a.u.}$$

which is approximately at two thirds of the whole treatment period  $\tau = 6$  a.u..

### 5.5 The Survival Probability of Tolerant Mutants

The deterministic part of this work revealed, that distinct tolerance mutations increase the effective fitness. However, a crucial result of the biologically relevant trade-off model was, that tolerance is beneficial, only if the fraction  $\phi = \frac{\lambda_{\min}}{\lambda_{\max}}$  decreases. Here, we find a comparable result for the survival probability.

It has proven to be useful, to visualize the quantity of interest in a two dimensional topography of the tolerance phenotypes. In the stochastic model, these are the

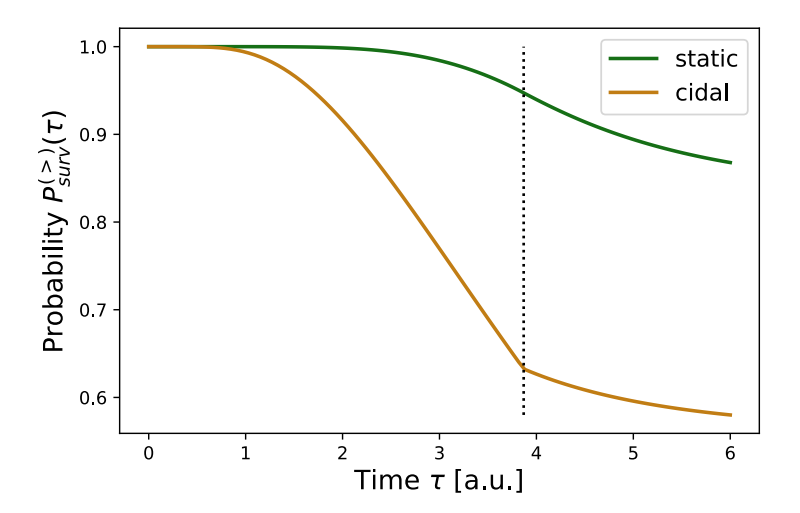


Figure 32: Survival Probability of  $n_0=10$  wild type bacteria as a function of time for the full period. The time where the MIC is reached by the concentration profile is indicated by the grey dots. It is again observed, that  $P_{\rm surv}^{\rm cidal} < P_{\rm surv}^{\rm static}$  for  $\tau>0$ . However, since we have g>d in the second phase, the  $\tau\to\infty$  limit of the survival probability in the second phase is  $1-\left(\frac{d}{g}\right)^{n_{\rm mic}}$  (by equation (52)). Essentially this limit is greater than zero.

growth rate g and the antibiotic susceptibility  $\eta_{\text{max}}$ .

For every possible pair of phenotypes we compute the survival probability at the end of one complete treatment period ( $\tau = 6 \, \text{t.u.}$ ) and visualize the result in a heat-map (figure 33).

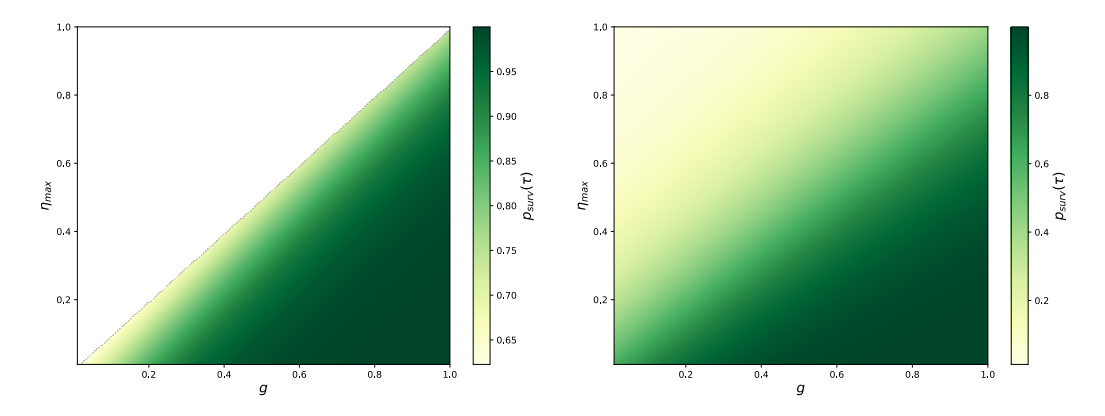


Figure 33: Heat maps of the survival probability for the tolerance trade-off phenotypes in the stochastic model (g and  $\eta_{\text{max}}$ ). The survival probability is computed for initial population sizes of  $N_0 = 10$  for the previously introduced PKPD model.

Left: Biostatic treatment. The upper triangular, where  $\eta_{\text{max}} > g$ , is neglected, since full growth inhibition is the best possible treatment.

Right: Biocidal treatment.

A comparison of key structural features in the landscape (such as the diagonal) indicates both quantitative and also qualitative differences between the two modes of action.

Unlike for the (normalized) effective fitness (figure 5), it is observed, that the survival probability of phenotypes with equal fraction  $\frac{\eta_{\text{max}}}{g}$  does not linearly relate. This observation becomes even more expressed, if we look at prolonged period times, here  $\tau = 20 \text{ t.u.}$ , in figure 34.

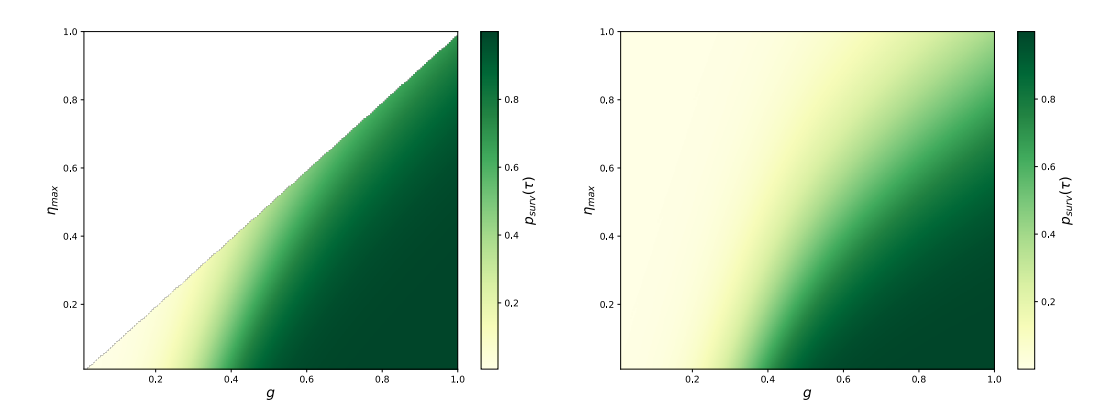


Figure 34: Heat maps of the survival probability for the tolerance trade-off phenotypes in the stochastic model (g and  $\eta_{\text{max}}$ ). The survival probability is computed for initial population sizes of  $N_0 = 10$  for a prolonged period time ( $\tau = 20 \, \text{t.u.}$ ). Other PKPD parameters remain unchanged.

Left: Biostatic treatment. The upper triangular, where  $\eta_{\text{max}} > g$ , is again neglected, since full growth inhibition is the best possible treatment.

Right: Biocidal treatment.

It is clearly observed, that the survival probability is not a constant for  $\frac{\eta_{\text{max}}}{g} = \text{const.}$  here.

However, this modified setup reveals, that the survival probability is a constant for some concave function  $\eta_{\text{max}}(g)$  with  $\frac{d}{dg}\eta_{\text{max}} > 1$ . Thus, in terms of the survival probability, a beneficial tolerant mutant has to increase its selective advantage (smaller  $\eta_{\text{max}}$ ) faster than linear in the cost (smaller g).

Here we choose  $g^{(\text{tol})} = 0.7 \,\text{time}^{-1}$  and  $\eta_{\text{max}}^{(tol)} = 0.4 \,\text{time}^{-1}$  while keeping the other PKPD parameters, especially also the death rate  $d^{(tol)}$  similar to the wild type. Repeating the survival probability analysis for the tolerant strain indicates, that tolerance is beneficial irrespective of the antibiotic mode of action (figure 35).

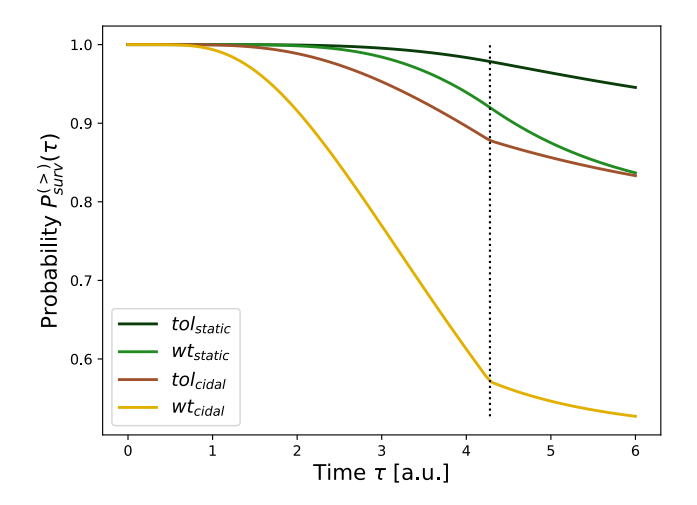


Figure 35: Survival Probability as a function of the period time  $\tau$  for the wild type and the tolerant mutant. For both modes of antibiotic action, tolerance increases the survival probability significantly. The grey dots indicate the transition from the super- to the sub-MIC regime.

### 6 Numerical Simulation of Periodic Treatment

In the previous section, we introduced the survival probability as an additional measure on some phenotype, to define its performance for one period of antibiotic stress. Assuming a mathematically modest step function dose-response curve, we were able to derive some insightful analytic results and showed that the type of antibiotic, as well as the bacterial phenotype, heavily influence the chance of survival.

In the following, we compare our previous findings to stochastic simulations. Using the well established Gillespie Algorithm [32] to implement time dependent population updates, we first verify our analytic results on the survival probability.

Later, we compare the stochastic model also to the effective fitness. Using large scale simulations, we show, that the deterministic description of a bacterial population becomes meaningful, when stochastic fluctuations are negligible.

Ultimately, by implementing a multi-genotype model, where we allow for mutations between the bacterial strains, we analyze how antibiotic tolerance can rescue a bacterial population from extinction.

### 6.1 Remarks on Competition

In section 5.4 we motivated, that any form of interaction between individuals is negligible, if population sizes are small. And we further derived an expression for the survival probability, if complete independence is guaranteed.

Therefore, we are interested to find an algorithm that is capable of describing extinction events for effectively independently replicating bacteria. However, we are eventually also interested to model rescue through tolerance evolution (section [7]).

If we were to assume complete independence among individuals, the rescuing strain, having a positive effective fitness, would grow unbounded over time. This not only poses computational challenges but also deviates significantly from biological reality, since competition for resources, for example space or nutrients, leads to logistic growth dynamics [33].

Therefore, we introduce an additional quantity K, the carrying capacity, in our numerical simulations. If not stated otherwise, we will assume that the competition affects the growth rate only (birth competition) and set K = 10000. Hence, the growth rate reads as:

$$g_{\text{comp}} = g \left( 1 - \frac{N}{K} \right).$$

For populations of size  $N_0 = 10$ , that we analyzed in section 5.4, the deviation in the growth rate is  $\approx 0.1 \%$  and the assumption of effective independence still holds.

In the following, we will immediately drop the subscript 'comp' again and always talk about g as the birth competition growth rate.

### 6.2 The Gillespie Algorithm

We use the Gillespie Algorithm [32] to model the stochastic population turnover of our periodic antibiotic treatment. This algorithm is exact for a continuous time process and capable of describing for example the number of bacteria  $N_i(t)$  of species i at time t. The birth and death process application has already been explored in previous studies [33] and we will modify the algorithm to simulate the periodic antibiotic dosing.

The most general system that is considered here includes two strains, a wild type (wt) and a tolerant mutant (tol), where mutations are assumed to occur only at birth events of the wt, where one of its offspring becomes a tol with probability  $q_{\text{mut}}$ .

Accordingly, we define  $k_{\text{tot}}$  as the sum of all possible transition rates at time t:

$$k_{\text{tot}}(t) = \underbrace{(g_{\text{wt}}(t) (1 - q_{\text{mut}}) + d_{\text{wt}}(t)) N_{\text{wt}}}_{wt \text{ turnover}} + \underbrace{(g_{\text{tol}}(t) + d_{\text{tol}}(t)) N_{\text{tol}}}_{tol \text{ turnover}} + \underbrace{(g_{\text{wt}}(t) q_{\text{mut}})) N_{\text{wt}}}_{wt \text{ mutation}}.$$

Furthermore, we define  $t_{\rm end}$  the end of treatment, which is in general different from the period length  $\tau$ .

Starting with some initial population size  $N_0 = (N_0^{(wt)}, N_0^{(tol)})$  at t = 0, we can iteratively update the size and time.

In each of these steps, we compute the growth and death rates of both subpopulations, according to equations (54), (55) and (59) for the respective mode of antibiotic action. Dividing these rates by the sum  $k_{\text{tot}}$  defines probabilities of the respective events. Note, that the birth of the wild type is separated into simple replication and mutation.

In one Gillespie-Step the next event is drawn from a uniform distribution with the according probabilities and the time increases by  $\Delta t \sim \exp(\frac{1}{k_{\rm tot}})$ . The birth, death or mutation event only executes if the environment is stable, i.e. when

$$\mod(t,\tau) < t_{\mathrm{MIC}} \quad \text{and} \quad \mod(t+\Delta t,\tau) \leq t_{\mathrm{MIC}}$$
 or 
$$\mod(t,\tau) \geq t_{\mathrm{MIC}} \quad \text{and} \quad \mod(t+\Delta t,\tau) \leq \tau.$$

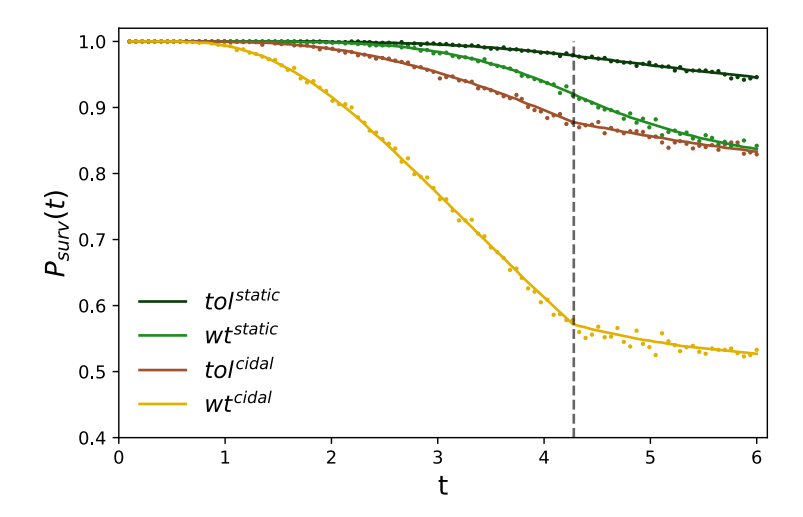


Figure 36: Survival Probability as a function of the period time  $\tau$  for the wild type and the tolerant mutant. Numerical results are visualized as dots around the theoretical expectation (solid lines). The grey dots indicate the transition from the super- to the sub-MIC regime. In all cases, the numerical and analytical results are in good agreement.

With the new time and population size, the update steps are repeated until the time has reached the end of treatment  $t_{\text{end}}$ .

# 6.3 Comparison of Simulations and the Survival Probability

In a first experiment, we want to quantify the survival probability in Gillespie simulations and compare to previous results. Accordingly, we choose  $t_{\rm end} = \tau$  for now. Moreover, since we are only interested in comparing homogeneous wt and tol populations here, we set the mutation probability to zero.

Running 2000 replicates of the respective wt and tol Gillespie simulation, we can check if any bacteria have survived after time  $\tau$  and compute the numerical survival probability as the arithmetic mean. Figure 36 summarizes the results for our previously introduces PKPD model and compares the empirical mean to the previous theoretical results from figure 35. We observe, that our numerical data is well described by the analytic predictions, validating our calculations and the Gillespie simulation.

### 6.4 Comparison of Simulations and the Effective Fitness

Until now, our stochastic model has focused on analyzing a single treatment period. We have shown, that results from the stochastic simulations are well described by the analytic results and found the survival probability as a useful quantity to describe how tolerance is beneficial. However, stochastic simulations over multiple periods are not yet discussed and will be the focus of this section. Moving away from the single period timescale, we are left with the effective fitness as our performance measure and we have to compare Gillespie simulations to the deterministic prediction.

We expect that stochastic deviations from the mean-field effective fitness description are important for small population sizes, particularly in the description of extinction events. However, these fluctuations are negligible in the limit  $N \to \infty$ . Thus, the Gillespie simulations are well predicted by the effective fitness, if the population size is large.

For the previously introduces reference strain, we can compute the effective fitness in the step function limit from equation (22), where we have  $\lambda_{\text{max}}$  and  $\lambda_{\text{min}}$  by (57) & (58). For initial population sizes  $N_0 = 10000$  and  $N_0 = 100$ , figure 37 visualizes the effective decrease in the wild type population for multiple treatment cycles. Note, that for this visualization we increased the carrying capacity to  $K = 10^7$  to neglect deviations from competition.

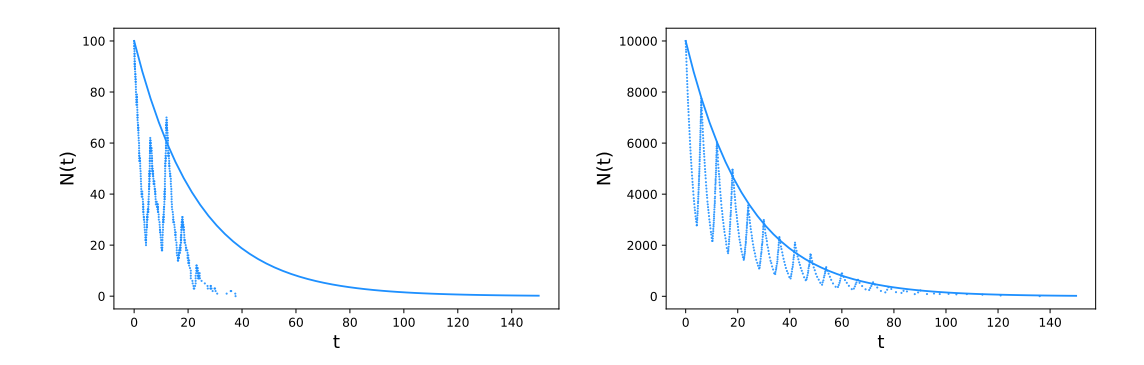


Figure 37: Time evolution of a wild type population of initial size  $N_0 = 100$  (*left*) and  $N_0 = 10000$  (*right*). A single replicate of a Gillespie simulation (blue dots) is shown together with the mean field expectation from the effective fitness (solid blue).

For large populations this mean field approximation is meaningful to describe the stochastic turnover of a bacterial population. However, for small populations stochastic fluctuations are relevant and the effective fitness fails to reliably describe the time evolution of the population size.

We observe, that Gillespie simulations follow the mean-field predictions for large populations, but significant deviations occur as the population size becomes smaller. Without further investigation, we have claimed, that our deterministic model does not describe small populations phenomena, such as extinction events, in a meaningful way. This is now ultimately proven here and justifies our discussion of a stochastic performance measure.

However, the mean field description becomes useful again, once we are interested in averages. For 500 replicates of a wild type simulation, we compute the average population size as a function of time for  $N_0 = 100$  and  $N_0 = 10000$ . Figure 38

illustrates, that the average and the effective fitness prediction align nicely.

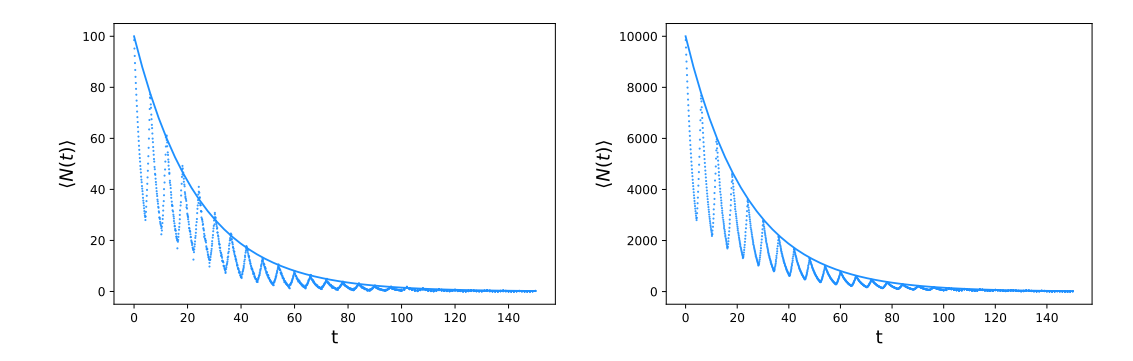


Figure 38: Mean time evolution of 500 wild type populations of initial size  $N_0 = 100 \ (left)$  and  $N_0 = 10000 \ (right)$ . The average of all Gillespie simulations (blue dots) is shown together with the mean field expectation from the effective fitness (solid blue). Comparing the results to figure [37] it is readily observed, that the deterministic prediction of the effective fitness well describes the average population size, particularly also for smaller  $N_0$ .

# 7 Population Rescue Through Antibiotic Tolerance

For the last part of this work we will move away from the analysis of clonal homogeneous bacterial populations and briefly discuss a more realistic scenario. We assume now, that our population consists of two phenotypes, a wild type and a tolerant mutant, which will be the same as in the previous section.

Assuming, that cell-cell interactions are still negligible, we can readily conclude form the multiplicative structure of the survival probability, that

$$P_{\mathrm{surv}}^{(wt)} < P_{\mathrm{surv}}^{(mixed)} < P_{\mathrm{surv}}^{(tol)}$$

holds. The presence of tolerant mutants is thus always beneficial for a wild type population.

However, the clinically relevant question, if tolerance can save a bacterial population from extinction and eventually evade the antibiotic treatment is yet unanswered. This question defines a typical rescue scenario, which is a central concern in evolutionary biology [34, 35].

We can readily check for the previously introduced tolerant mutant, that

$$\Lambda_{\mathrm{Step}}^{(wt)} < 0 < \Lambda_{\mathrm{Step}}^{(tol)}$$
.

holds for the effective fitness. Thus, a homogeneous wild type population will eventually go extinct for  $t \to \infty$ , while a tolerant population grows to the carrying capacity, once it has established.

Using Gillespie simulations, we quantify this establishment probability of a tolerant mutant numerically in two distinct scenarios: (1) Rescue through standing genetic variation without mutation and (2) rescue through de novo mutation.

## 7.1 Standing Genetic Variation

It has been shown in various studies, that standing genetic variation increases the probability of resistance establishment in suddenly changing environments [85, 86, 87]. Here, we analyze a similar scenario for antibiotic tolerance. We show that initial heterogeneity in the population can prevent extinction, even if the initial frequency of tolerant mutants is small.

For population sizes of  $N_0 = 100$  with different initial frequencies, we ask if the whole population has survived after 50 periods of antibiotic treatment. If so, the population counts as rescued. Otherwise it has gone extinct.

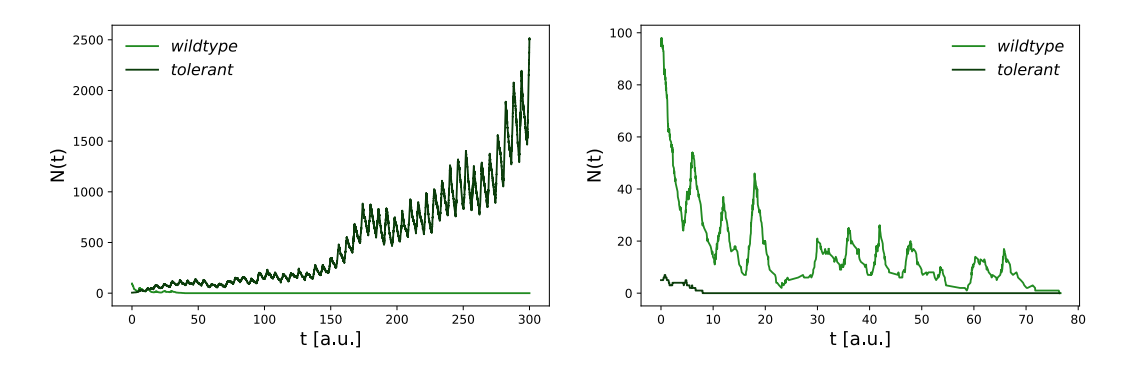


**Figure 39:** Time evolution of the population size for a heterogeneous population with  $N_0^{(wt)} = 95$  and  $N_0^{(wt)} = 5$ . The pharmacokinetic parameters remain unchanged, such that  $\tau = 6$  and  $t_{\text{MIC}} \approx 3.87 \, \text{a.u.}$ 

Left: The tolerant subpopulation survives at initially small size and establishes in the population.

Right: Both subpopulation eventually go extinct.

Both figures present a single Gillespie simulation of a 5% tolerant population under biostatic treatment. Note the different scales in the two panels.

The two scenarios are visualized in figure [39].

We repeat these Gillespie simulations for different frequencies of the tolerant mutant in a mixed population of  $N_0 = 100$  and evaluate the establishment probability numerically from 500 equivalent repetitions. A population is considered to be established, if it survived until  $t = 50 \tau$ , otherwise it has gone extinct at previous time  $t < 50 \tau$ . In the following, the probability of establishment is also called 'rescue probability'.

This quantity is now capable to measure the probability that clinical treatment fails after multiple drug applications, due to the presence of a tolerant mutant. Since the wild type eventually goes extinct by construction of the problem, the rescue probability crucially depends on the dynamics of the tolerant subpopulation (see figure [39]). If the subpopulation goes extinct in the beginning of the treatment, the rescue probability is zero in the absence of de novo mutations. Hence, the rescue probability crucially depends on the survival probability in the first treatment period, where the subpopulation size is small.

However, the extinction probability remains nonzero afterwards and thus several subsequent treatment periods contribute to the chance of long term rescue. The probability of these further extinction events crucially depends on the time for which the tolerant subpopulation remains small, which was termed the time at high risk by Gomulkiewicz and Holt [35]. The right plot in Figure [39] illustrates a case where the tolerant subpopulation becomes extinct during the second drug application.

Accordingly, the probability of rescue increases when the tolerant mutant reaches

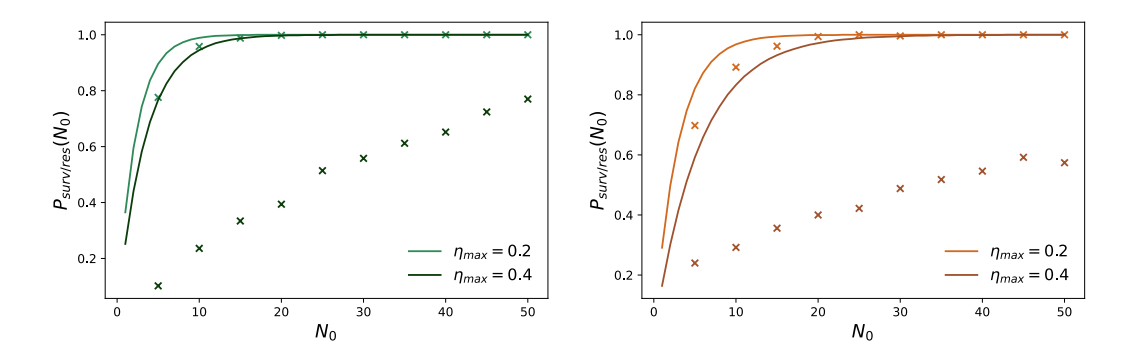


Figure 40: Comparison of the rescue probability (crossed markers) to the survival probability of the respective tolerant strain for biostatic (left) and biocidal (right) treatment. Additionally to our tolerant mutant ( $\eta_{\text{max}} = 0.4$ )), we illustrate a further rescue scenario with an *enhanced tolerant mutant* ( $\eta_{\text{max}} = 0.2$ ).

We observe that for the mutant with  $\eta_{\text{max}} = 0.4$ , the rescue probability deviates significantly from the survival probability, indicating that late-stage extinction events play a non-negligible role. However, as the effective fitness of the tolerant strain increases, the single-period survival probability provides an increasingly accurate approximation of the rescue probability.

a critical size quickly, i.e. if the effective fitness is large. In this sense, the rescue probability has contributions from both our discussed performance measures, the survival probability, and the effective fitness.

Figure 40 illustrates the numerically observed rescue probability for different initial frequencies of the tolerant mutant. The result is compared to the survival probability of a homogeneous tolerant population with the same initial size as the subpopulation in the heterogeneous case. Note, that rescue and survival probability have different timescales.

#### 7.2 De Novo Mutation

In the first part of this work, we discussed the genotypic TIL-model, explaining the evolution of antibiotic tolerance via mutation. In this model, we considered a bi-allelic genotype of L loci and evolutionary paths involved multiple sequential mutations, eventually also reverse mutations.

Here, we only consider two genotypes where mutation can happen from the wild type to the tolerant mutant in a single step. Mutations from the tolerant mutant to the wild type are not considered.

We model this dynamic in Gillespie simulations again, but we choose the mutation probability during the wild type replication as  $q_{\text{mut}} = 10^{-2}$  now. The initial tolerance frequency is set to zero, i.e. we start with a homogeneous wild type population.

Similar to the standing genetic variation, we can numerically evaluate the rescue probability from repeated simulations, where a single simulation is either extinct or rescued (see figure 41).

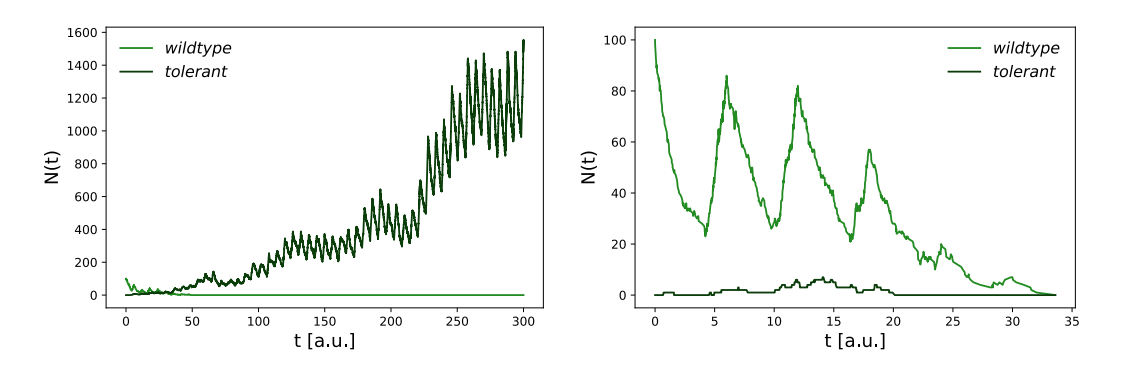


**Figure 41:** Time evolution of the population size for a heterogeneous population with  $N_0^{(wt)} = 100$ ,  $N_0^{(tol)} = 0$  and mutation probability  $q_{\text{mut}} = 10^{-2}$ .

Left: A tolerant mutant appears, survives at initially small size and establishes in the population.

Right: A tolerant mutant appears, but goes extinct again.

Both figures present a single Gillespie simulation under biostatic treatment. Note the different scales in the two panels.

In analogy to the discussion above, we evaluate the establishment after 50 drug applications and identify the rescue probability with 500 Gillespie replicates.

Since the probability of de novo tolerant mutants is nonzero, as long as the wild type population has not gone extinct, we cannot compare the rescue probability to the survival probability of a homogeneous subpopulation here.

Figure 42 visualizes the final result on the rescue probability for different mutation probabilities  $q_{\text{mut}}$  in the numerical Gillespie simulations.

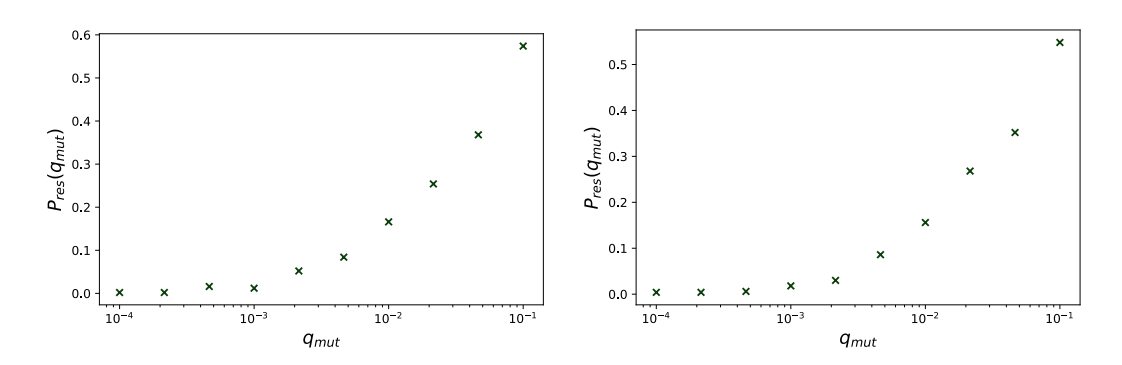


**Figure 42:** Rescue probability of a heterogeneous (initially homogeneous) population of  $N_0 = 100$  as a function of the mutation probability  $q_{\text{mut}}$ . Note that the x-axis is shown on a logarithmic scale.

Left: Biostatic treatment.

Right: Biocidal treatment.

Again, we note that both modes of antibiotic action seem qualitatively equivalent, however, the rescue probability is quantitatively higher for the biostatic treatment.

## 8 Discussion

#### 8.1 Conclusion

In the present work, we have explored how the size of a bacterial population evolves under periodic antibiotic treatment. Building up on the theory of Hill-shaped Dose Response Curves [20], we were interested to quantify the performance of different phenotypes in a time dependent concentration profile. Particularly, we introduced a simple exponential decay as a pharmacokinetic function, that alternates around the MIC.

For the purpose of this study, we devoted ourselves to the analysis of antibiotic tolerance. Following Brauner et al. [7], we defined tolerance as the ability to reduce the killing rate at high antibiotic concentrations.

Throughout this thesis, we assumed that any such tolerance mutation comes with a cost in the null fitness, while leaving the MIC unchanged. This was termed tolerance trade-off.

Within this work we introduced the effective fitness and the survival probability as two crucial measures of performance under periodic stress and demonstrated, that such tolerant mutants can have a selective advantage over the wild type. We concluded, that the presence or the development of tolerant mutants can potentially rescue a population from extinction and ultimately lead to treatment failure.

The effective fitness was discussed as the main result of the deterministic analysis. Integrating the dose-response curve over the exponential pharmacokinetic function, we were able to derive a closed form of the average replication rate over one period. For the two most discussed dose-response curves, the Hill- and the step-profile, it was discussed that the sign of the effective fitness essentially depends on the fraction between the maximum killing rate  $\lambda_{\min}$  and the null fitness  $\lambda_{\max}$ , assuming all the other parameters remain unchanged. Thus, a beneficial tolerance trade-off was found for phenotypes that decrease the fraction  $\phi$  compared to the wild type.

Based on this result, we used the model of trade-off induced fitness landscapes to assign genotypes with an effective fitness. Focusing on setups, where mutations with a beneficial trade-off can occur, we systematically analyzed the structure of the emerging fitness landscape. A crucial finding was, that the fitness rank order of the genotypes is conserved, if detrimental mutations, i.e. mutations that have  $\bar{\phi}^i > 1$ , cannot occur by construction. This guaranteed the peak accessibility for TIL models where  $\lambda^i_{\min}$  and  $\lambda^i_{\max}$  are chosen from non-overlapping uniform intervals.

Furthermore, running a naive random adaptive walk on the fitness graph revealed

the previously observed biphasic evolution, where non-optimal trade-offs are compensated by reverting certain mutations. Crucially, mutations along such paths were successively increasing the effective fitness, ultimately shifting it from negative to positive.

The effective fitness analysis revealed results for the average growth or death behavior of a large population for long treatment times. However, because the clinical goal is to eradicate pathogenic populations, we aimed to develop a stochastic framework in the second part of this thesis. Such a model captures simultaneous growth and death events on the timescale of a single treatment period and we were able to quantify extinction probabilities for small populations.

Instead of using the instantaneous net replication rates  $\lambda_{\min}$  and  $\lambda_{\max}$ , this model describes population dynamics more precisely through a growth rate g, a death rate d, and an antibiotic-induced killing rate  $\eta$ . We distinguished between biocidal and biostatic interpretations of  $\eta$ .

Using previous results on the simple birth-death process and a step like dose-response curve, we derived an analytically exact solution of the extinction probability for one period of treatment. This result revealed that tolerance, which is understood as a simultaneous reduction of g and  $\eta$  here, can increase the probability of survival. This remained true irrespective of the mode of antibiotic action. The analytical predictions were validated through numerical Gillespie simulations, demonstrating excellent agreement.

Moreover, the Gillespie algorithm provides a measure on the rescue probability of a small heterogeneous populations. Since this is a stochastic process over multiple treatment periods, neither the effective fitness, nor the presented survival probability is capable of describing rescue scenarios. However, it was discussed, that high survival probabilities and a large effective fitness correlate with high rescue probabilities.

Thus, the analysis on the rescue probability combines both central quantities of this work, describing clinically relevant scenarios of evolutionary rescue. This measure was numerically analyzed in two fundamentally different setups and we could determine some rescue enhancing parameters. However, a rigorous analytic derivation on the rescue probability remains for future work and is briefly discussed in section 8.2.3.

#### 8.2 Outlook

### 8.2.1 Modified Gillespie Algorithm

Our stochastic birth and death model considers that waiting times until the next event are exponentially distributed. In a system where the death rate is zero and no antibiotic is present, the division probability of any cell is the highest immediately after the previous birth event. Because of this assumption, our considered model is markovian. However, this is far from biological reality, since the cell cycle is generally history dependent, i.e. the cell has to synthesize DNA and grow in size upon division. Thus, the empirically observed distribution of cell cycle times significantly deviates from a simple exponential distribution [88].

Nevertheless, it is desirable to restrict ourselves to markovian systems of moderate mathematical complexity. Therefore, previous studies proposed to model multi stage division processes, where any cell cycle consists of multiple subsequent exponentially distributed waiting times [88]. In the simplest case of two stages, we interpret this as a first phase of maturation and a second phase of division. Accordingly, young cells have to spend some time growing upon replication.

This feature could be implemented in our Gillespie algorithm if we expand the number states and consider two distinct types, a mature and an immature, of every phenotype. An immature cell would then grow to a mature cell of the same phenotype, while mature cells divide or mutate into the immature state. Every such type would then again have the Markov property and performs the next event after exponentially distributed waiting times.

Other studies have proposed novel Gillespie algorithms for non-markovian stochastic processes [89, 90], where general hyperexponential waiting time distributions [88] can be implemented directly.

#### 8.2.2 Biphasic Evolution in the Stochastic Model

In section 3 we applied a previously established model on trade-off induced fitness landscapes 29 to the effective fitness and thoroughly discussed the evolution of antibiotic tolerance. We have seen, that evolutionary paths on the emerging fitness landscapes exhibit a characteristic biphasic behavior. We interpret such paths as cost-compensating, where non-optimal trade-offs are reversed in the late stage of evolution. Furthermore, we showed, that the number of mutational steps is in general large.

However, our stochastic model operates on a much simpler landscape, where only two genotypes, the wild type and a single *tolerant mutant*, are considered. Essentially, this describes the limit of a single peak landscape, where genotypes that are not a fitness peak have very large mutation probabilities. Thus, the

fitness peak is readily found by the evolution.

A more sophisticated stochastic model would consider a third strain, the *tolerant-compensated mutant*, that has compensated some of the cost in the growth rate g. This accounts for the cost-compensating characteristic in the evolution on trade-off induced landscapes and would have an influence on the rescue probability of a general heterogeneous population.

In the context of resistance evolution, a stochastic model of cost compensation has been analyzed in previous studies [91].

#### 8.2.3 Analytic Results on the Rescue Probability

In section 5 we introduced the survival probability as a novel quantity to measure the performance of some phenotype. Throughout this section, we considered a single dose of antibiotic and presented the survival probability as a function of the period time  $\tau$ . However, we cannot readily extent the result to multiple successive treatment periods, since the survival probability in the k-th period depends on the population size  $n_{k-1}$  at the end of the previous period. This would require to know the propagator of the probability vector  $\mathbf{p_n} = (p_0, p_1, \dots, p_N)$ , which, to my knowledge, has not been derived.

Nevertheless, we discussed the rescue probability, which is nothing but the survival probability after multiple drug cycles, in numerical Gillespie simulations (see section 6). However, we did not obtain a closed-form analytical expression for the survival probability in this work.

We already mentioned, that Alexander 54 computed the survival probability in the long time limit for the Hill function PKPD model. Using standard results on the general, particularly time independent birth-death process 30, 92, we can find the extinction probability of a single individual at time t as:

$$P_{\text{ext}}(t) = \frac{G(t)}{1 + G(t)} \tag{67}$$

where

$$G(t) = \int_0^t d(t') \exp\left[\int_0^{t'} (g(t'') - d(t'') - \eta(t'')) dt''\right] dt'.$$
 (68)

We note, that the term in the exponential is nothing but the time integral of the dose-response curve and closely relates to the well discussed effective fitness. However, evaluating this integral remains challenging.

In the limit of infinitely many completed cycles of antibiotic dosing, Alexander evaluated (68) for the Hill function PKPD model [86].

Since the effective fitness is also known for the step function, evaluating (68) should be feasible. This allows for an analytical derivation of the rescue prob-

ability in a heterogeneous population without mutation, as discussed in Section [7.1], which can then be compared to results obtained from Gillespie simulations. Unfortunately, a suitable analytical measure for processes involving mutation remains largely unavailable.

#### 8.2.4 First Passage Times

In section 7.2 we have discussed the model of rescue through de novo mutation. It is generally hard to obtain analytical results on the probability distribution here, since the mutation probability couples the previously independent differential equations of both subpopulations. However, if the mutation probability is small, i.e. there is at most one mutation before the wild type population goes extinct, the establishment of a tolerant population will depend only on the probability that a single tolerant mutant rescues the whole population, given that this mutant appears before the wild type population goes extinct.

It is therefore desirable to quantify the mean first passage time of the n=0 state for a wild type population. Previous studies investigated this for a special case with certain constraints on the sum  $\lambda = b - d$  [93], or for constant population size [91]. However, for the general time inhomogeneous birth-death process, deriving the first passage time of extinction remains for future research.

# A Remarks on the Dose-Response Curve and the Effective Fitness

## A.1 Reformulation of the Dose-Response Curve

We have the dose-response curve

$$\lambda(c(t)) = \lambda_{max} - k \frac{c^{\nu}}{K_m^{\ \nu} + c^{\nu}} \tag{69}$$

with apparent growth rate  $\lambda_{max}$ , drug-cell reaction rate k, antibiotic concentration c (in general time dependent) and Michaelis-Menten saturation constant  $K_m$ . We note, that for high concentrations ( $c \gg K_m$ ) the DRC saturates to the maximal possible death rate ( $-\lambda_{min}$ ) (where the "-" sign is convention). Hence,

$$\lambda(c \gg K_m) = -\lambda_{min} = \lambda_{max} - k.$$

Furthermore, the saturation constant  $K_m$  can be described as a function of the MIC:

$$K_m^{\ \nu} = a\,MIC^{\nu}$$

and we determine a, such that  $\lambda(MIC) \stackrel{!}{=} 0$  [20]:

$$0 = \lambda_{max} - (\lambda_{max} + \lambda_{min}) \frac{MIC^{\nu}}{a MIC^{\nu} + MIC^{\nu}}$$

$$\iff \frac{\lambda_{max} + \lambda_{min}}{\lambda_{max}} = a + 1$$

$$\iff a = \frac{\lambda_{min}}{\lambda_{max}}$$

Given this result, equation (69) becomes:

$$\lambda(c(t)) = \lambda_{max} - (\lambda_{max} + \lambda_{min}) \frac{c^{\nu}}{\frac{\lambda_{min}}{\lambda_{max}} MIC^{\nu} + c^{\nu}}$$
 (70)

$$\lambda(c(t)) = \lambda_{max} - (\lambda_{max} + \lambda_{min}) \frac{\left(\frac{c}{MIC}\right)^{\nu}}{\left(\frac{c}{MIC}\right)^{\nu} + \frac{\lambda_{\min}}{\lambda_{\max}}}.$$
 (71)

## A.2 Analytic Solution of the DRC Integral

The Integral of the dose-response curve is introduced as  $\tilde{\Lambda}$ . For the Hill type DRC

$$\lambda_{\text{Hill}}(c(t)) = \lambda_{max} - (\lambda_{max} + \lambda_{min}) \frac{\left(\frac{c(t)}{MIC}\right)^{\nu}}{\left(\frac{c(t)}{MIC}\right)^{\nu} + \frac{\lambda_{\min}}{\lambda_{\max}}}$$

together with a simple exponential concentration profile

$$c(t) = c_{\text{max}} e^{-\alpha (t - t_0)}$$

and  $0 < t \le \tau$  the integral becomes

$$\begin{split} \tilde{\Lambda}(t) &= \int_{t_0}^{t_0+t} \lambda(c(t'))dt' \\ &= \lambda_{\max} t - (\lambda_{\max} + \lambda_{\min}) \, C^{\nu} \int_{t_0}^{t_0+t} dt' \frac{e^{-\alpha \nu (t_0-t')}}{C^{\nu} \, e^{-\alpha \nu (t_0-t')} + \frac{\lambda_{\min}}{\lambda_{\max}}} \end{split}$$

with  $C = \frac{c_{\text{max}}}{MIC}$ .

We now substitute:

$$u = C^{\nu} e^{-\alpha \nu (t_0 - t')} + \frac{\lambda_{\min}}{\lambda_{\max}}$$

which leaves us with

$$\tilde{\Lambda}(t) = \lambda_{\max} t - \frac{(\lambda_{\max} + \lambda_{\min})}{-\alpha \nu} \int_{u(t_0)}^{u(t_0+t)} du \, \frac{1}{u}.$$

This is a standard integral to solve and yields

$$\tilde{\Lambda}(t) = \lambda_{\max} t + \frac{\lambda_{\max} (1 + \phi)}{\alpha \nu} \ln \left( \frac{C^{\nu} e^{-\alpha \nu t} + \phi}{C^{\nu} + \phi} \right)$$

where  $\phi = \frac{\lambda_{\min}}{\lambda_{\max}}$  was introduced. Notably, the result is independent of  $t_0$ , since the treatment efficacy should (naively) not depend on the starting point of the treatment.

## A.3 Limits of the Effective Fitness

In this part, different limits of the presented effective fitness

$$\Lambda_{\text{Hill}}(\tau) = \lambda_{\text{max}} \left[ 1 + \frac{(1+\phi)}{\nu \alpha \tau} \ln \left( \frac{C^{\nu} e^{-\nu \alpha \tau} + \phi}{C^{\nu} + \phi} \right) \right]$$
 (72)

are discussed in more detail. However, this section focuses on the analytic perspective of the problem, while more illustrative interpretations are provided in the main text.

#### A.3.1 On the Pharmacokinetic Parameter $\tilde{\alpha}$

The limit of  $\tilde{\alpha} \to \infty$ :

$$\lim_{\tilde{\alpha} \to \infty} \Lambda_{\text{Hill}} = \lambda_{\text{max}} \left[ 1 + \underbrace{\lim_{\tilde{\alpha} \to \infty} \frac{(1+\phi)}{\nu \, \tilde{\alpha}} \, \ln\left(\frac{C^{\nu} e^{-\nu \, \tilde{\alpha}} + \phi}{C^{\nu} + \phi}\right)}_{=0} \right]$$
$$= \lambda_{\text{max}}$$

The limit of  $\tilde{\alpha} \to 0$ :

$$\begin{split} \lim_{\tilde{\alpha} \to 0} \Lambda_{\mathrm{Hill}} &= \lambda_{\mathrm{max}} \left[ 1 + \lim_{\tilde{\alpha} \to 0} \frac{(1+\phi)}{\nu \, \tilde{\alpha}} \, \ln \left( \frac{C^{\nu} e^{-\nu \, \tilde{\alpha}} + \phi}{C^{\nu} + \phi} \right) \right] \\ &\stackrel{\mathrm{L' \; Hospital}}{=} \lambda_{\mathrm{max}} \left[ 1 + \frac{(1+\phi)}{\nu} \lim_{\tilde{\alpha} \to 0} \frac{-\nu \, C^{\nu} \, e^{-\tilde{\alpha} \, \nu}}{C^{\nu} \, e^{-\tilde{\alpha} \, \nu} + \phi} \right] \\ &= \lambda_{\mathrm{max}} \left[ 1 + \frac{C^{\nu} (1+\phi)}{C^{\nu} + \phi} \right] \end{split}$$

#### A.3.2 On the Hill Exponent $\nu$

Here, the limit of  $\nu \to 0$  is not very meaningful, since the dose-response curve (71) will be zero everywhere in this case. Hence, only the case  $\nu \to \infty$  is discussed:

$$\lim_{\nu \to \infty} \Lambda_{\text{Hill}} = \lambda_{\text{max}} \left[ 1 + \underbrace{\lim_{\nu \to \infty} \frac{(1+\phi)}{\nu \, \tilde{\alpha}} \, \left( \ln \left( C^{\nu} e^{-\nu \, \tilde{\alpha}} + \phi \right) - \ln \left( C^{\nu} + \phi \right) \right)}_{(\star)} \right] \tag{73}$$

The limit will depend on the value of  $C e^{-\tilde{\alpha}}$  and we have to distinguish  $C e^{-\tilde{\alpha}} \leq 1$  (A) and  $C e^{-\tilde{\alpha}} > 1$  (B). Furthermore it is considered, that C > 1, i.e. the initial concentration is bigger than the MIC.

For Case A the first term of  $(\star)$  vanishes and we are left with:

$$\begin{split} \lim_{\nu \to \infty} \Lambda_{\mathrm{Hill}} &= \lambda_{\mathrm{max}} \left[ 1 - \lim_{\nu \to \infty} \frac{(1 + \phi)}{\nu \, \tilde{\alpha}} \, \ln \left( C^{\nu} + \phi \right) \right] \\ &= \lambda_{\mathrm{max}} \left[ 1 - \lim_{\nu \to \infty} \frac{(1 + \phi)}{\nu \, \tilde{\alpha}} \, \left( \nu \ln(C) + \underbrace{\ln \left( 1 + \frac{\phi}{C^{\nu}} \right)}_{\to 0} \right) \right] \\ &= \lambda_{\mathrm{max}} \left[ 1 - \frac{1 + \phi}{\tilde{\alpha}} \, \ln \left( C \right) \right] \end{split}$$

For Case B, we will also factorize the terms inside the logarithm and write them as a sum:

$$(\star) = \lim_{\nu \to \infty} \frac{(1+\phi)}{\nu \,\tilde{\alpha}} \left( \nu \, \ln\left(C \, e^{-\tilde{\alpha}}\right) + \underbrace{\ln\left(1 + \frac{\phi}{C^{\nu} \, e^{-\nu \,\tilde{\alpha}}}\right)}_{\to 0} - \nu \ln(C) - \underbrace{\ln\left(1 + \frac{\phi}{C^{\nu}}\right)}_{\to 0} \right)$$

$$= \frac{(1+\phi)}{\tilde{\alpha}} \left( \ln(C) - \tilde{\alpha} - \ln(C) \right)$$

$$= 1 + \phi$$

If we now plug this result back into (73), we obtain:

$$\lim_{\nu \to \infty} \Lambda_{\text{Hill}} = -\lambda_{\text{min}} \tag{74}$$

Hence:

$$\lim_{\nu \to \infty} \Lambda_{\text{Hill}} = \begin{cases} \lambda_{\text{max}} \left( 1 - \frac{1+\phi}{\tilde{\alpha}} \ln \left( C \right) \right) & \text{for } \tilde{\alpha} \ge \ln(C) \\ -\lambda_{\text{min}} & \text{for } \tilde{\alpha} < \ln(C) \end{cases}$$
 (75)

## A.4 Derivation of Effective Fitness for the Step DRC

We start with the presented step profile:

$$\lambda_{\text{step}} = \begin{cases} \lambda_{\text{max}} & \text{for } c(t) < MIC \\ -\lambda_{\text{min}} & \text{for } c(t) > MIC \end{cases}$$
 (76)

and integrate this function over one period of length  $\tau$ :

$$\tilde{\Lambda}_{\text{Step}}(\tau) = \int_{t_0}^{t_0 + \tau} \lambda_{\text{step}}(c(t'))dt'$$
(77)

We assume the familiar simple exponential profile for the pharmacokinetics:

$$c(t) = c_{\text{max}} e^{-\alpha t}.$$

If it is again assumed, that the initial concentration is bigger than the MIC (C > 1), we only distinguish two scenarios:

**Scenario A:** The concentration is higher than the MIC over the whole period length  $\tau$ . This is the case, if

$$\tau < t_{\rm MIC} = \frac{1}{\alpha} \ln \left( \frac{c_{\rm max}}{MIC} \right) \tag{78}$$

$$\Leftrightarrow \quad \tilde{\alpha} < \ln(C) \tag{79}$$

where  $t_{\rm MIC}$  is the time at which the concentration dropped to the MIC and  $\tilde{\alpha} = \alpha \tau$  as before.

For this case, the solution of the integral is trivial and we compute:

$$\tilde{\Lambda}_{\mathrm{Step}}(\tau) = -\lambda_{\min} \, \tau$$

Scenario B: The concentration drops below the MIC at time  $t_{\text{MIC}} < \tau$ . Hence, the integral (77) can be written as:

$$\begin{split} \tilde{\Lambda}_{\text{Step}}(\tau) &= -\int_{t_0}^{t_0 + t_{\text{MIC}}} \lambda_{\text{min}} dt' + \int_{t_0 + t_{\text{MIC}}}^{t_0 + \tau} \lambda_{\text{max}} dt' \\ &= \lambda_{\text{max}} \left( \tau - t_{\text{MIC}} \right) - \lambda_{\text{min}} \, t_{\text{MIC}} \\ &= \lambda_{\text{max}} \, \tau - \left( \lambda_{\text{max}} + \lambda_{\text{min}} \right) \frac{1}{\alpha} \, \ln \left( \frac{c_{\text{max}}}{MIC} \right) \\ &= \lambda_{\text{max}} \left( \tau - \frac{1 + \phi}{\alpha} \ln(C) \right) \end{split}$$

Summarizing the two discussed scenarios, one obtains:

$$\Lambda_{\text{step}} = \frac{1}{\tau} \tilde{\Lambda}_{\text{Step}}(\tau) = \begin{cases} \lambda_{\text{max}} \left( 1 - \frac{1+\phi}{\alpha \tau} \ln \left( C \right) \right) & \text{for } \tilde{\alpha} \ge \ln(C) \\ -\lambda_{\text{min}} & \text{for } \tilde{\alpha} < \ln(C) \end{cases}$$
(80)

which is the same as (75).

# A.5 Analysis on the Normalized Effective Fitness as a Function of $\kappa$

In this section, some of the main results of the  $\kappa$  dependency of the effective fitness are proven.

## A.5.1 The Limit of Large Death Rates $(\kappa \to \infty)$

We start with (27):

$$\frac{\Lambda_{\rm Hill}}{\lambda_{\rm max}}\left(\kappa\right) = 1 + \frac{\left(1+\kappa\right)}{\nu\,\tilde{\alpha}}\,\ln\left(\frac{C^{\nu}e^{-\nu\,\tilde{\alpha}}+\kappa}{C^{\nu}+\kappa}\right)$$

We take  $\kappa \to \infty$  now and obtain:

$$\lim_{\kappa \to \infty} \frac{\Lambda_{\text{Hill}}}{\lambda_{\text{max}}} (\kappa) = 1 + \frac{1}{\nu \,\tilde{\alpha}} \lim_{\kappa \to \infty} \frac{\ln \left( \frac{C^{\nu} e^{-\nu \,\tilde{\alpha}} + \kappa}{C^{\nu} + \kappa} \right)}{\frac{1}{(1+\kappa)}}$$

$$\stackrel{\text{L' Hospital}}{=} 1 - \frac{C^{\nu} \left( 1 - e^{-\nu \,\tilde{\alpha}} \right)}{\nu \,\tilde{\alpha}} \underbrace{\lim_{\kappa \to \infty} \frac{\left( 1 + \kappa \right)^2}{\left( C^{\nu} e^{-\nu \,\tilde{\alpha}} + \kappa \right) \left( C^{\nu} + \kappa \right)}_{\to 1}$$

$$= 1 + \frac{C^{\nu}}{\tilde{\alpha} \, \nu} \left( e^{-\tilde{\alpha} \, \nu} - 1 \right)$$

#### A.5.2 What Happens for Finite $\kappa$

In the main part 2.4.4 it was argued, that the effective fitness (27) has a maximum point and we want to show now, that this maximum is unique, if

$$\frac{e^{\tilde{\alpha}\nu} - 1}{\tilde{\alpha}\nu C^{\nu}} - 1 > 0 \tag{81}$$

and

$$1 + \frac{C^{\nu}}{\tilde{\alpha}\,\nu} \left( e^{-\tilde{\alpha}\,\nu} - 1 \right) < 0 \tag{82}$$

holds. So lets assume (81) and (82). In this case, the effective fitness is positive (negative) for some small (large)  $\kappa$  and thus has a second zero point  $\kappa_0 \in [0, \infty)$  and there exists at least one extrema (maximum).

We furthermore compute, that the second derivative

$$\frac{\partial^{2}}{\partial\kappa^{2}}\frac{\Lambda_{\mathrm{Hill}}}{\lambda_{\mathrm{max}}}\left(\kappa\right) = \frac{\left(e^{\tilde{\alpha}\nu}-1\right)C^{\nu}\left(-2\kappa e^{\tilde{\alpha}\nu}+2C^{2\nu}+\left(\kappa-1\right)\left(e^{\tilde{\alpha}\nu}+1\right)C^{\nu}\right)}{\tilde{\alpha}\nu\left(C^{\nu}+\kappa\right)^{2}\left(\kappa e^{\tilde{\alpha}\nu}+C^{\nu}\right)^{2}}$$

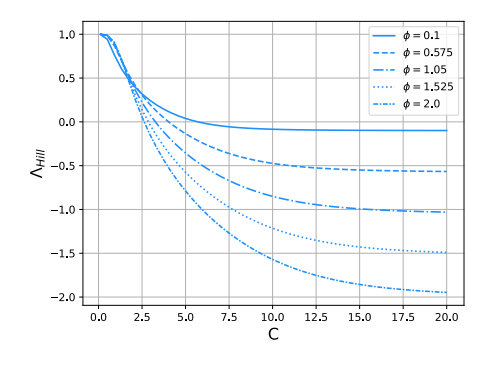
becomes zero for

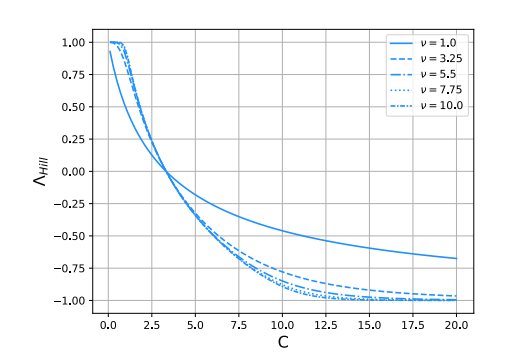
$$\kappa_{\text{crit}} = \frac{C^{\nu} \left( e^{\tilde{\alpha}\nu} - 2C^{\nu} + 1 \right)}{\left( e^{\tilde{\alpha}\nu} + 1 \right) C^{\nu} - 2e^{\tilde{\alpha}\nu}} \tag{83}$$

which means, that the effective fitness is concave for  $\kappa \in (0, \kappa_{\rm crit})$  and convex otherwise. Since this is the only solution to  $\frac{\partial^2}{\partial \kappa^2} \frac{\Lambda_{\rm Hill}}{\lambda_{\rm max}}(\kappa) = 0$ , one concludes, that the effective fitness has a maximum at some  $\kappa \in (0, \kappa_{\rm crit})$  and the effective fitness converges to the limit from above:

$$\lim_{\kappa \to \infty} \frac{\Lambda_{\rm Hill}}{\lambda_{\rm max}} \left( \kappa \right) = 1 + \frac{C^{\nu}}{\tilde{\alpha} \, \nu} \left( e^{-\tilde{\alpha} \, \nu} - 1 \right)$$

## A.6 The Effective Fitness Under Changes of the MIC





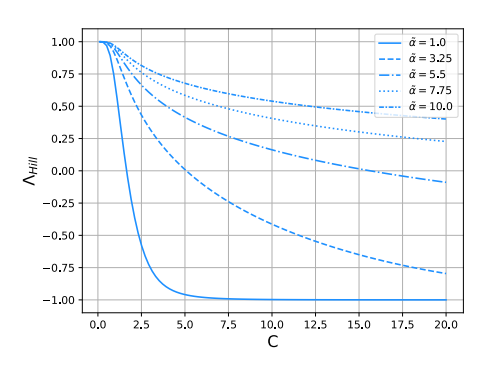


Figure A.1: Visualization of the effective fitness  $\Lambda_{\rm Hill}$  as a function of the resistance parameter C in different environments. If not varied, the system parameters are set to:  $\lambda_{\rm min} = \lambda_{\rm max} = 1$ ,  $\tilde{\alpha} = 2.4$  and  $\nu = 4$ . Note, that the variation in  $\phi$  (upper left plot) is induced be a variation in  $\lambda_{\rm min}$  while  $\lambda_{\rm max} = 1$  is kept constant. Hence,  $\phi = \lambda_{\rm min}$  here.

For every choice of parameters we observe, that the effective fitness is a monotonically decreasing function in C and converges to the maximum death rate  $-\lambda_{\min}$  (or  $\phi$  in the upper left plot).

## B Remarks on the TIL Model

## B.1 Proof of the Ordering-Accessibility Equivalence

In the accessibility analysis of the general TIL landscapes in the main text (section 3.3.2), we argued that these landscapes are not accessible, because they do not fulfill the ordering condition. For this argument to hold, we need to prove at least, that the ordering condition from 29 is necessary for the subset-superset accessibility property. However, since we already know that the ordering condition is sufficient 29, we can directly prove the equivalence.

Therefore let us consider a general fitness graph  $\mathcal{F} \equiv \mathbb{H}_2^L$  of genotypes  $\boldsymbol{\sigma}$ . Let us denote any additional mutation in the i-th locus by  $\Delta_i$ . Thus, in the example of L=4, we have  $\Delta_3 \boldsymbol{\sigma} = \{1,3\}$  for  $\boldsymbol{\sigma} = \{1\}$  and  $\boldsymbol{\sigma} \subset \Delta_i \boldsymbol{\sigma} \ \forall i$ . The symbol  $\Delta_{ij}$  indicates a mutation in the i-th and in the j-th locus.

In order to prove, that  $\mathcal{F}$  has the ordering condition, if it has the subset-superset accessibility property, we show the opposite. So lets assume, that  $\mathcal{F}$  does not have the ordering condition. Considering a general two face of  $\mathcal{F}$ , our assumption implies, that at least one of the following statements is fulfilled:

- 1. We can find a two-face, where the double mutant is the fittest genotype and the background genotype is not the least fit.
- 2. We can find a two-face, where the background genotype is the fittest and the double mutant is not the least fit.

Note, that the ordering condition does not make a statement about two-faces where one of the single mutants has the highest fitness.

In both of the above cases, at least one of the single mutant has to be less fit than the background (1.) or the double mutant (2.). This immediately breaks the accessibility of the fittest genotype through all direct paths from its subset (1.) or superset (2.) respectively.

If the fittest genotype of the two-face is also a fitness peak of  $\mathcal{F}$ , our statement already follows. If the fittest genotype of the two-face is not a fitness peak of  $\mathcal{F}$ , it must be in the sub-or superset of at least one fitness peak of  $\mathcal{F}$  [69]. However, since the previously analyzed two-face also has to be in the sub- or superset of these fitness peaks, the subset-superset accessibility property is also violated.

Accordingly, we have shown, that any fitness graph  $\mathcal{F}$  that does not have the ordering condition also does not have the subset-superset accessibility property. Thus, the ordering condition is a necessary condition for the accessibility to hold and together with the argument from [29] the equivalence follows.

# B.2 Results for Trade-Off Landscapes with 4 Loci and Constant Variance

In the main text (figure 3.3.2) the average number of peaks and the accessibility property has been analyzed as a function of the average trade-off  $\langle \phi^i \rangle$  for  $\hat{\mu}_{\min}$ . Here, we show the results for different choices of the  $\lambda_{\max}$  interval.

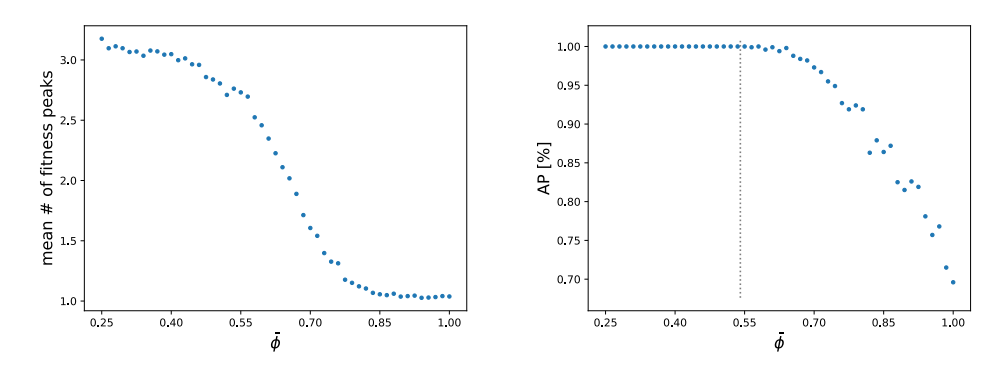
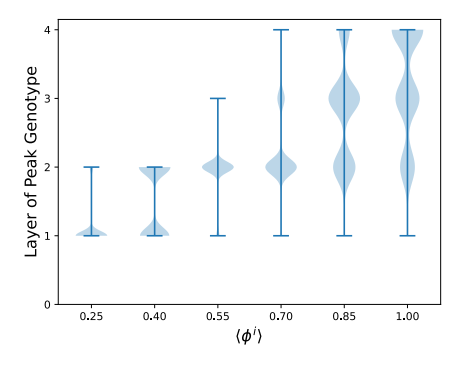


Figure B.1: Mean number of peaks (left) and percent of AP-fulfilling landscapes (right) as functions of the associated trade-off. Every point represents an average over 500 realizations on every setup. Each setup has  $\lambda_{\max} \in [0.7, 1.0)$  and therefore  $\langle \phi^i \rangle = \frac{\langle \lambda_{\min} \rangle}{0.85}$ .



**Figure B.2:** Violin Plot of the peak genotype layer for five exemplary setups. Each setup has  $\lambda_{\text{max}} \in [0.7, 1.0)$  and therefore  $\langle \phi^i \rangle = \frac{\langle \lambda_{\text{min}} \rangle}{0.85}$ .

### B.3 Normalization of the Fitness Peak Count

We already discussed in the main text, that large systems will have many genotypes with large topological distance to the high fitness layer. The number of such peaks increases non-linearly with the system size, since every layer of n mutations consists of  $\binom{L}{n}$  genotypes. Therefore, we would severely overestimate the number of fitness peaks, if we assume that the number of peaks grows proportional to the system size.

Therefore, we include a probability mass function (pmf), estimating the number of genotypes relevant for fitness peaks  $n_{\rm rel}$ . This pmf is obtained numerically from

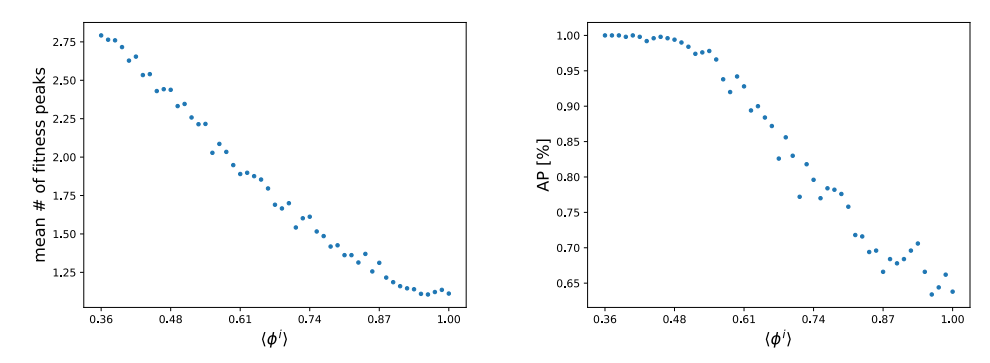
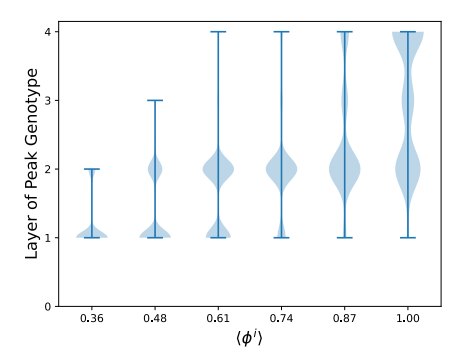


Figure B.3: Mean number of peaks (left) and percent of AP-fulfilling landscapes (right) as functions of the associated trade-off. Every point represents an average over 500 realizations on every setup. Each setup has  $\lambda_{\text{max}} \in [0.3, 0.6)$  and therefore  $\langle \phi^i \rangle = \frac{\langle \lambda_{\text{min}} \rangle}{0.45}$ .



**Figure B.4:** Violin Plot of the peak genotype layer for five exemplary setups. Each setup has  $\lambda_{\text{max}} \in [0.3, 0.6)$  and therefore  $\langle \phi^i \rangle = \frac{\langle \lambda_{\text{min}} \rangle}{0.45}$ .

a layer histogram for the respective number of loci L (similar to the violin plots) and we thus obtain:

$$n_{\rm rel} = \sum_{n=0}^{L} {L \choose n} P(n)$$
 (84)

where P(n) is the probability of finding a peak in layer n. In general, this probability depends on the number of loci L, but in order to compare different system sizes, we assume, that the probability mass function does not change with L. For the purpose of this work, we used L=4 to determine P(n) and used this distribution in order to determine the number of relevant genotypes as a function of the number of loci.

## **B.4** Evolution Algorithm

For the purpose of this work, we run a simple random adaptive walk, where every fitter genotype is equally likely [74]. Starting from a given genotype (usually the wild type), we:

1. Generate a list of candidates/neighbors.

- 2. Randomly select one genotype from the list of candidates.
  3. Check effective fitness of selected candidate.
  a Accept candidate as new genotype if fitness increased and repeat from 1.
  b Delete genotype from candidates if fitness decreased.
  4. Check if list is empty.
- a Stop if list is empty (Peak).
- b Repeat from 2 if list is not empty.

# C Robustness of the Deterministic Tolerance Evolution Model

#### C.1 Robustness of the Effective Fitness

We have introduced the effective fitness  $\Lambda_{Hill}$  as an appropriate fitness proxy for homogeneous bacterial colonies exposed to periodic stress. However, the derivation of the analytic result (15) required a simple exponential approximation of the concentration profile and the explicit form of the Hill-Function.

Here, we discuss how our fitness proxy, i.e. the effective fitness behaves if any of these two functions is changed. More explicitly, we show that for any general concentration profile c(t) the normalized effective fitness remains a function of the fraction  $\phi$ . Furthermore, we will numerically compute the two dimensional fitness topography for a double exponential concentration profile (equation [9]). In this parametrization, we assume that the drug uptake rate  $\beta$  is small compared to the degradation rate  $\alpha$  and demonstrate that the previous findings largely remain valid. Finally, we will also comment on the robustness against changes in the shape of the dose-response curve.

Given a general concentration profile c(t), we can write the integral of the dose-response curve as

$$\tilde{\Lambda}_{\text{Hill}}(t) = \int_0^{\tau} \lambda_{\text{Hill}}(c(t'))dt' \tag{85}$$

$$\tilde{\Lambda}_{\text{Hill}}(t) = \lambda_{\text{max}} \left[ \tau - (1 + \phi) \int_0^{\tau} \frac{\left(\frac{c(t')}{MIC}\right)^{\nu}}{\left(\frac{c(t')}{MIC}\right)^{\nu} + \phi} dt' \right]. \tag{86}$$

Dividing by the null fitness  $\lambda_{\text{max}}$  gives a general expression for the normalized effective fitness. We immediately find, that this quantity depends only on the fraction  $\phi$  again, if anything but  $\lambda_{\text{min}}$  and  $\lambda_{\text{max}}$  are held constant.

Accordingly, even for a general concentration profile, bacteria can switch from effective death to growth only if the fraction  $\phi$  changes.

As an example, we solve the integral (8) numerically for the double exponential profile (9) and find the effective fitness as:

$$\Lambda_{\text{Hill}}(t) = \lambda_{\text{max}} - \frac{\lambda_{\text{max}} (1 + \phi)}{\tau} \int_0^{\tau} \frac{C^{\nu} \left( e^{-\alpha t'} - e^{-\beta t'} \right)^{\nu}}{C^{\nu} \left( e^{-\alpha t'} - e^{-\beta t'} \right)^{\nu} + \phi} dt'.$$
 (87)

Figure C.1 visualizes two numerical results of the two dimensional topography of the double exponential effective fitness. We observe a qualitatively very similar picture as figure 5 and find a fraction  $\phi_{\text{crit}}$  where the effective fitness is zero in

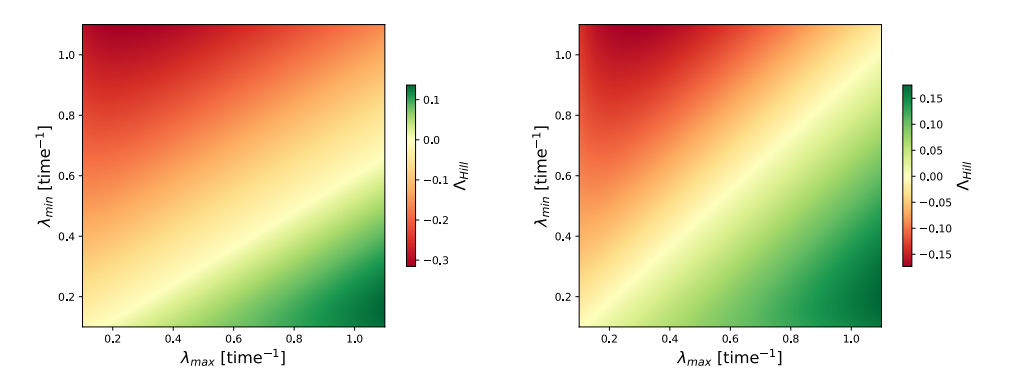


Figure C.1: The Effective Fitness in a two dimensional landscape of null fitness  $(\lambda_{\text{max}})$  and maximum death rate  $(\lambda_{\text{min}})$ . The left scenario corresponds to a rather fast drug uptake  $(\beta \gg \alpha)$ , while the right plot illustrates a rather slow drug drug availability  $(\beta > \alpha)$ .  $\Lambda_{\text{Hill}}$  is numerically computed for a double exponential concentration protocol with  $\tilde{\alpha} = 2.4$ ,  $\tilde{\beta} \equiv \beta \tau = 100/10$  (left/right),  $c_{\text{max}} = 4\,MIC$  and with a Hill parameter  $\nu = 4$ . In accordance with previous observations, we find a fraction  $\phi_{\text{crit}}$  where the effective fitness is zero in both scenarios.

both scenarios. However, this critical point changes with  $\tilde{\beta} \equiv \beta \tau$  and we observe that  $\Lambda_{\text{Hill}}$  increases as rate of drug absorption decreases.

Experimental studies on the pharmacokinetics usually find very large drug absorption rates [44], [94]. Hence, the left plot in figure [C.1], which qualitatively aligns with previous results, depicts the effective fitness for a realistic concentration profile.

Consequently, the simple exponential decay provides a useful approximation of the more complicated, double exponential concentration profile.

We will therefore proceed with

$$c(t) = c_{\text{max}} e^{-\alpha (t - t_0)} \tag{88}$$

and focus on the shape of the dose-response curve in the following.

In the framework that is presented, any computation of an effective fitness  $\Lambda$  requires an integration of the respective dose-response curve  $\lambda(c(t))$ , such that

$$\Lambda = \frac{1}{\tau} \int_0^{\tau} \lambda(c(t')) dt'.$$

Studies on bacterial fitness commonly assume Hill-type dose-response curves [68], [95], [82], which is a monotonic decreasing function of the antibiotic concentration. It is generally reasonable to consider any decreasing function, since higher doses are expected to gradually inhibit bacterial growth. However, it has been shown that some unusual non-monotonic behavior can occur under extreme conditions [82], which is not further considered here.

For simple exponential concentration profiles, the fitness function, i.e. the doseresponse curve, is a monotonic function in time and the effective fitness is readily computed by the fundamental theorem of calculus:

$$\Lambda = \frac{1}{\tau} \left( F(c(\tau)) - F(c_{\text{max}}) \right) \tag{89}$$

if the antiderivative F(c) of  $\lambda(c)$  exists for the whole interval  $[0, \tau]$ .

We can extend this to partially defined dose-response curves:

$$\Lambda = \frac{1}{\tau} \sum_{i} \left( F^{(i)}(c(t_{i+1})) - F^{(i)}(c(t_i)) \right)$$
 (90)

where the antiderivative of  $\lambda(c)$  exists on the interval  $[t_i, t_{i+1}]$ .

We will therefore construct an alternative dose-response curve that has a region of maximum growth/death and an intermediate region that is a decreasing function of c (figure C.2). For simplicity, we will only consider linear intermediate functions here, but generally this could be any suitable function.

Notably, this definition does not necessarily fix the mic, since we can find the

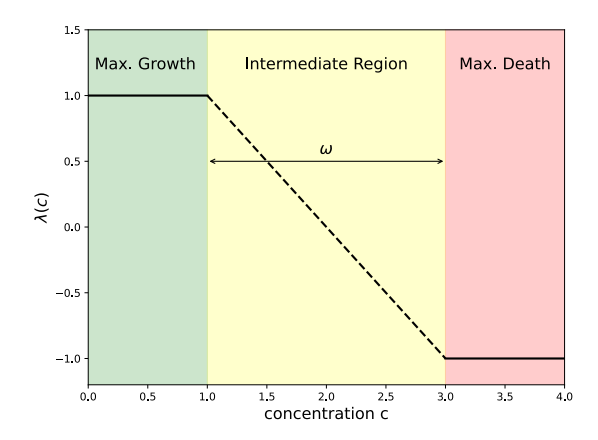


Figure C.2: Construction scheme for alternative DRC's. The function is assumed to be constant at low/high concentrations and the intermediate part of width  $\omega$  can be any decreasing function of the concentration (here linear) that continuously connects the null fitness and the max. death rate.

root of the dose-response curve anywhere in  $\left(\rho - \frac{\omega}{2}, \rho + \frac{\omega}{2}\right)$ , where  $\rho$  is the MIC of a DRC with  $\lambda_{\min} = \lambda_{\max}$ . Thus, changing the ratio  $\phi = \frac{\lambda_{\min}}{\lambda_{\max}}$  will also change the MIC to some extent.

For such dose-response curves, the normalized effective fitness will always be a function of the fraction

$$\frac{\Lambda}{\lambda_{\text{max}}} = G\left(\frac{\lambda_{\text{min}}}{\lambda_{\text{max}}}\right)$$

and thus remains constant if  $\phi = \frac{\lambda_{\min}}{\lambda_{\max}}$  is not changed.

The previously discussed step dose-response curve is a simple non trivial example of such a function width intermediate width  $\omega = 0$ . We have not yet illustrated the full two dimensional fitness topography for the step profile, but we can readily convince ourselves, that the sign of  $\Lambda_{\text{step}}$  only depends on the fraction  $\phi$ :

$$\Lambda_{\mathrm{step}} = \frac{\lambda_{\mathrm{max}}}{\tau} \left( \phi \left( t_{\mathrm{mic}} \right) + \left( \tau - t_{\mathrm{mic}} \right) \right).$$

The parameter  $t_{\text{mic}}$  is the time at which the antibiotic concentration dropped to the MIC. Accordingly, the fitness topography maintain their characteristic feature that effective growth and death are separated by a boundary at constant  $\phi$  (see figure  $\mathbb{C}.3$ ).

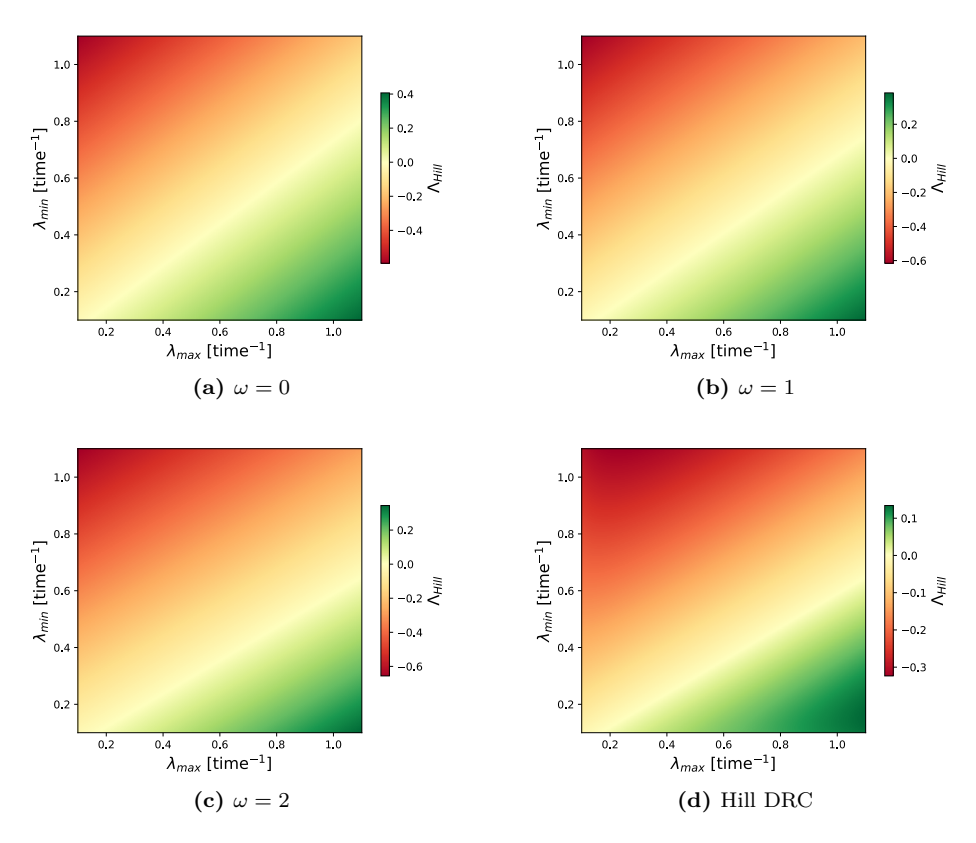


**Figure C.3:** Topography of the effective fitness for a dose-response curve with constant growth/death for low/high concentrations of the antibiotics and a linear intermediate decrease of width  $\omega$  (as in figure C.2). Furthermore, also the topography of the Hill model with the usual system parameters  $(C, \nu, \tilde{\alpha}) = (4, 4, 2.4)$  is provided.

With increasing width  $\omega$  the fraction  $\phi$  where the effective fitness is zero decreases and compares to the Hill equivalent.

Yet, it was already noted that such a partially defined dose-response curve does not fix the MIC and is not everywhere differentiable. Therefore, we do not observe the Hill-model intrinsic phenomena that the dose-response curve becomes zero everywhere if  $\lambda_{\min} = 0$  or  $\lambda_{\max} = 0$ . Hence, there is no global maximum in

the effective fitness  $\Lambda$  as a function of  $\phi$  (see figure  $\overline{\text{C.4}}$ ).

However, in the relevant regime, i.e. regimes where the Hill-model phenomena become irrelevant, the effective fitness of every presented dose-response curve is qualitatively equal (approximately linear) and the Hill result converges to the respective step result.

Empirical studies on  $\beta$ -lactam antibiotics usually observe dose-response curves that are very steep around the MIC [82]. A binary step DRC can therefore be a good approximation in some cases.

Notably, the width  $\omega$  of the intermediate region does not have a major effect on the effective fitness as a function of the fraction  $\phi$  (figure C.4).

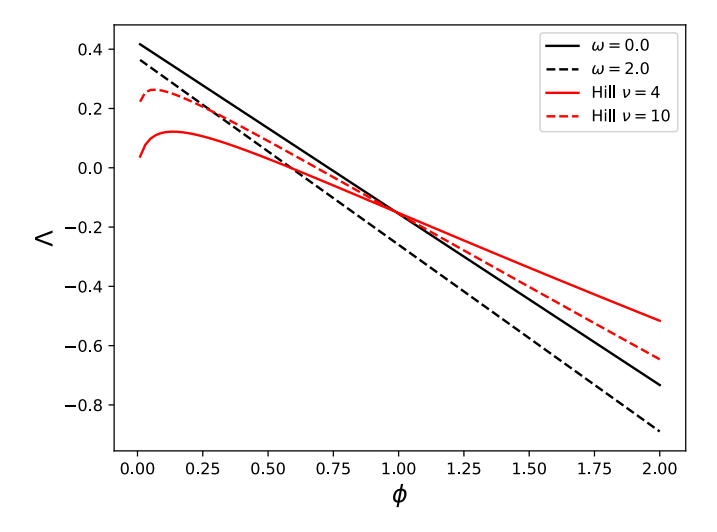
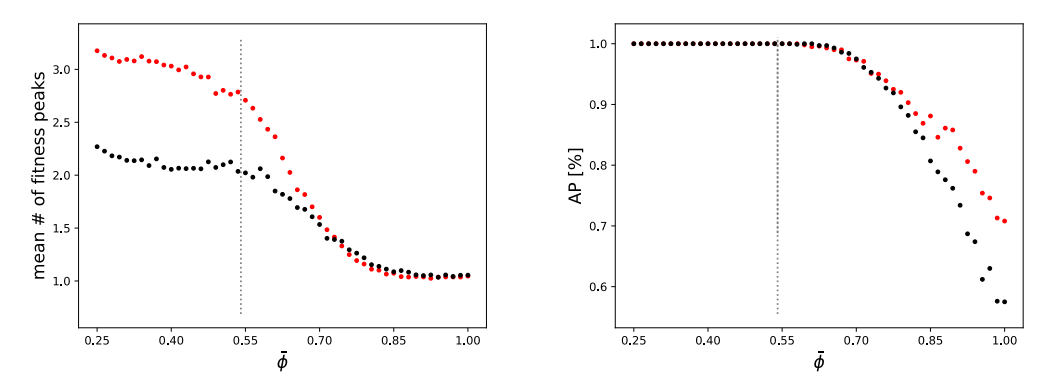


Figure C.4: Effective fitness  $\Lambda$  as a function of the ratio  $\phi$  for the constructed DRC with  $\omega=0$  (step function) and  $\omega=2$  (linear decrease) and for the Hill DRC with  $\nu=4$  (as before) and  $\nu=10$  (steep profile). For all models we set  $c_{\rm max}=4\,MIC$  and  $\tilde{\alpha}=2.4$ . All the provided functions show a qualitatively similar (approximately linear) behavior in the relevant regime and the Hill effective fitness converges to the Step result as  $\nu$  becomes large.

## C.2 Robustness of the TIL-Model Analysis

Finally, we repeat the analysis of the TIL-model for the step dose-response curve (in black) and compare to our previous Hill analysis (in red). Again, the qualitative behavior of all examined observables is very similar in both cases and many of the arguments also hold for the step profile. However, the effective fitness of the step dose-response curve (and also the linear intermediate decrease) does not have a maximum. The only fitness peak of an associated toy model would therefore always be the *full mutant* (or the wild type if the phenotypes increase  $\phi$ ) and the optimal number of mutations  $n_{\rm opt} = L$ . Intermediate layers with many

genotypes are thus never highly likely to have a fitness peaks and especially intermediate peak layers do not occur. Consequently, the number of fitness peaks in the step model is substantially smaller than for the Hill equivalent. Figure C.5-C.7 summarize the results on the Step DRC TIL model.



**Figure C.5:** Mean number of peaks (left) and percent of AP-fulfilling landscapes (right) as functions of the associated trade-off  $\bar{\phi}$ . Both observables are shown for the Hill model (red) and the Step DRC model (black).

For small  $\bar{\phi}$ , i.e. highly favorable trade-offs, the step dose-response curve has  $\mathcal{O}(1)$  fewer fitness peaks than the hill model equivalent. We again observe that the number of fitness peaks significantly decreases, as the accessibility property is lost (vertical dotted line) and for  $\bar{\phi} \to 1$  both landscapes are single peaked.

Every point represents an average over 1000 realizations on every setup with the usual system parameters  $(C, \nu, \tilde{\alpha}) = (4, 4, 2.4)$ . Each setup has  $\lambda_{\max}^i \in [0.5, 0.8)$  and therefore  $\bar{\phi} = \frac{\langle \lambda_{\min}^i \rangle}{0.65}$ .

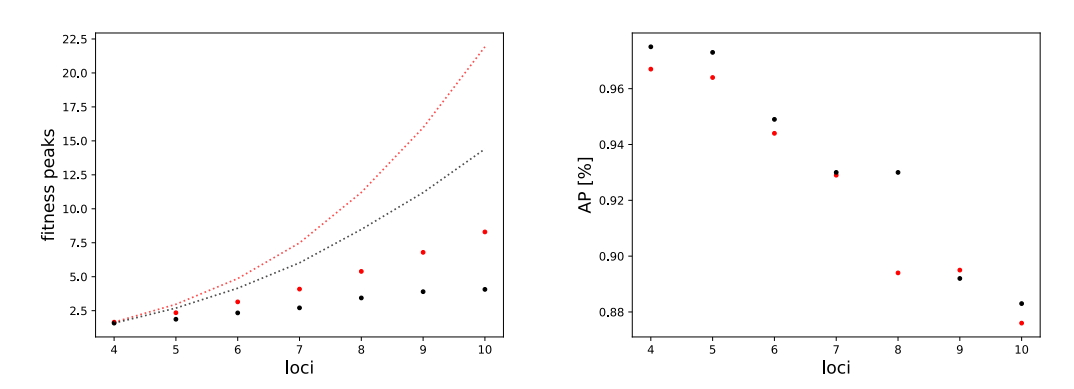
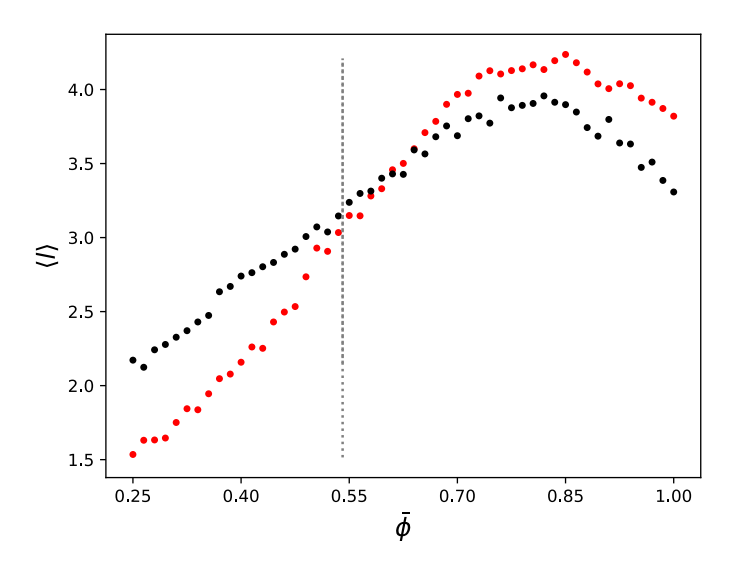


Figure C.6: Left: Total number of peaks for the Hill model (red dots) and the Step DRC model (black dots) together with a respective theoretical estimate (dotted lines). For this estimate, we assumed that the number of peaks is proportional to the size of the relevant sub-landscape. Right: Percent of AP-fulfilling landscapes as functions of the number of loci L. In both plots every data point represents an average over 1000 realizations on the respective number of loci with  $\lambda_{\text{max}} \in [0.5, 0.8)$  and  $\lambda_{\text{min}} \in [0.3, 0.6)$ .

Ultimately, visualizing the evolutionary path in the full two dimensional topography, we observe the same biphasic exchange compensation as in the Hill model (see figure C.8).



**Figure C.7:** Length of evolutionary paths for the Hill Model (red) and the step DRC model (black) as a function of  $\bar{\phi}$  for L=4. The dotted line visualizes the transition from setups that analytically must have the accessibility property to those that do not have it. The path length of both models is qualitatively very similar and can be explained as deviation from the path of the

from an associated toy model. Though, the Step DRC model realizes longer paths than the Hill model if the landscape has the accessibility property, while shorter paths are realized if the AP is lost. For this visualization we chose  $\lambda_{\max}^i \in [0.5, 0.8)$  and therefore  $\bar{\phi} = \frac{\langle \lambda_{\min}^i \rangle}{0.65}$ .

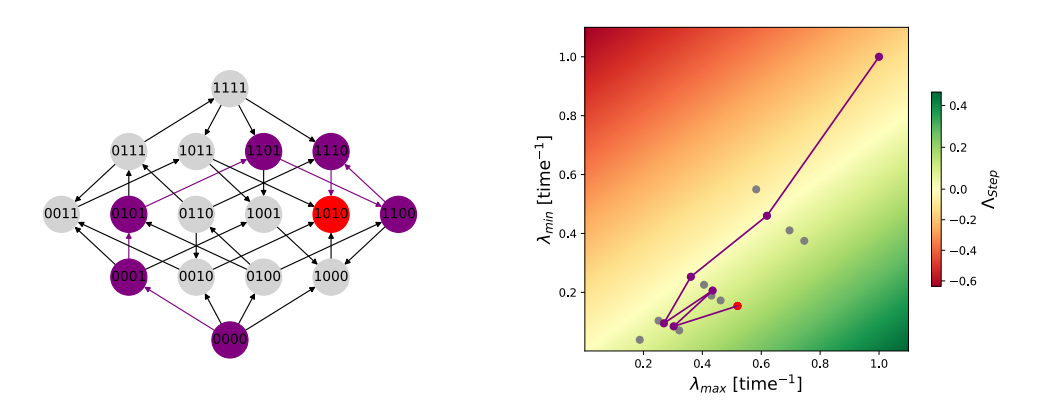


Figure C.8: Exemplary evolution from the wild type to a fitness peak (red). The genetic path (purple) is shown on the fitness graph (left), as well as in the full two dimensional topography (right). Similar to the Hill model, we observe a biphasic trade-off compensation behavior here. The growth-death trade-off landscape was constructed with  $\lambda_{\text{max}} \in [0.5, 0.8)$  and  $\lambda_{\text{min}} \in [0.3, 0.6)$ .

# D Size Distributions in the Simple Birth–Death Process

In the chapter on the simple and homogeneous birth-death process  $\boxed{4.2}$ , we discussed the time evolution of the extinction probability, i.e. the probability  $P_n(t)$  of the absorbing state n=0. However, this quantity does not describe extinction probabilities in changing environments, particularly also not for our periodic step function PKPD profile. In order to compute the survival probability after a full period with sub and super MIC concentration regimes, it was necessary to evaluate the size distribution  $P_n(t)$  (equation  $\boxed{48}$  and  $\boxed{49}$ ) at  $t=t_{\rm MIC}$ . This has been done for every theoretical result in section  $\boxed{5}$ . Here, we want to discuss the shape and the time dynamics of the size distribution briefly for the wild type and the tolerant mutant under biostatic or, respectively, biocidal treatment.

Throughout the main analysis, we demonstrated that the survival probability of bacteria is lower under biocidal treatment relative to the corresponding biostatic case. Thus, we expect to see differences in the shape of the full distribution as well.

Figure D.1 presents the probability distributions for the reference strain (wild type) under both biostatic and biocidal treatment, shown together in a single histogram at selected time points. Similarly, figure D.2 explains this for the tolerant strain. We show the time evolution of the histogram for  $t \leq t_{\text{MIC}} \approx 4.28$ , which is the interesting regime for the PKPD model in section 5.

For both strains, we observe, that the initially peaked probability distribution broadens rapidly, where the variance of the biocidal distribution is always bigger than for the respective biostatic case at any time t > 0. Furthermore, for both modes of antibiotic action, the size distribution drifts towards smaller population sizes. Accordingly, the biocidal distribution reaches the state n = 0 earlier, than the biostatic one. This is an absorbing state, i.e. there is no out flux, and therefore  $P_0(t)$  is an increasing function of time.

Notably, these visualizations illustrate the observed difference in extinction probabilities between biocidal and biostatic treatments. In the next section [sec:proof\_cidal\_static we follow up on this finding and find a rigorous proof for the simple birth and death process.

Furthermore, the analysis of figure  $\boxed{\text{D.1}}$  and  $\boxed{\text{D.2}}$  reveals, that the dispersion of the distribution of the tolerant mutant is slightly faster, than for the wild type. However, the drift velocity towards the absorbing state n=0 appears smaller for the tolerant mutant. Accordingly, also the full distribution explains, that our tolerant strain has an increased chance of surviving antibiotic treatment, compared to the wild type.

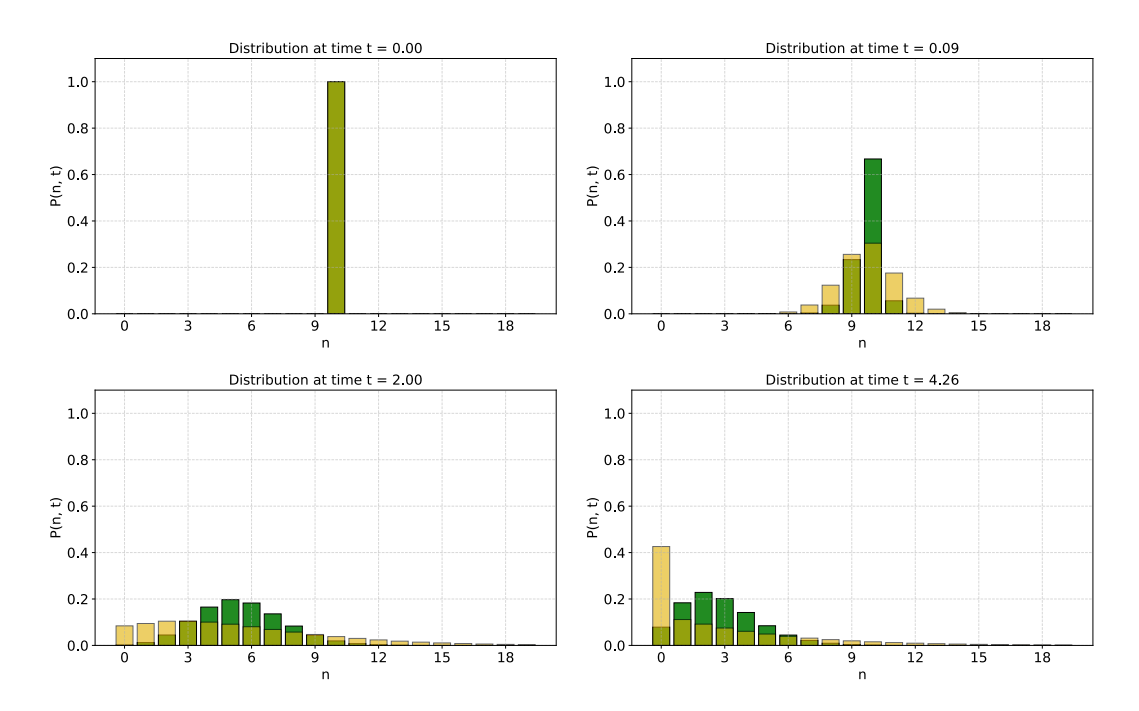


Figure D.1: Time evolution of the wild type size distribution from t = 0 to  $t \approx t_{\text{MIC}}$ . Every histogram shows the distribution of the biostatic (green) and the biocidal (yellow) scenario respectively. Olive colors are the overlap. Both distributions are computed for initial population sizes  $N_0 = 10$ .

We observe, that the width of the biocidal distribution increases faster that the biostatic one and the extinction probability at the  $t = t_{\text{MIC}}$  ( $P_0(t_{\text{MIC}})$ ) is significantly higher for biocidal treatment.

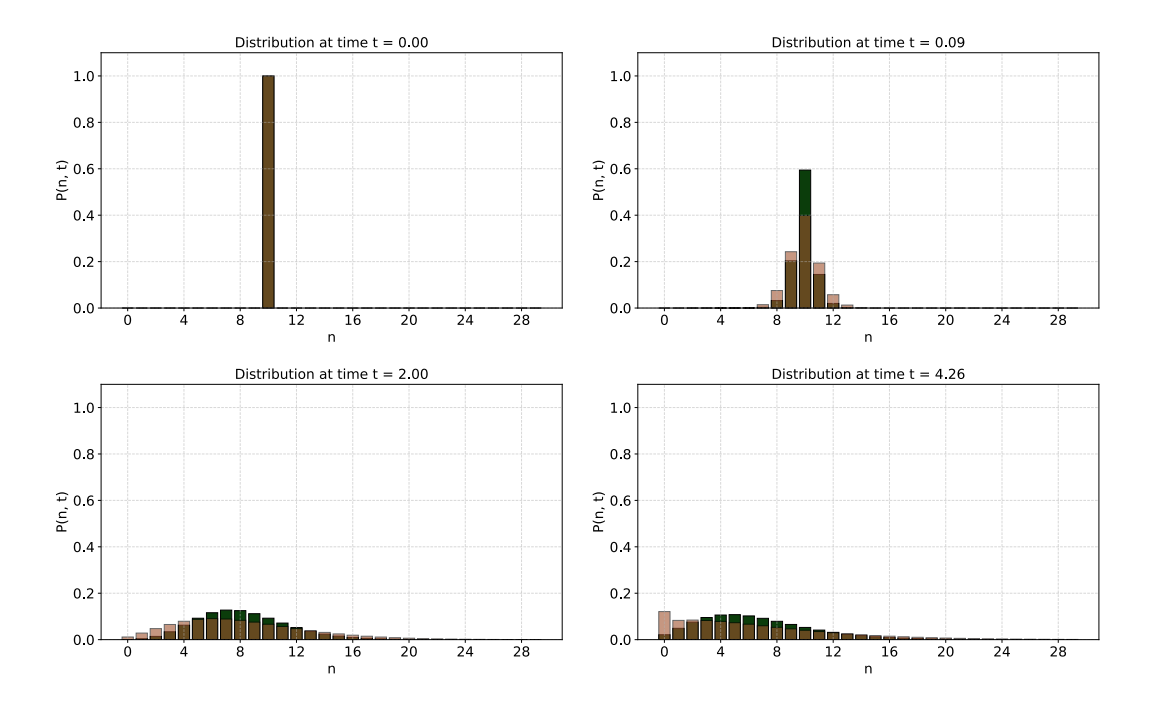


Figure D.2: Time evolution of the tolerant strain size distribution from t=0 to  $t\approx t_{\rm MIC}$ . Every histogram shows the distribution of the biostatic (dark-green) and the biocidal (light-brown) scenario respectively. Brown colors are the overlap. Both distributions are computed for initial population sizes  $N_0=10$ .

We observe, that the width of the biocidal distribution increases faster that the biostatic one and the extinction probability at the  $t = t_{\text{MIC}} (P_0(t_{\text{MIC}}))$  is significantly higher for biostatic treatment.

# E Survival Probability for Biostatic and Biocidal Treatment

# E.1 Proof that $P_{\text{surv}}^{\text{cidal}} < P_{\text{surv}}^{\text{static}}$

We want to prove here, that the survival probability under biocidal treatment is smaller than for the biostatic case. By looking at the expressions (61) and (62), we note, that it is enough to show, that

$$\frac{d\left(e^{(g-d-\eta_{\max})\tau}-1\right)}{(g-\eta_{\max})\lambda-d}<\frac{d+\eta_{\max}\left(e^{(g-d-\eta_{\max})\tau}-1\right)}{g\lambda-d-\eta_{\max}}.$$

#### Case 1: We assume:

$$(g - \eta_{\text{max}}) > d$$
 and thus  $\lambda := e^{(g - d - \eta_{\text{max}})\tau} > 1$ .

Furthermore, we define:

$$c := \frac{d}{(g - \eta_{\text{max}})\lambda - d}, \quad s := \frac{(d + \eta_{\text{max}})}{g\lambda - d - \eta_{\text{max}}}$$

By definition, we know, that:

$$\eta \max \lambda \ (g - d - \eta \max) > 0.$$

Adding zeros and factoring, we obtain:

$$\Leftrightarrow \underbrace{dg\lambda - d^2 - d\eta_{\max} + g\eta_{\max}\lambda - \eta_{\max}d\lambda - \eta_{\max}^2\lambda}_{\text{d}\lambda - \eta_{\max}} \underbrace{-\underbrace{dg\lambda + d^2 + \eta_{\max}d}_{\text{max}}}_{\text{d}\lambda - \eta_{\max}\lambda - \eta_{\max}\lambda - d)} > 0$$

$$\Leftrightarrow \underbrace{(d + \eta_{\max})((g - \eta_{\max})\lambda - d)}_{\text{d}\lambda - d} \underbrace{-d(g\lambda - d - \eta_{\max})}_{\text{d}\lambda - d} > 0$$

Since  $d(g\lambda - d - \eta_{\text{max}})$  and  $(g - \eta_{\text{max}})\lambda - d$  are positive, we readily find:

$$\Leftrightarrow c (\lambda - 1) > s (\lambda - 1)$$

which proves our statement.

Case 2: Same setup, but now  $\lambda < 1$ , ie. we assume  $(g - \eta_{\text{max}}) < d$ . We therefore know, that

$$\eta_{\text{max}} \lambda \left( g - d - \eta_{\text{max}} \right) < 0.$$

Repeating the steps from above, we obtain

$$\Leftrightarrow (d + \eta_{\max}) ((g - \eta_{\max})\lambda - d) - d(g\lambda - d - \eta_{\max}) < 0$$
  
$$\Leftrightarrow (d + \eta_{\max}) ((g - \eta_{\max})\lambda - d) < d(g\lambda - d - \eta_{\max}).$$

We note, that by definition, we have  $(g\lambda - d - \eta_{\text{max}}) < 0$  and also  $((g - \eta_{\text{max}})\lambda - d) < 0$ . Therefore:

$$\Leftrightarrow c < s$$

multiplying both sides with  $(\lambda - 1) < 0$  yields the desired expression:

$$\Leftrightarrow c (\lambda - 1) > s (\lambda - 1)$$

We have therefore proven that:

$$P_{\rm surv}^{\rm cidal} < P_{\rm surv}^{\rm static}$$

for all parameter regimes where  $\eta_{\text{max}} > 0$ .

# E.2 Proof that $P_{ ext{surv}}^{ ext{cidal}} > P_{ ext{surv}}^{ ext{static}}$ for $\eta_{ ext{max}} < 0$

We consider the survival probability

$$P_{\text{surv}}^{(>)}(g,d) = 1 - \left[ \frac{d(e^{(g-d)\tau} - 1)}{ge^{(g-d)\tau} - d} \right]^{n_0},$$

For this function we have shown above, that:

$$P_{\text{surv}}^{(>)}(g, d + \eta_{\text{max}}) < P_{\text{surv}}^{(>)}(g - \eta_{\text{max}}, d) < P_{\text{surv}}^{(>)}(g, d)$$

where the last inequality follows, because decreasing the growth rate, or increasing the death rate, will always decrease the survival probability.

Now we want to show, that the opposite order is true if we revert sign of  $\eta_{\text{max}}$ , i.e.

$$P_{\text{surv}}^{(>)}(g, d - \eta_{\text{max}}) > P_{\text{surv}}^{(>)}(g + \eta_{\text{max}}, d) > P_{\text{surv}}^{(>)}(g, d).$$

Let us again denote

$$\lambda := e^{(g-d+\eta_{\max})\tau}$$

now with a plus in front of the  $\eta_{\text{max}}$ , and focus on the expressions inside the survival function:

$$c(\lambda - 1) = \frac{(d - \eta_{\text{max}})(\lambda - 1)}{g\lambda - (d - \eta_{\text{max}})}, \quad s(\lambda - 1) = \frac{d(\lambda - 1)}{(g + \eta_{\text{max}})\lambda - d}.$$

We aim to prove that

$$c(\lambda - 1) < s(\lambda - 1)$$

which implies, that

$$P_{\text{surv}}^{(>)}(g, d - \eta_{\text{max}}) > P_{\text{surv}}^{(>)}(g + \eta_{\text{max}}, d).$$

Let us assume, that g > d, which is well justified, since bacteria would not have established otherwise. Then  $\lambda - 1 > 0$  and we are left to show, that

$$c < s$$

$$\Leftrightarrow \frac{d - \eta_{\max}}{g\lambda - d + \eta_{\max}} < \frac{d}{g\lambda + \eta_{\max}\lambda - d}$$

$$\stackrel{\lambda \geq 1}{\Leftrightarrow} (d - \eta_{\max})(g\lambda + \eta_{\max}\lambda - d) < d(g\lambda - d + \eta_{\max})$$

Subtracting the LHS from the RHS:

$$\Leftrightarrow \quad 0 \quad < \left[ dg\lambda - d^2 + d\eta_{\max} \right] - \left[ dg\lambda + d\eta_{\max}\lambda - d^2 - \eta_{\max}g\lambda - \eta_{\max}^2\lambda + \eta_{\max}d \right]$$

$$\Leftrightarrow \quad 0 \quad < -d\eta_{\max}\lambda + \eta_{\max}g\lambda + \eta_{\max}^2\lambda$$

$$\Leftrightarrow 0 < \eta_{\max} \lambda (g - d + \eta_{\max})$$

Since  $\eta_{\text{max}} > 0$ ,  $\lambda > 1$ , and  $g - d + \eta_{\text{max}} > 0$ , this expression is strictly positive, which proves

$$c(\lambda - 1) < s(\lambda - 1) \implies P_{\text{surv}}^{(>)}(g, d - \eta_{\text{max}}) > P_{\text{surv}}^{(>)}(g + \eta_{\text{max}}, d).$$

It is easy to check that increasing either g or decreasing d increases the survival probability. Thus the full chain holds:

$$P_{\text{surv}}^{(>)}(g, d - \eta_{\text{max}}) > P_{\text{surv}}^{(>)}(g + \eta_{\text{max}}, d) > P_{\text{surv}}^{(>)}(g, d).$$

## References

- [1] Alexander Fleming. "On the antibacterial action of cultures of a penicillium, with special reference to their use in the isolation of B. influenzae". In: British journal of experimental pathology 10.3 (1929), p. 226.
- [2] W. A. Adedeji. "The Treasure Called Antibiotics". In: *Annals of Ibadan postgraduate medicine* 14.2 (2016), pp. 56-57. ISSN: 1597-1627. URL: https://www.ncbi.nlm.nih.gov/pmc/articles/PMC5354621/.
- [3] National Center for Health Statistics. FastStats. 2024. URL: https://www.cdc.gov/nchs/fastats/life-expectancy.htm (visited on 08/30/2024).
- [4] Rustam I. Aminov. "A brief history of the antibiotic era: lessons learned and challenges for the future". In: Frontiers in microbiology 1 (2010), p. 134. DOI: 10.3389/fmicb.2010.00134. URL: https://www.ncbi.nlm.nih.gov/pmc/articles/PMC3109405/.
- [5] Annie Browne et al. "Global antibiotic consumption and usage in humans, 2000–18: a spatial modelling study". In: *The Lancet Planetary Health* 5 (2021). DOI: 10.1016/S2542-5196(21)00280-1.
- [6] Edward P Abraham and Ernst Chain. "An enzyme from bacteria able to destroy penicillin". In: Nature 146.3713 (1940), pp. 837–837.
- [7] Asher Brauner et al. "Distinguishing between resistance, tolerance and persistence to antibiotic treatment". In: Nature Reviews Microbiology 14.5 (2016), pp. 320–330. ISSN: 1740-1526. DOI: 10.1038/nrmicro.2016.34. URL: https://doi.org/10.1038/nrmicro.2016.34.
- [8] Amit Gaurav et al. "Role of bacterial efflux pumps in antibiotic resistance, virulence, and strategies to discover novel efflux pump inhibitors". In: *Microbiology* 169.5, 001333 (2023). ISSN: 1465-2080. DOI: https://doi.org/10.1099/mic.0.001333. URL: https://www.microbiologyresearch.org/content/journal/micro/10.1099/mic.0.001333.
- [9] Nadine Kraupner et al. "Interaction between Mutations and Regulation of Gene Expression during Development of De Novo Antibiotic Resistance". In: Antimicrobial agents and chemotherapy 58 (2014). DOI: 10.1128/AAC. 02892-14.

- [10] Herman Goossens et al. "Outpatient antibiotic use in Europe and association with resistance: a cross-national database study". In: *The Lancet* 365.9459 (2005), pp. 579-587. ISSN: 0140-6736. DOI: https://doi.org/10.1016/S0140-6736(05)17907-0. URL: https://www.sciencedirect.com/science/article/pii/S0140673605179070.
- [11] WHO. Antimicrobial resistance. 2024. URL: https://www.who.int/news-room/fact-sheets/detail/antimicrobial-resistance (visited on 08/29/2024).
- [12] Mohsen Naghavi et al. "Global burden of bacterial antimicrobial resistance 1990–2021: a systematic analysis with forecasts to 2050". In: *The Lancet* 404.10459 (2024), pp. 1199–1226.
- [13] Joseph W. Bigger. "Treatment of Staphylococcal Infections with Penecilin by Intermittent Sterilisation". In: *The Lancet* 244.6320 (1944). Originally published as Volume 2, Issue 6320, pp. 497–500. ISSN: 0140-6736. DOI: https://doi.org/10.1016/S0140-6736(00)74210-3. URL: https://www.sciencedirect.com/science/article/pii/S0140673600742103.
- [14] Sandra Handwerger and Alexander Tomasz. "Antibiotic tolerance among clinical isolates of bacteria". In: *Reviews of Infectious Diseases* (1985), pp. 368–386.
- [15] Jemila Kester and Sarah Fortune. "Persisters and beyond: Mechanisms of phenotypic drug resistance and drug tolerance in bacteria". In: *Critical reviews in biochemistry and molecular biology* 49 (2013). DOI: 10.3109/10409238.2013.869543.
- [16] Irit Levin-Reisman et al. "Antibiotic tolerance facilitates the evolution of resistance". In: Science 355.6327 (2017), pp. 826-830. DOI: 10.1126/science. aaj2191. URL: https://www.science.org/doi/abs/10.1126/science.aaj2191.
- [17] Kim Lewis. "The science of antibiotic discovery". In: *Cell* 181.1 (2020), pp. 29–45.
- [18] Ashley T. Deventer et al. "Antibiotic tolerance among clinical isolates: mechanisms, detection, prevalence, and significance". In: Clinical Microbiology Reviews 37.4 (2024). DOI: 10.1128/cmr.00106-24. URL: https://journals.asm.org/doi/abs/10.1128/cmr.00106-24.
- [19] Gabriel Carvalho, Christiane Forestier, and Jean-Denis Mathias. "Antibiotic resilience: a necessary concept to complement antibiotic resistance?" In: *Proceedings of the Royal Society B* 286.1916 (2019), p. 20192408.

- [20] Roland R. Regoes et al. "Pharmacodynamic Functions: a Multiparameter Approach to the Design of Antibiotic Treatment Regimens". In: Antimicrobial Agents and Chemotherapy 48.10 (2004), pp. 3670–3676. DOI: 10.1128/aac.48.10.3670-3676.2004. URL: https://journals.asm.org/doi/abs/10.1128/aac.48.10.3670-3676.2004.
- [21] J.G. Wagner. "Kinetics of pharmacologic response I. Proposed relationships between response and drug concentration in the intact animal and man". In: Journal of Theoretical Biology 20.2 (1968), pp. 173-201. ISSN: 0022-5193. DOI: https://doi.org/10.1016/0022-5193(68)90188-4. URL: https://www.sciencedirect.com/science/article/pii/0022519368901884.
- [22] Jaap J. Hoogeterp et al. "The Efficacy of Rifampicin against Staphylococcus aureus in Vitro and in an Experimental Infection in Normal and Granulocytopenic Mice". In: Scandinavian Journal of Infectious Diseases 20.6 (1988). PMID: 2975827, pp. 649–656. DOI: 10.3109/00365548809035666. URL: https://doi.org/10.3109/00365548809035666.
- [23] A Nolting et al. "Pharmacokinetic-pharmacodynamic modeling of the antibiotic effect of piperacillin in vitro". In: *Pharmaceutical research* 13.1 (1996), pp. 91–96. ISSN: 0724-8741. DOI: 10.1023/a:1016085402278. URL: https://doi.org/10.1023/a:1016085402278.
- [24] Lewis B. Sheiner et al. "Simultaneous modeling of pharmacokinetics and pharmacodynamics: Application to d-tubocurarine". In: Clinical Pharmacology & Therapeutics 25.3 (1979), pp. 358-371. DOI: https://doi.org/10.1002/cpt1979253358. URL: https://ascpt.onlinelibrary.wiley.com/doi/abs/10.1002/cpt1979253358.
- [25] Jurriaan E. M. de Steenwinkel et al. "Time-kill kinetics of anti-tuberculosis drugs, and emergence of resistance, in relation to metabolic activity of Mycobacterium tuberculosis". In: *Journal of Antimicrobial Chemotherapy* 65.12 (2010), pp. 2582–2589. ISSN: 0305-7453. DOI: 10.1093/jac/dkq374. URL: https://doi.org/10.1093/jac/dkq374.
- [26] Carmela T. M. Mascio, Jeff D. Alder, and Jared A. Silverman. "Bactericidal Action of Daptomycin against Stationary-Phase and Nondividing Staphylococcus aureus Cells". In: Antimicrobial Agents and Chemotherapy 51.12 (2007), pp. 4255–4260. DOI: 10.1128/aac.00824-07. URL: https://journals.asm.org/doi/abs/10.1128/aac.00824-07.
- [27] Helle Krogh Johansen et al. "Antagonism between penicillin and erythromycin against Streptococcus pneumoniae in vitro and in vivo". In: *Journal of An*-

- timicrobial Chemotherapy 46.6 (2000), pp. 973-980. ISSN: 0305-7453. DOI: 10.1093/jac/46.6.973. URL: https://doi.org/10.1093/jac/46.6.973.
- [28] I P Thonus, P Fontijne, and M F Michel. "Ampicillin susceptibility and ampicillin-induced killing rate of Escherichia coli". In: *Antimicrobial Agents and Chemotherapy* 22.3 (1982), pp. 386–390. DOI: 10.1128/aac.22.3.386. URL: https://journals.asm.org/doi/abs/10.1128/aac.22.3.386.
- [29] Suman G Das et al. "Predictable properties of fitness landscapes induced by adaptational tradeoffs". In: *eLife* 9 (2020), e55155. ISSN: 2050-084X. DOI: 10.7554/eLife.55155. URL: https://doi.org/10.7554/eLife.55155.
- [30] David G. Kendall. "On the Generalized "Birth-and-Death" Process". In: *The Annals of Mathematical Statistics* 19.1 (1948), pp. 1–15. ISSN: 00034851. URL: http://www.jstor.org/stable/2236051.
- [31] Norman TJ Bailey. The elements of stochastic processes with applications to the natural sciences. John Wiley & Sons, 1991. Chap. 8, pp. 84–105.
- [32] Daniel T. Gillespie. "Exact stochastic simulation of coupled chemical reactions". In: *The Journal of Physical Chemistry* 81.25 (1977), pp. 2340–2361. DOI: 10.1021/j100540a008. eprint: https://doi.org/10.1021/j100540a008. URL: https://doi.org/10.1021/j100540a008.
- [33] Peter Czuppon et al. "A stochastic analysis of the interplay between antibiotic dose, mode of action, and bacterial competition in the evolution of antibiotic resistance". In: *PLOS Computational Biology* 19.8 (2023), pp. 1–20. DOI: [10.1371/journal.pcbi.1011364]. URL: [https://doi.org/10.1371/journal.pcbi.1011364].
- [34] John Maynard Smith. "The causes of extinction". In: *Philosophical Transactions of the Royal Society of London. B, Biological Sciences* 325.1228 (1989), pp. 241–252.
- [35] Richard Gomulkiewicz and Robert D. Holt. "When does Evolution by Natural Selection Prevent Extinction?" In: *Evolution* 49.1 (1995), pp. 201–207. ISSN: 00143820, 15585646. URL: http://www.jstor.org/stable/2410305.
- [36] Irith Wiegand, Kai Hilpert, and Robert EW Hancock. "Agar and broth dilution methods to determine the minimal inhibitory concentration (MIC) of antimicrobial substances". In: Nature protocols 3.2 (2008), pp. 163–175.

  DOI: https://doi.org/10.1038/nprot.2007.521. URL: https://www.nature.com/articles/nprot.2007.521.
- [37] Ofer Fridman et al. "Optimization of lag time underlies antibiotic tolerance in evolved bacterial populations". In: *Nature* 513.7518 (2014), pp. 418–421. DOI: https://doi.org/10.1038/nature13469.

- [38] Viktória Lázár et al. "Antibiotic combinations reduce Staphylococcus aureus clearance". In: *Nature* 610 (2022), pp. 1–7. DOI: 10.1038/s41586-022-05260-5.
- [39] Anat Bren et al. "Tradeoffs in bacterial physiology determine the efficiency of antibiotic killing". In: *Proceedings of the National Academy of Sciences* 120.51 (2023), e2312651120. DOI: 10.1073/pnas.2312651120. URL: https://www.pnas.org/doi/abs/10.1073/pnas.2312651120.
- [40] Anna J. Lee et al. "Robust, linear correlations between growth rates and beta-lactam-mediated lysis rates". In: *Proceedings of the National Academy of Sciences* 115.16 (2018), pp. 4069–4074. DOI: 10.1073/pnas.1719504115. URL: https://www.pnas.org/doi/abs/10.1073/pnas.1719504115.
- [41] Eshan S. King, Anna E. Stacy, and Jacob G. Scott. "A low-footprint, fluorescence-based bacterial time-kill assay for estimating dose-dependent cell death dynamics". In: bioRxiv (2024). DOI: 10.1101/2024.03.08. 584154. URL: https://www.biorxiv.org/content/early/2024/03/19/2024.03.08.584154.
- [42] Gerhard Levy. "Kinetics of pharmacologic effects". In: Clinical Pharmacology & Therapeutics 7.3 (1966), pp. 362-372. DOI: https://doi.org/10.1002/cpt196673362. URL: https://ascpt.onlinelibrary.wiley.com/doi/abs/10.1002/cpt196673362.
- [43] Gerhard Levy, Milo Gibaldi, and William J. Jusko. "Multicompartment Pharmacokinetic Models and Pharmacologic Effects". In: *Journal of Pharmaceutical Sciences* 58.4 (1969), pp. 422–424. ISSN: 0022-3549. DOI: https://doi.org/10.1002/jps.2600580406. URL: https://www.sciencedirect.com/science/article/pii/S0022354915368179.
- [44] Hartmut Derendorf. "Pharmacokinetic evaluation of β-lactam antibiotics". In: Journal of Antimicrobial Chemotherapy 24.3 (1989), pp. 407–413. ISSN: 0305-7453. DOI: 10.1093/jac/24.3.407. URL: https://doi.org/10.1093/jac/24.3.407.
- [45] Markus Mueller, Amparo de la Peña, and Hartmut Derendorf. "Issues in Pharmacokinetics and Pharmacodynamics of Anti-Infective Agents: Kill Curves versus MIC". In: Antimicrobial Agents and Chemotherapy 48.2 (2004), pp. 369–377. DOI: 10.1128/aac.48.2.369-377.2004. URL: https://journals.asm.org/doi/abs/10.1128/aac.48.2.369-377.2004.

- [46] William J. Jusko. "Pharmacodynamics of Chemotherapeutic Effects: Dose-Time-Response Relationships for Phase-Nonspecific Agents". In: *Journal of Pharmaceutical Sciences* 60.6 (1971), pp. 892–895. ISSN: 0022-3549. DOI: https://doi.org/10.1002/jps.2600600618. URL: https://www.sciencedirect.com/science/article/pii/S0022354915379594.
- [47] Jianguo Zhi, Charles H. Nightingale, and Richard Quintiliani. "A Pharmacodynamic Model for the Activity of Antibiotics Against Microorganisms under Nonsaturable Conditions". In: Journal of Pharmaceutical Sciences 75.11 (1986), pp. 1063–1067. ISSN: 0022-3549. DOI: https://doi.org/10.1002/jps.2600751108. URL: https://www.sciencedirect.com/science/article/pii/S002235491547265X.
- [48] Jianguo Zhi, Charles H. Nightingale, and Richard Quintiliani. "Microbial pharmacodynamics of piperacillin in neutropenic mice of systematic infection due toPseudomonas aeruginosa". In: Journal of Pharmacokinetics and Biopharmaceutics 16 (1988), pp. 355–375. URL: https://api.semanticscholar.org/CorpusID:32788972.
- [49] S. Corvaisier et al. "Comparisons between Antimicrobial Pharmacodynamic Indices and Bacterial Killing as Described by Using the Zhi Model". In: Antimicrobial Agents and Chemotherapy 42.7 (1998), pp. 1731–1737. DOI: 10.1128/aac.42.7.1731. URL: https://journals.asm.org/doi/abs/10.1128/aac.42.7.1731.
- [50] Michel J.Y. Bouvier d Yvoire and Pascal H. Maire. "Dosage Regimens of Antibacterials". In: Clinical Drug Investigation 11.4 (1996), pp. 229-239.
  ISSN: 1173-2563. DOI: 10.2165/00044011-199611040-00006. URL: https://link.springer.com/article/10.2165/00044011-199611040-00006#
  citeas.
- [51] Elisabet I. Nielsen, Otto Cars, and Lena E. Friberg. "Pharmacokinetic / Pharmacodynamic (PK/PD) Indices of Antibiotics Predicted by a Semimechanistic PKPD Model: a Step toward Model-Based Dose Optimization". In: Antimicrobial Agents and Chemotherapy 55.10 (2011), pp. 4619–4630. DOI: 10.1128/aac.00182-11. URL: https://journals.asm.org/doi/abs/10.1128/aac.00182-11.
- [52] D. Andes and W.A. Craig. "Animal model pharmacokinetics and pharmacodynamics: a critical review". In: International Journal of Antimicrobial Agents 19.4 (2002), pp. 261–268. ISSN: 0924-8579. DOI: https://doi.org/10.1016/S0924-8579(02)00022-5. URL: https://www.sciencedirect.com/science/article/pii/S0924857902000225.

- [53] Jasmine Foo et al. "Effects of pharmacokinetic processes and varied dosing schedules on the dynamics of acquired resistance to erlotinib in EGFR-mutant lung cancer". In: *Journal of Thoracic Oncology* 7.10 (2012), pp. 1583–1593.
- [54] Helen K. Alexander. "The Roles of Stochasticity and Life History in the Evolutionary Population Dynamics of Pathogens". en. Doctoral Thesis. Zurich: ETH Zurich, 2014. DOI: 10.3929/ethz-a-010388652.
- [55] Eugene A Yurtsev et al. "Bacterial cheating drives the population dynamics of cooperative antibiotic resistance plasmids". In: *Molecular systems biology* 9.1 (2013), p. 683.
- [56] Sivan Pearl Mizrahi, Akshit Goyal, and Jeff Gore. "Community interactions drive the evolution of antibiotic tolerance in bacteria". In: *Proceedings of the National Academy of Sciences* 120.3 (2023), e2209043119. DOI: 10.1073/pnas.2209043119. URL: https://www.pnas.org/doi/abs/10.1073/pnas.2209043119.
- [57] Elaine Tuomanen et al. "The Rate of Killing of Escherichia coli by Beta-Lactam Antibiotics is Strictly Proportional to the Rate of Bacterial Growth". In: Journal of general microbiology 132 (1986), pp. 1297–304. DOI: https://doi.org/10.1099/00221287-132-5-1297. URL: https://doi.org/10.1099/00221287-132-5-1297.
- [58] Irit Levin-Reisman et al. "Epistasis between antibiotic tolerance, persistence, and resistance mutations". In: *Proceedings of the National Academy of Sciences* 116.29 (2019), pp. 14734–14739. DOI: 10.1073/pnas.1906169116. URL: https://www.pnas.org/doi/abs/10.1073/pnas.1906169116.
- [59] Fernando Baquero and Bruce R Levin. "Proximate and ultimate causes of the bactericidal action of antibiotics". In: *Nature Reviews Microbiology* 19.2 (2021), pp. 123–132.
- [60] Orit Gefen et al. "TDtest: Easy detection of bacterial tolerance and persistence in clinical isolates by a modified disk-diffusion assay". In: *Scientific Reports* 7 (2017), p. 41284. DOI: 10.1038/srep41284.
- [61] Clément Vulin et al. "Prolonged lag time results in small colony variants and reflects a sub-population of persisters in vivo". In: bioRxiv (2018). DOI: 10.1101/279968. URL: https://www.biorxiv.org/content/early/2018/03/12/279968.
- [62] Vanina Dengler Haunreiter et al. "In-host evolution of Staphylococcus epidermidis in a pacemaker-associated endocarditis resulting in increased antibiotic tolerance". In: *Nature communications* 10.1 (2019), p. 1149.

- [63] José Camacho Mateu, Matteo Sireci, and Miguel A. Muñoz. "Phenotypic-dependent variability and the emergence of tolerance in bacterial populations". In: *PLOS Computational Biology* 17.9 (2021), e1009417. ISSN: 1553-7358. DOI: 10.1371/journal.pcbi.1009417. URL: http://dx.doi.org/10.1371/journal.pcbi.1009417.
- [64] Tom Cronenberg et al. "Antibiotics modulate attractive interactions in bacterial colonies affecting survivability under combined treatment". In: *PLOS Pathogens* 17.2 (2021), pp. 1–20. DOI: 10.1371/journal.ppat.1009251. URL: https://doi.org/10.1371/journal.ppat.1009251.
- [65] Isabelle Wielert et al. "Pilin antigenic variants impact gonococcal lifestyle and antibiotic tolerance by modulating interbacterial forces". In: *PLOS Biology* 23.1 (2025), pp. 1–27. DOI: 10.1371/journal.pbio.3003022. URL: https://doi.org/10.1371/journal.pbio.3003022.
- [66] Diane Horne and Alexander Tomasz. "Tolerant Response of Streptococcus sanguis to β-Lactams and Other Cell Wall Inhibitors". In: Antimicrobial Agents and Chemotherapy 11.5 (1977), pp. 888–896. DOI: 10.1128/aac. 11.5.888. URL: https://journals.asm.org/doi/abs/10.1128/aac.11.5.888.
- [67] Michael A. Stiffler, Doeke R. Hekstra, and Rama Ranganathan. "Evolvability as a Function of Purifying Selection in TEM-1 β-Lactamase". In: *Cell* 160.5 (2015), pp. 882–892. ISSN: 0092-8674. DOI: https://doi.org/10.1016/j.cell.2015.01.035. URL: https://www.sciencedirect.com/science/article/pii/S0092867415000781.
- [68] Suman G. Das, Joachim Krug, and Muhittin Mungan. "Driven Disordered Systems Approach to Biological Evolution in Changing Environments". In: *Phys. Rev. X* 12 (2022), p. 031040. DOI: 10.1103/PhysRevX.12.031040. URL: https://link.aps.org/doi/10.1103/PhysRevX.12.031040.
- [69] Joachim Krug and Daniel Oros. "Evolutionary accessibility of random and structured fitness landscapes". In: Journal of Statistical Mechanics: Theory and Experiment 2024.3 (2024), p. 034003. DOI: 10.1088/1742-5468/ad3197. URL: https://dx.doi.org/10.1088/1742-5468/ad3197.
- [70] Kristina Crona, Devin Greene, and Miriam Barlow. "The peaks and geometry of fitness landscapes". In: *Journal of Theoretical Biology* 317 (2013), pp. 1–10. ISSN: 0022-5193. DOI: https://doi.org/10.1016/j.jtbi.2012. 09.028. URL: https://www.sciencedirect.com/science/article/pii/S0022519312005061.

- [71] Kristina Crona et al. "Inferring genetic interactions from comparative fitness data". In: *eLife* 6 (2017). Ed. by Dan Weinreich, e28629. ISSN: 2050-084X. DOI: [10.7554/eLife.28629]. URL: [https://doi.org/10.7554/eLife.28629].
- [72] Suman G. Das, Muhittin Mungan, and Joachim Krug. "Epistasis-mediated compensatory evolution in a fitness landscape with adaptational tradeoffs". In: *Proceedings of the National Academy of Sciences* 122.15 (2025), e2422520122. DOI: 10.1073/pnas.2422520122. URL: https://www.pnas.org/doi/abs/10.1073/pnas.2422520122.
- [73] Yue Shan et al. "Genetic Basis of Persister Tolerance to Aminoglycosides in Escherichia coli". In: mBio 6.2 (2015), 10.1128/mbio.00078-15. DOI: 10. 1128/mbio.00078-15. URL: https://journals.asm.org/doi/abs/10. 1128/mbio.00078-15.
- [74] Stuart Kauffman and Simon Levin. "Towards a general theory of adaptive walks on rugged landscapes". In: Journal of Theoretical Biology 128.1 (1987), pp. 11-45. ISSN: 0022-5193. DOI: https://doi.org/10.1016/S0022-5193(87)80029-2. URL: https://www.sciencedirect.com/science/article/pii/S0022519387800292.
- [75] Sam P. Brown, R. Fredrik Inglis, and François Taddei. "Synthesis: Evolutionary ecology of microbial wars: within-host competition and (incidental) virulence". In: *Evolutionary Applications* 2.1 (2009), pp. 32–39. DOI: https://doi.org/10.1111/j.1752-4571.2008.00059.x. URL: https://onlinelibrary.wiley.com/doi/abs/10.1111/j.1752-4571.2008.00059.x.
- [76] Michael E Hibbing et al. "Bacterial competition: surviving and thriving in the microbial jungle". In: *Nature reviews microbiology* 8.1 (2010), pp. 15–25.
- [77] Elisa T. Granato, Thomas A. Meiller-Legrand, and Kevin R. Foster. "The Evolution and Ecology of Bacterial Warfare". In: Current Biology 29.11 (2019), R521-R537. ISSN: 0960-9822. DOI: https://doi.org/10.1016/j.cub.2019.04.024. URL: https://www.sciencedirect.com/science/article/pii/S0960982219304221.
- [78] Rene Niehus et al. "The evolution of strategy in bacterial warfare via the regulation of bacteriocins and antibiotics". In: *eLife* 10 (2021), e69756. ISSN: 2050-084X. DOI: 10.7554/eLife.69756. URL: https://doi.org/10.7554/eLife.69756.

- [79] Christin Nyhoegen, Sebastian Bonhoeffer, and Hildegard Uecker. "The many dimensions of combination therapy: How to combine antibiotics to limit resistance evolution". In: *Evolutionary Applications* 17.8 (2024). e13764 EVA-2023-262-OA.R1, e13764. DOI: <a href="https://doi.org/10.1111/eva.13764">https://doi.org/10.1111/eva.13764</a>. URL: <a href="https://onlinelibrary.wiley.com/doi/abs/10.1111/eva.13764">https://onlinelibrary.wiley.com/doi/abs/10.1111/eva.13764</a>.
- [80] Outpatient Antibiotic Use: Retail Pharmacy Prescription Data | A.R. & Patient Safety Portal. 2025. URL: https://arpsp.cdc.gov/profile/antibiotic-use/all-classes?utm\_source=chatgpt.com&year-select-rate-map=year2023 (visited on 07/09/2025).
- [81] Daniel Florin Pancu et al. "Antibiotics: Conventional Therapy and Natural Compounds with Antibacterial Activity—A Pharmaco-Toxicological Screening". In: Antibiotics 10.4 (2021). ISSN: 2079-6382. DOI: 10.3390/antibiotics10040401. URL: https://www.mdpi.com/2079-6382/10/4/401.
- [82] S Andreas Angermayr et al. "Growth-mediated negative feedback shapes quantitative antibiotic response". In: Molecular Systems Biology 18.9 (2022), e10490. DOI: https://doi.org/10.15252/msb.202110490. eprint: https://www.embopress.org/doi/pdf/10.15252/msb.202110490. URL: https://www.embopress.org/doi/abs/10.15252/msb.202110490.
- [83] David Dubnau and Melanie Blokesch. "Mechanisms of DNA Uptake by Naturally Competent Bacteria". In: Annual Review of Genetics 53. Volume 53, 2019 (2019), pp. 217-237. ISSN: 1545-2948. DOI: https://doi.org/10.1146/annurev-genet-112618-043641. URL: https://www.annualreviews.org/content/journals/10.1146/annurev-genet-112618-043641.
- [84] Rotem Gross et al. "Collective  $\beta$ -lactam resistance in *Escherichia coli* due to  $\beta$ -lactamase release upon cell death". In: bioRxiv (2024). DOI: 10.1101/2024.10.14.618215.
- [85] H. Allen Orr and Robert L. Unckless. "Population Extinction and the Genetics of Adaptation." In: *The American Naturalist* 172.2 (2008). PMID: 18662122, pp. 160–169. DOI: 10.1086/589460. URL: https://doi.org/10.1086/589460.
- [86] Helen K. Alexander and Sebastian Bonhoeffer. "Pre-existence and emergence of drug resistance in a generalized model of intra-host viral dynamics". In: *Epidemics* 4.4 (2012), pp. 187–202. ISSN: 1755-4365. DOI: https://doi.org/10.1016/j.epidem.2012.10.001. URL: https://www.sciencedirect.com/science/article/pii/S1755436512000485.

- [87] Rowan DH Barrett and Dolph Schluter. "Adaptation from standing genetic variation". In: *Trends in ecology & evolution* 23.1 (2008), pp. 38–44.
- [88] Christian A Yates, Matthew J Ford, and Richard L Mort. "A multi-stage representation of cell proliferation as a Markov process". In: *Bulletin of mathematical biology* 79.12 (2017), pp. 2905–2928.
- [89] Naoki Masuda and Luis E. C. Rocha. "A Gillespie Algorithm for Non-Markovian Stochastic Processes". In: SIAM Review 60.1 (2018), pp. 95–115. ISSN: 1095-7200. DOI: 10.1137/16m1055876. URL: http://dx.doi.org/10.1137/16M1055876.
- [90] Marian Boguñá et al. "Simulating non-Markovian stochastic processes". In: *Physical Review E* 90.4 (2014). ISSN: 1550-2376. DOI: 10.1103/physreve. 90.042108. URL: http://dx.doi.org/10.1103/PhysRevE.90.042108.
- [91] Loïc Marrec and Anne-Florence Bitbol. "Quantifying the impact of a periodic presence of antimicrobial on resistance evolution in a homogeneous microbial population of fixed size". In: Journal of Theoretical Biology 457 (2018), pp. 190–198. ISSN: 0022-5193. DOI: https://doi.org/10.1016/j.jtbi.2018.08.040. URL: https://www.sciencedirect.com/science/article/pii/S0022519318304284.
- [92] Emanuel Parzen. Stochastic processes. SIAM, 1999. Chap. 7, pp. 276–306.
- [93] Virginia Giorno and Amelia G. Nobile. "On some integral equations for the evaluation of first-passage-time densities of time-inhomogeneous birth-death processes". In: *Applied Mathematics and Computation* 422 (2022), p. 126993. ISSN: 0096-3003. DOI: https://doi.org/10.1016/j.amc.2022. 126993. URL: https://www.sciencedirect.com/science/article/pii/S0096300322000790.
- [94] Mark R. Deziel et al. "Effective Antimicrobial Regimens for Use in Humans for Therapy of *Bacillus anthracis* Infections and Postexposure Prophylaxis". In: *Antimicrobial Agents and Chemotherapy* 49.12 (2005), pp. 5099–5106. DOI: 10.1128/aac.49.12.5099-5106.2005. URL: https://journals.asm.org/doi/abs/10.1128/aac.49.12.5099-5106.2005.
- [95] Nikola Ojkic et al. "A roadblock-and-kill model explains the dynamical response to the DNA-targeting antibiotic ciprofloxacin". In: bioRxiv (2019). DOI: 10.1101/791145. URL: https://www.biorxiv.org/content/early/2019/10/10/791145.

## Supplementary Material

All TIL-Model and Gillespie simulations ran on Python programming language. The code will be available on GitHub:

https://github.com/PeriodicSandworm/ToleranceEvolutionModel.git

## Eidesstattliche Versicherung

Hiermit versichere ich an Eides statt, dass ich die vorliegende Arbeit selbstständig und ohne die Benutzung anderer als der angegebenen Hilfsmittel angefertigt habe. Alle Stellen, die wörtlich oder sinngemäß aus veröffentlichten und nicht veröffentlichten Schriften entnommen wurden, sind als solche kenntlich gemacht. Die Arbeit ist in gleicher oder ähnlicher Form oder auszugsweise im Rahmen einer anderen Prüfung noch nicht vorgelegt worden. Ich versichere, dass die eingereichte elektronische Fassung der eingereichten Druckfassung vollständig entspricht.

Jonas Günzl

Köln, den 19.08.2025

